Politecnico di Milano

Scuola di Ingegneria Industriale e dell'Informazione

Corso di Laurea Magistrale in Ingegneria Fisica

Dipartimento di Fisica

Study of rotational dynamics in impulsively aligned molecules by high-order harmonic generation

Tesi di Laurea Magistrale di:

Luca Cardellino

Matr. N. 766136

Relatore: Prof. Salvatore Stagira
Correlatore: Prof.ssa Caterina Vozzi

Anno Accademico 2013-2014

Dedicato con affetto ai miei genitori

Contents

List of Figures

Abstract

Study of rotational dynamics in impulsively aligned molecules by high-order harmonic generation

Luca cardellino

High Order Harmonic Generation (HHG) is a nonlinear process that occurs when an intense femtosecond laser pulse interacts with matter. The HHG process is important principally because it can be exploited as a coherent source of attosecond pulse train and it represents a sensitive probe of the wave functions of the bound states involved in the process. In this thesis work the HHG process is performed in impulsively aligned molecular gases. The molecules are aligned by a lower intensity laser pulse (pump) at $800\,\text{nm}$ with a duration shorter than the molecular rotational period. The pump excites a rotational wave-packet that periodically rephases at such instant of time called revivals corresponding to multiple or fraction of the rotational period of the molecule. The harmonic emission, generated by an intense laser pulse (probe) at $1450\,\text{nm}$ from an aligned molecular gas, is sensitive to the angle formed by the molecular axis with respect to the polarization direction of the probe. Such angle varies with respect to the time delay between pump and probe and this reflects on the HHG yield by an intensity modulation at the time delays corresponding to the revivals. The fractional revivals that appear in the HHG spectra are connected to the symmetry of the *highest occupied molecular orbital* (HOMO) and to the geometry of the molecules. The observation of the fractional revivals allows to get spectroscopic information about the structure and dynamics of the molecules in the gas.

Riassunto

La generazione di armoniche di ordine elevato (HHG:*High Harmonic Genera-tion*) é un processo non lineare che avviene quando un impulso laser a femtosecondi di intensitá molto elevata (dell'ordine di $10^{14}W/cm^2$) interagisce con la materia. Per via dell'interazione un elettrone viene ionizzato per effetto tunnel da un atomo o da una molecola e successivamente accelerato nel continuo dal campo elettrico del laser. Data l'elevata frequenza di oscillazione del campo elettrico, l'elettrone segue l'andamento del campo e quando questo cambia verso viene fatto ricollidere con lo ione parente. L'elettrone, ritornando allo stato legato, si diseccita e libera l'energia cinetica acquisita nel continuo sotto forma di radiazione nella regione spettrale dell'estremo ultravioletto (XUV). Tale processo si ripete ogni semi-ciclo ottico del campo producendo un treno di impulsi di durata dell'ordine degli attosecondi il cui spettro discreto é costituito dalle sole armoniche dispari della frequenza fondamentale. In un mezzo gassoso, l'emissione di radiazione XUV da parte di tutti gli atomi o di tutte le molecole si somma coerentemente dando luogo ad un'interferenza costruttiva soltanto lungo una direzione specifica. Per questa ragione il processo di HHG puó essere usato in mezzi gassosi come sorgente coerente ad attosecondi. La generazione di armoniche é estremamente importante anche perchè rappresenta un'ottima sonda delle proprietá delle funzioni d'onda degli stati legati coinvolti nel processo, in quanto la probabilità di ricollisione dipende dalla forma funzionale dell'orbitale da cui é stato emesso. Nel caso specifico del lavoro di tesi la generazione di armoniche di ordine elevato, prodotta da un laser nel medio infrasosso (1450 nm) é stata applicata ad un gas di molecole allineate

in regime impulsivo, ovvero mediante un impulso laser allineante (a $800\,\mathrm{nm}$) di durata inferiore al periodo rotazionale della molecola che permette di avere allineamento anche in assenza di campo. Ció é dovuto all'eccitazione di un pacchetto rotazionale i cui stati rientrano in fase tra loro in corrispondenza di certi istanti di tempo chiamati 'revival' che possono essere multipli del periodo rotazionale della molecola oppure sue frazioni. Se in un esperimento di tipo pump-probe, in cui l'impulso allineante rappresenta il pump e l'impulso generante il probe, facciamo variare il ritardo tra il pump e il probe, si ottiene una mappa costituita da spettri di armoniche acquisite a vari ritardi di tempo. L'angolo tra l'asse molecolare e la direzione di polarizzazione del probe è un parametro chiave nel processo di ricombinazione dell'elettrone, il quale a sua volta è legato alla forma dell'orbitale con cui l'elettrone ricollide. Il risultato é una modulazione dell'intensitá dell'emissione di armoniche al variare del ritardo, che si presenta in corrispondenza di quei ritardi di tempo in cui l'asse molecolare si riallinea con il campo, ovvero nei revival. Il lavoro di tesi è incentrato sullo studio della presenza di revival frazionari in CO_2 e N_2O e sulla ricerca di eventuali modifiche della forma del revival al variare dell'ordine di armonica.

Introduction

The (HHG) *High Harmonic Generation* represents an important process within the study of the laser-matter interaction in the strong-field regime. The HHG is a non linear process that occurs when an intense femtosecond laser pulse ($I \sim 10^{13} - 10^{14} \, W/cm^2$) interacts with atoms or molecules and generates high order harmonics of the fundamental laser frequency. Under the effect of the electric field an electron can be tunnel ionized from a molecule or an atom and, in the semiclassical view [4], it is accelerated in the continuum by the electric field with some probability to recollide with its parent ion. The recolliding electron emits a photon in the spectral range of the XUV (extreme ultraviolet) and soft X-rays. This process repeats every optical semi-cycle and thus the emitted radiation is characterized by an attosecond pulse train whose spectrum is constituted by only odd harmonics. Owing to its nature, HHG can be exploited as a coherent source of XUV-soft X-ray attosecond pulses [5]. The recollision probability, and thus the HHG spectra, depends on the properties of the wave function of the bound state involved. This fact allows to extract information about the property of the wave function of the bound state involved in the process. The recolliding electron can be used as a probe. Indeed the emitted energy, and thus the harmonic spectra, depends on the time between the ionization instant and the recollision instant. Different energies of the emitted photons correspond to different recollision probabilities of the electron. We can perform spatial and temporal measures by exploiting HHG process with high temporal ($\sim as$) and spatial resolution ($\sim$Å): the temporal duration of the electronic wave packet is shorter than the half optical

cycle.

We can use HHG process in coherently aligned molecules in order to extract, for example, the dynamic molecular structure [6, 7]. This can be seen as a pump-probe technique in molecular gases where the pump is the aligning pulse and the probe is the generating pulse (in particular the recolliding electron wave-packet). The alignment establishes a quantum coherence among the rotational states that vanishes and is recovered at multiples or fractions of the rotational period (revivals). The revivals shape encodes the information about the molecular structure by the dependence of the harmonic emission on the angle formed by the molecular axis with respect to the probe polarization direction. The observation of the appearance of revivals, in particular of the fractional revivals, and the study of their shape variations with respect to the harmonic order could lead towards more spectroscopic information about the molecular structure. The thesis work is focused on the study of fractional revivals, and thus the rotational dynamics of impulsively aligned molecules, in CO_2 and N_2O.

Chapter 1

HHG: *High Harmonic Generation*

High-order harmonic generation (HHG) is a coherent, highly nonlinear optical process. This effect can be understood in terms of a nonlinear dependence of the polarization vector of the medium on the incident laser electric field and so the generation of new frequencies, integer multiples of the incident laser frequency, occurs. Atoms and molecules exposed to a strong laser field emit a light bursts with a sub- femtosecond duration whose spectra has a universal characteristic shape. Coherence, instead, is due to the fact that the HHG signal is a coherent superposition of radiation emission from all the medium points [8]. The new genereted frequencies are in the spectral region between extreme ultraviolet (XUV) and soft X-ray and only odd multiples of the laser frequency ω appear. HHG is the only method able to obtain a source of coherent light in the spectral region of XUV and soft X-ray. The spectrum has repeatable features if the photon energy $\hbar\omega$ is much smaller then the ionization potential of the medium. Owing to the high intensity ($I \sim 10^{13} - 10^{16}\, W/cm^2$) the laser field is comparable or larger than the Coulomb field seen by the outer electrons of the target molecule/atom. For this reason, a non perturbative approach is required for modelling the HHG process. These intensities can be reached using short laser pulse (femtosecond). The chapter presents an excursus on the HHG process and provide a model for understanding the phenomenon, first in a microscopic range (one atom or molecule) and then in a macroscopic system (ensemble of atoms or molecules). I will first introduce a

semiclassical model which is useful to understand the process, then I will proceed with a more accurate quantum treatment and I will conclude with the explanation of what happens in a macroscopic ensemble of atoms/molecules.

1.1 The semiclassical Three-Step Model

The semiclassical model was introduced by Corkum [4] and Kulander, Schafer and Krause in 1993 and it is based on the assumption of strong-field and single-active-electron (SAE), so the laser intensity is high enough and we consider a single electron ionized per atom/molecule. We call this approach semiclassical since it uses both quantum and classical mechanics: the ionization by laser field is a quantum phenomenon and the electron motion in the continuum is described classically. The model divide the process in three step, hence is called *Three-Step model*:

1. **Tunnel ionization**: electron extraction occurs through *tunnel effect* which is in competition with other phenomena.

2. **Propagation**: once ionized, the electron propagates in the continuum following the electric field trend; it is characterized by a nearly-plane wave function and the more it travels in the continuum the more its wave function broadens.

3. **Recombination**: when the electron is in the continuum it has a certain probability to collide with its parent ion and recombine with it. When it returns in a bound state, owing to energy conservation, the kinetic energy acquired during propagation is converted into one emitted photon; this emission is classically seen as an emission of radiation for *Bremsstrahlung* after the recollision with the ion.

1.1.1 First step: tunnel ionization

There are many possible ionization mechanisms depending on the *Keldysh* parameter:

$$\gamma = \sqrt{\frac{I_p}{2U_p}} \tag{1.1}$$

where I_p is the ionization potential of the atom and U_p is the ponderomotive energy of the electron,

$$U_p = \frac{e^2 E_0^2}{4 m_e \omega_0^2} \tag{1.2}$$

which is the average energy of an electron moving in an oscillating electric field. In the previous equation, e is the electron charge, m_e the electron mass, E_0 is the laser electric field amplitude and ω_0 its oscillation frequency (fundamental frequency):

$$\vec{E}(t) = \vec{E_0} \cos(\omega_0 t). \tag{1.3}$$

We distinguish two cases:

$\gamma \gg 1$: it can be used a perturbative approach, LOPT (*Lower Order Perturbative Theory*)

$\gamma \ll 1$: a non perturbative approach is necessary.

An atom exposed to an intense laser field experiences two processes competing with each other: multi-photon ionization, which predominate if $\gamma \gg 1$, and tunnel ionization, which predominate if $\gamma \ll 1$. Since U_p depends on the square of the electric field amplitude, the higher is the intensity the lower is the γ parameter, so with relative low intensity the problem can be treated with the perturbation theory at the first order (photon energy much lower than ionization potential), instead for high intensity (10^{13}-10^{14} W/cm^2) the perturbative approach can't be used. In multi-photon ionization the electron can reach the continuum absorbing an integer number n of photon such that

$$n \hbar \omega_0 \geqslant I_p \ . \tag{1.4}$$

(a) Tunnel ioniz.
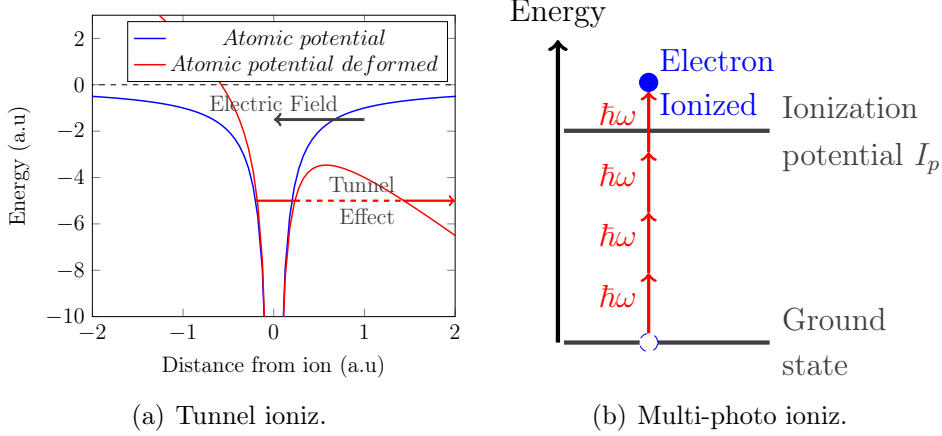
(b) Multi-photo ioniz.

Figure 1.1: *Tunnel ionization (a) and multi-photon ionization (b) schemes.*

In this case the *ionization rate* (ionization probability per unit of time, so the number of emitted electron per unit of time) is $\Gamma_n = \sigma_n I^n$, where I is the laser intensity and σ_n the cross section of the process. If the electron absorbs more photons than necessary, the exceeding photons give a contribution to the increasing of the electron kinetic energy; this process is known as *above threshold ionization* (ATI) [4].

In the tunnel ionization, which occurs if the perturbative approach isn't applicable, the laser electric field distorts the Coulombian field and the atomic potential is deformed. The electron will thus find a potential barrier which it can pass through thanks to tunnel effect. In this case the tunneling ionization rate can be calculated with the ADK (Ammosov, Delone, Krainov) theory [9] in which the tunneling time t_t, the time necessary to the electron for crossing the barrier, is much lower than the oscillation period of the electric field T_0. It can be demonstrated that

$$\gamma = \frac{t_t}{T_0/2} \ , \tag{1.5}$$

so when $\gamma \ll 1$, that is the condition for which the tunnel effect predominates on other ionization forms, is also $t_t \ll T_0$ [10]. t_t is the time that spends the electron to pass through the barrier. This condition allows to consider the electric

field *quasi-static* and thus the barrier, generated by the field, keep on unmodified for a time long enough to make tunneling process completed. The hypothesis for which the frequency ω_0 is much lower than $\omega_t = 1/t_t$, so that we can neglect the change of the field during the passage of the electron through the barrier, is called *adiabatic approximation*. The γ parameter tell us the degree of adiabaticity of the motion through the barrier. For laser in the spectral region of infrared and visible, like the lasers used for HHG experiments, the approximation is valid. The ionization rate can be calculated by

$$W(t) = -\frac{1}{N(t)}\frac{dN}{dt} = \omega_p |C_{n^*}|^2 \left(\frac{4\omega_p}{\omega_t}\right)^{2n^*-1} \exp\left(-\frac{4\omega_p}{3\omega_t}\right) \qquad (1.6)$$

where N(t) is the atom fraction that is still unionized at the time t.
In (1.6):

$$\omega_p = \frac{I_p}{\hbar} \qquad (1.7)$$

$$\omega_t = \frac{eE(t)}{\sqrt{2m_e I_p}} \qquad (1.8)$$

$$n^* = Z\sqrt{\frac{I_{ph}}{I_p}} \qquad (1.9)$$

$$|C_{n^*}|^2 = 2^{2n^*}\frac{1}{n^*\Gamma(n^*+1)\Gamma(n^*))} \qquad (1.10)$$

where I_{ph} is the Hydrogen ionization potential and Γ is the Eulero *Gamma* function. Combining the equations above we find:

$$\frac{\omega_p}{\omega_t} = \frac{I_p}{\hbar}\frac{\sqrt{2m_e I_p}}{eE(t)}$$

$$\Downarrow$$

$$\exp\left(-\frac{4\omega_p}{2\omega_t}\right) = \exp\left(-\frac{2\sqrt{m_e}(2I_p)^{\frac{3}{2}}}{3\hbar eE}\right)$$

Finally we obtain the following dependence for the ionization rate

$$W \propto \exp\left(-\frac{\sqrt{m_e}2(2I_p)^{\frac{3}{2}}}{3\hbar eE}\right) \qquad (1.11)$$

Indeed W depends on the probability density that there is immediately after the barrier, at the end of crossing, and this leads to estimate a dependence from $\exp\left(-I_p/E\right)$, where I_p/E is closely connected to the width of the barrier (through γ). For these calculations the electric field isn't constant during the electron passage, but it have a rising edge. In the case $\gamma \ll 1$ we can still use the adiabatic approximation, and so the ADK model, to calculate the ionization rate by averaging it over an optical period of laser or using the saturation intensity I_s that is the intensity for which the ionization rate is near to one. In the experiments realized the ionization potential is $I_p \sim 15eV$ and the focalization intensity is $I \sim 10^{14}W/cm^2$ so $\gamma \ll 1$ and tunnel ionization prevails.

1.1.2 Second step: propagation

Once the electron is ionized, it passes from a condition in which it could occupy only a certain quantized energy state to one in which it can assume a continuum of energies, as if it was free. The condition in which electron can take every energy value with continuity is called *continuum*. In the continuum the electron can be treated classically and we can apply the classical mechanics to describe the electron motion and find its trajectories. Its motion can be thought as that of a charge in oscillating electric field. We consider electron subjected only to the force produced by the incident laser electric field; in fact in the Lorentz force the magnetic field is weighed by v/c hence this contribution become important only for relativistic electrons. It is worth mentioning that, in the strong-field approximation, the Coulomb field of the ion can be neglected with respect to the laser field. We consider an electric field of the form:

$$\vec{E}(t) = \vec{E_0}\cos\left(\omega_0 t\right) \tag{1.12}$$

We choose a reference system where electric field has one component in a specific direction, supposed the x-direction. The electron is accelerated in the direction of the electric field oscillation. The Newton equation for the motion of a charge

in electric field can be written as:

$$\ddot{x}(t) = \frac{q}{m_q} E_0 \cos\left(\omega_0 t\right) \tag{1.13}$$

where q is the charge and m_q its mass. We call t_i the ionization instant and t_r the recombination instant. Integrating the equation 1.13 using the initial condition $\dot{x}(t_i) = 0$, $x(t_i) = 0$, we obtain:

$$\dot{x}(t) = \frac{qE_0}{m_q\omega_0}\left(\sin\left(\omega_0 t\right) - \sin\left(\omega_0 t_i\right)\right) \tag{1.14}$$

Finally the trajectories are:

$$x(t) = -\frac{qE_0}{m_q\omega_0^2}\left(\cos\left(\omega_0 t\right) - \cos\left(\omega_0 t_i\right) + \sin\left(\omega_0 t_i\right)(t - t_i)\omega_0\right) \tag{1.15}$$

For an electron $q = -e$:

$$\dot{x}(t) = -\frac{eE_0}{m_e\omega_0}\left(\sin\left(\omega_0 t\right) - \sin\left(\omega_0 t_i\right)\right) \tag{1.16}$$

$$x(t) = \frac{eE_0}{m_e\omega_0^2}\left(\cos\left(\omega_0 t\right) - \cos\left(\omega_0 t_i\right) + \sin\left(\omega_0 t_i\right)(t - t_i)\omega_0\right) \tag{1.17}$$

At different ionization instants t_i correspond different trajectories which depend also on laser frequency and electric field amplitude (it's only a scale factor).

1.1.3 Third step: recombination

The electron oscillating with the electric field has a certain probability to collide with the parent ion in a specific time. The more it rests in the continuum, the more its wave function broads, the more the superposition with the wave function of the bound state decreases and lower is the probability to collide with the ion. We can find the instant $t = t_r$ in which the electron recombine with his parent ion solving the equation:

$$\cos\left(\omega_0 t\right) - \cos\left(\omega_0 t_i\right) + \sin\left(\omega_0 t_i\right)(t - t_i)\omega_0 = 0 \tag{1.18}$$

All couples (t_i, t_r) solutions of this equation individuates a specific trajectory of the electron.
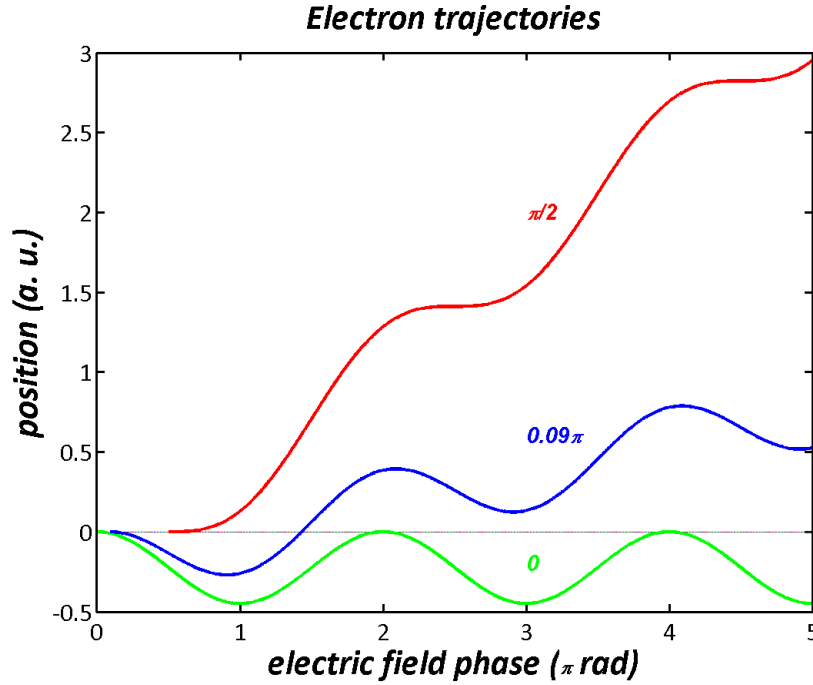
Figure 1.2: *Electrons trajectories for three different values of the initial phase of the electric field: 0 rad (infinite recollisions with zero energy), 0.09π rad (only one recollision), $\frac{\pi}{2}$ rad (no recollision).*

As figure 1.2 shows, there is an instant t_i from which the electron generated never recombines with its parent ion. In particularly the maximum electric field phase for which electron can be ionized in order to get recombination is about $\pi/2$ every semi-period. Precisely electrons recombine if they have generated when the electric field phase is:

$$0° \leqslant \omega_0 t_i \leqslant 80°$$

$$180° \leqslant \omega_0 t_i \leqslant 260°$$

This process in fact happens every semi-period of electric field in opposite direction, so with a periodicity of π. The (1.18) is a transcendental equation that can be solved graphically or numerically. The $t_r = t_r(t_i)$ function is plotted in figure 1.3 in terms of the phases of the electric field at ionization and recombination time. When $\omega_0 t_i = 0° + k\pi, k \in \mathbb{N}$ the electron recombines infinite times, but with zero velocity and so zero energy. The recombination is possible only for linearly
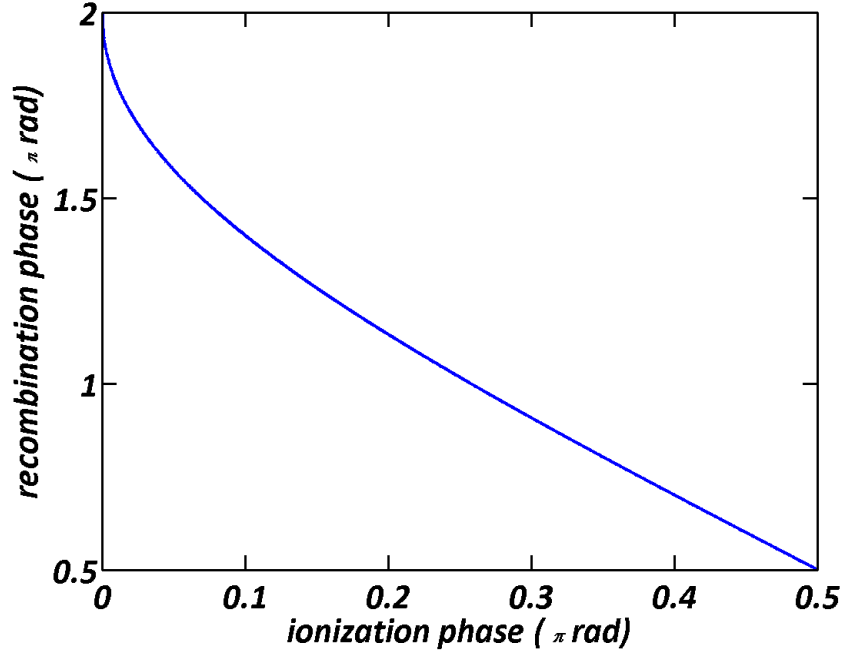
Figure 1.3: *Electric field phase at the electron recombination in unit of π rad versus electric field phase at the electron ionization in unit of π rad.*

polarized pulses. For the conservation of energy the recombination of electron is followed by the radiation emission that can be seen as a photon emission when electron returns in its fundamental state:

$$\mathcal{E}_{hhg} = I_p + K = I_p + \frac{1}{2}m_e\dot{x}^2 \tag{1.19}$$

Putting the equation 1.14 into the equation 1.19:

$$\mathcal{E}_{hhg} = \hbar\omega_{hhg} = I_p + 2U_p[\sin(\omega_0 t_r) - sin(\omega_0 t_i)]^2 \tag{1.20}$$

The maximum energy achieved by electron in the continuum is obtained for $\omega_0 t_i = 0.09\pi + k\pi, k \in \mathbb{N}$ and $\omega_0 t_r = 1.4\pi + k\pi, k \in \mathbb{N}$:

$$\mathcal{E}_{hhg,MAX} = \hbar\omega_{cut} = I_p + 3.17U_p \tag{1.21}$$

$$\omega_{cut} = \frac{I_p + 3.17U_p}{\hbar} \tag{1.22}$$

The (1.21) is defined as energy *cut-off*.
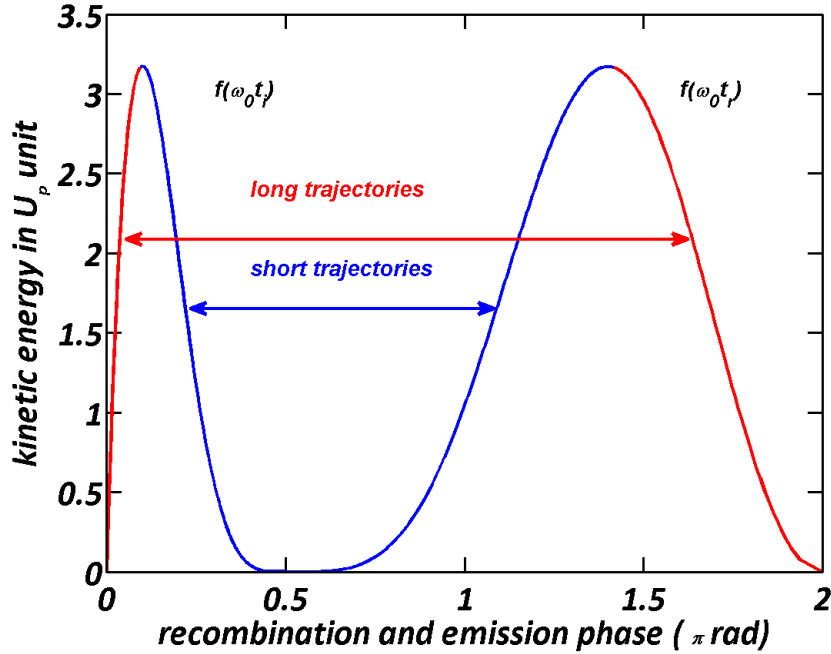
Figure 1.4: *Kinetic energy in U_p units for long (red) and short (blue) trajectories depending on emission time t_i (right) and on recombination time t_r (left).*

The spectrum irradiated for Bremsstrahlung, due to the sharp deceleration of the electron, is continuous and it's characterized by a *plateau* followed by a *cut-off*. In the figure 1.4 we can notice that for recollision energies lower than the cutoff one there are two trajectories available for each energy value; in fact we can distinguish a long trajectory for $0 \leqslant t_i \leqslant 0.09\pi$, whereby the electron remains longer in the continuum, and a short trajectory for $0.09\pi \leqslant 0.5\pi$. The two trajectories degenerate in only one in the cut-off. The recollision times corresponding to short trajectories are restricted to a temporal interval shorter than a half-cycle of the laser, hence the radiation burst generated by such contributions has a duration of the order hundreds of attoseconds. Moreover the figure suggests us that a chirp is present, in fact for short trajectories electron with higher kinetic energy recollides later. In this case energy, and so frequency, increase with time, thus the chirp is positive.

The power radiated by an oscillating dipole is calculated by the Larmor formula in

which the power $P(t) \propto < a(t) >^2$, where $a(t)$ is the acceleration of the electron and $< a(t) >$ is its average over all ionization times, since the ionization is a quantum process and we can only determine the probability that it happens in a certain time interval [11]: in the average the various $a(t; t_i)$ are weighed by the probability of ionization at the instant t_i, $p_i(t_i)$. Under the approximation of electric dipole, the electric field radiated by the dipole, taking into account only the recollisions in one optic cycle, is proportional to $< a(t) >$ and its spectrum is a continuum characterized by a plateau and a cut-off. Considering N optical cycles, the total dipole acceleration is the sum of $2N$ terms because in one cycle there are two recollision events. The spectral power density is:

$$S(\omega) = |\hat{a}(\omega)|^2 \tag{1.23}$$

If we think N approaching to infinity the spectrum becomes more and more discrete. Taking into account all optical cycles, the temporal signal is ideally a train of bursts, spaced by $T_0/2$:

$$\epsilon_{XUV}(t) = \epsilon_{burst} * h(t) \tag{1.24}$$

where

$$h(t) = \sum_{n=-\infty}^{+\infty} e^{in\pi} \delta\left(t - n\frac{T_0}{2}\right) \tag{1.25}$$

The Fourier transform of signal is:

$$\mathcal{F}[\tilde{\epsilon}_{XUV}](\omega) = \tilde{\epsilon}_{burst}(\omega)\tilde{h}(\omega) \tag{1.26}$$

The train of Dirac delta can be expanded in Fourier series, since its a T_0 periodic signal:

$$h(t) = 2\sum_{m=1}^{+\infty} a_n \cos\left(m\frac{2\pi}{T_0}t\right) \tag{1.27}$$

with

$$a_n = \frac{1}{T_0} \int_0^{T_0} \cos\left(m\frac{2\pi}{T_0}t\right) \sum_{n=-\infty}^{+\infty} e^{in\pi}\delta\left(t - n\frac{T_0}{2}\right)dt \tag{1.28}$$

$$= \frac{1}{T_0} \int_0^{T_0} \cos\left(m\frac{2\pi}{T_0}t\right)\left[\delta(t) - \delta\left(t - \frac{T_0}{2}\right)\right]dt \tag{1.29}$$

$$= \frac{1}{T_0}[1 - \cos(m\pi)] \tag{1.30}$$

The coefficients are not zero for only odd harmonics, that is m must be an odd integer:

$$m = 2k + 1 \tag{1.31}$$

The absence of even harmonics can be also understood thinking to the medium non linear susceptibility, due to the anharmonicity introduced by electron recollisions. Since the medium has inversion symmetry (centrosymmetric medium) the expansion in power series of non linear susceptibility contains only odd orders. If we consider a pulse of finite duration the harmonic line width is proportional to the inverse of the pulse duration. The more the pulse is short the more the spectrum is similar to a continuum. The limit is a pulse with one optical cycle for which the spectrum is continuous. The presence of pulsed radiation causes that:

1. the number of optical cycles is finite and so the spectrum is characterized by broader peaks for shorter driving pulses;

2. the peaks in the cutoff region of the XUV spectrum are found to be shifted with respect to the expected harmonic frequencies owing to the phase shift between spectra emitted from consecutive recollision events, which occur at different laser intensities [12].

1.2   The Lewenstein model

A quantum model is necessary to overcome the hard limitations of the semiclassical model, such as quantum diffusion of electron wave packets, elastic scattering

by ion of electron, quantum interference between wave packets of different generation time and in particular the initial condition $x(t_i) = 0, \dot{x}(t_i) = 0$. This model was proposed by Lewenstein *et al.* [8] and is based on some hypothesis:

1. SAE (Single Active Electron)

2. Strong field (SFA): allows to neglect Coulomb ion field with respect to the laser field; its validity is confirmed for high order harmonics because typically electron is ionized when electric field is maximum and at the recollision the kinetic energy is much higher than the ionization energy.

3. Depletion of the fundamental state neglected: U_p not too much high.

4. Contribution of bound states, except ground state, neglected: valid if ω_0 is much far from intermediate resonances between the various states and when tunnel ionization is dominant.

We consider initially a single atom. The Time Dependent Schrödinger Equation (TDSE) is:

$$i\hbar \frac{\partial |\psi(\vec{r},t)\rangle}{\partial t} = \left[-\frac{\hbar^2}{2\mu} \nabla^2_{\vec{r}} + V_0(\vec{r}) + e\vec{r} \cdot E(t) \right] |\psi(\vec{r},t)\rangle \qquad (1.32)$$

where V_0 is the Coulomb potential and $E(t)$ is the laser electric field. The electron emission happens for tunnel effect. Initially, when the electric field is off, the electron is on the ground state:

$$|\psi(\vec{r},t_0)\rangle = |\psi_0(\vec{r},t)\rangle = e^{-i\frac{\mathcal{E}_0}{\hbar}t} \phi_0(\vec{r}) \qquad (1.33)$$

where $\mathcal{E}_0 = -I_p$.

The solution is written as a superposition of ground state and continuum states:

$$|\psi(\vec{r},t)\rangle = e^{i\frac{I_p}{\hbar}t} \left[|\phi_0(\vec{r})\rangle + \frac{1}{\sqrt{(2\pi)^2}} \int b(\vec{k},t) \left| e^{i\vec{k}\cdot\vec{r}} \right\rangle d^3k \right] \qquad (1.34)$$

Temporal evolution is completely determined by $b(\vec{k},t)$ that are complex quantities. The (1.34) satisfies the eigenvalues equation:

$$\left(-\frac{\hbar^2}{2\mu}\nabla_{\vec{r}}^2 + V_0(\vec{r})\right)|\phi_0(\vec{r})\rangle = -I_p|\phi_0(\vec{r})\rangle \qquad (1.35)$$

Using the (1.35), neglecting the potential $V_0(\vec{r})$ for SFA and choosing a reference system such that electric field results polarized in x direction, we obtain the following equation in b:

$$\frac{\partial}{\partial t}b(\vec{k},t) = -\frac{i}{\hbar}\left(\frac{\hbar^2 k^2}{2\mu} + I_p\right)b(\vec{k},t) - \frac{i}{\hbar}eE(t)d_x(\vec{k}) + \frac{e}{\hbar}E(t)\frac{\partial}{\partial k_x}b(\vec{k},t) \qquad (1.36)$$

where $d_x(\vec{k}) = \left\langle e^{-i\vec{k}\cdot\vec{r}} \middle| x \middle| \phi_0(\vec{r})\right\rangle = \frac{1}{\sqrt{(2\pi)^2}}\int e^{-i\vec{k}\cdot\vec{r}}x\phi_0(\vec{r})d\vec{r}$ is the transition dipole between the ground state and the continuum state $\left\langle \vec{k}\right\rangle$ along the electric field direction. I_p and $\phi_0(\vec{r})$ bring the information about $V_0(\vec{r})$ even though it doesn't appear explicitly in the equation 1.36.

The (1.36) is linear and first order equation, so it can be analytically integrated finding $b(\vec{k},t)$ and thus $|\psi(\vec{r},t)\rangle$. On the basis of the solutions of (1.36), we can calculate the expectation value of dipole moment, source of harmonics field. The harmonics spectrum $\tilde{\vec{E}}_{XUV}(\omega)$ generated by the interaction between the laser electric field and a single molecule or atom can be calculated as the Fourier transform $\mathcal{F}_t$ of the dipole acceleration, defined as the expectation value of dipole momentum operator $\hat{\vec{a}} = -\frac{i}{\mu}\vec{\nabla}_r V(\vec{r})$ ('acceleration gauge'):

$$\tilde{\vec{E}}_{XUV}(\omega) = \mathcal{F}_t\left[\left\langle \psi(\vec{r},t)\middle|\hat{\vec{a}}\middle|\psi(\vec{r},t)\right\rangle\right] \qquad (1.37)$$

According to the Ehrenfest theorem the $\langle\hat{\vec{a}}\rangle$ operator can be replaced by $\frac{d\langle\hat{\vec{p}}\rangle}{dt}$ ('velocity gauge'), where $\hat{\vec{p}} = -i\vec{\nabla}_r$ is the dipole momentum operator, or by $\frac{d^2\langle\hat{\vec{r}}\rangle}{dt^2}$ ('length gauge'), where $\hat{\vec{r}} = \vec{r}$ is the dipole moment operator in units of electron charge e. The harmonics spectrum can be rewrite as following depending on the

gauge choice:

$$\tilde{\vec{E}}_{XUV}(\omega) = \mathcal{F}_t\left[\frac{d}{dt}\left\langle \psi(\vec{r},t)\left|\hat{\vec{p}}\right|\psi(\vec{r},t)\right\rangle\right] = i\omega\mathcal{F}_t\left[\left\langle \psi(\vec{r},t)\left|\hat{\vec{p}}\right|\psi(\vec{r},t)\right\rangle\right] \quad (1.38)$$

$$\tilde{\vec{E}}_{XUV}(\omega) = \mathcal{F}_t\left[\frac{d^2}{dt^2}\left\langle \psi(\vec{r},t)\left|\hat{\vec{r}}\right|\psi(\vec{r},t)\right\rangle\right] = -\omega^2\mathcal{F}_t\left[\left\langle \psi(\vec{r},t)\left|\hat{\vec{r}}\right|\psi(\vec{r},t)\right\rangle\right] \quad (1.39)$$

The three forms are not equivalent if we consider the recolliding wave as a combination of plane wave and the best choice is not known *a priori*. We can express generically the three operators with the operator $\hat{\vec{\rho}}$ whose expectation value is $\vec{\rho}(t) = \langle\hat{\vec{\rho}}\rangle = \left\langle \psi(\vec{r},t)\left|\hat{\vec{\rho}}\right|\psi(\vec{r},t)\right\rangle$. More simply if we have a dipole moment $\vec{d}(t) = -e\vec{r}(t) = -e\vec{r}_0\cos(\omega t)$ oscillating at ω frequency, it's possible to calculate classically the emitting electric field value far from the dipole at the ω frequency which is given by:

$$\tilde{\vec{E}}(\omega) \propto -\omega^2\mathcal{F}_t[\vec{r}(t)] = -\omega^2\mathcal{F}_t\left[\left\langle \phi_{(}\vec{r},t)\left|\hat{\vec{r}}\right|\phi_{(}\vec{r},t)\right\rangle\right] \quad (1.40)$$

Neglecting transitions between continuum states that give no contribution to HHG, we can write the dipole moment as:

$$\langle\vec{r}(t)\rangle = -i\int_{\vec{p}}\int_{t'=0}^{\infty}\frac{e}{\hbar^4}\vec{E}(t')\cdot\vec{d}(\vec{p}+e\vec{A}(t'))\vec{d}^*(\vec{p}+e\vec{A}(t))e^{-\frac{i}{\hbar}S(\vec{p},t,t')}d\vec{p}dt'+c.c. \quad (1.41)$$

where

- $S(\vec{p},t,t')$ is the quasiclassical action,

- in $\vec{p}+e\vec{A}(t)$, $\vec{p}$ is the canonical momentum which is a constant of the motion if $V_0(\vec{r})$ is neglected,

- $\vec{A}(t)$ is the vector potential of the laser electric field,

- $\vec{d}(\vec{p}+e\vec{A}(t))$ transition dipole from ground state to continuum state $\left|\vec{k}(t)\right\rangle = \frac{1}{\sqrt{(2\pi)^2}}e^{i\vec{k}\cdot\vec{r}}$.

$$S(\vec{p}, t, t') = \int_{t'}^{t} \left[\frac{|\vec{p} + e\vec{A}(t'')|^2}{2\mu} + I_p \right] dt'' \tag{1.42}$$

$$\hbar\vec{k}(t) = \vec{p} + e\vec{A}(t) \tag{1.43}$$

$$\vec{d}(\vec{p} + e\vec{A}(t)) = \vec{d}(\vec{k}(t)) = \frac{1}{\sqrt{(2\pi)^2}} \int e^{i\vec{k}\cdot\vec{r}} \vec{r} \phi_0(\vec{r}) d\vec{r} \tag{1.44}$$

The terms inside (1.41) have the following physical interpretation:

- $\vec{E}(t') \cdot \vec{d}[\vec{p} + e\vec{A}(t')]$ stands for the probability that occurs a transition from ground state to continuum $\left| \vec{k}(t') \right\rangle$ at the time t'.

- $e^{-\frac{i}{\hbar}S(\vec{p},t,t')}$ represents the phase acquired by electron during the propagation from the instant t' to a generic instant t. Electron during the propagation changes its state from the initial one $\left| \vec{k}(t') \right\rangle$ to $\left| \vec{k}(t) \right\rangle$.

- $\vec{d}^*(\vec{p} + e\vec{A}(t))$ stands for the probability that occurs the electron recombination at generic time t from the continuum $\left| \vec{k}(t) \right\rangle$ to ground state. Between t' and t the canonical momentum is preserved.

Putting the expression (1.41) of dipole momentum into the equation (1.40) we obtain:

$$\tilde{E}_{XUV}(\omega) \propto i\omega^2 \int_t \int_{\vec{p}} \int_{t'=0}^{\infty} \frac{e}{\hbar^4} \vec{E}(t') \cdot \vec{d}(\vec{p} + e\vec{A}(t')) \vec{d}^*(\vec{p} + e\vec{A}(t)) e^{-\frac{i}{\hbar}S(\vec{p},t,t')} d\vec{p} dt' e^{i\omega t} dt \tag{1.45}$$

The equation (1.45) gives the amplitude spectrum of HHG and it's the integral over all possible quantum trajectories characterized by a ionization time t', a recombination time t and a canonical momentum $\vec{p}$ which doesn't change during the propagation.

We can also define the phase term

$$\Phi_{XUV}(\vec{p}, t, t') = \omega t - S(\vec{p}, t, t') \tag{1.46}$$

In order to extract an analytical solution for this integral, we can use an important approximation, called *saddle point* approximation, which among all possible

trajectories selects only few of them that give a significant contribution to the XUV radiation. If the phase term $e^{-\frac{i}{\hbar}S(\vec{p},t,t')}$ changes quickly with $\vec{p}$ respect to the matrix elements, the integrand is an oscillating function with zero average value. The other terms can then be brought out from the integral in $\vec{p}$ and then the term containing the quasiclassical action can be expanded in Taylor series near the *saddle point* $\vec{p}_s$; the major contribution comes from those trajectories whose $S(\vec{p},t,t')$ function is stationary:

$$\vec{\nabla}_{\vec{p}}S(\vec{p},t,t')|_{\vec{p}_s} = 0 \tag{1.47}$$

$$S(\vec{p},t,t') \approx S(\vec{p}_s,t,t') + \frac{1}{2}\nabla_{\vec{p}}^2 S(\vec{p},t,t')|_{\vec{p}_s}(\vec{p}-\vec{p}_s)^2 \tag{1.48}$$

The (1.48) is called "*Saddle Point Approximation*". Moreover

$$\vec{\nabla}_{\vec{p}}S(\vec{p},t,t')|_{\vec{p}_s} = \vec{r}_{\vec{p}_s}(t) - \vec{r}_{\vec{p}_s}(t') = 0 \tag{1.49}$$

From 1.49 we understand that the predominant contribution to harmonics generation comes from electrons which recombine in the same position where they are emitted. This fact recalls the assumptions made in the semiclassical model.

The integral in $\vec{p}$ after the approximation becomes

$$I(t,t') = \int_{\vec{p}} e^{-\frac{i}{\hbar}S(\vec{p},t,t')}d\vec{p} \tag{1.50}$$

and thus we obtain the following dipole moment:

$$\langle \vec{r}(t) \rangle = -i \int_{t'=0}^{\infty} \frac{e}{\hbar^4} \left(\frac{\pi\mu\hbar}{\alpha + i\frac{(t-t')}{2}} \right)^{\frac{3}{2}} \vec{E}(t') \cdot \vec{d}(\vec{p}_s + e\vec{A}(t')) \cdot \\ \cdot \vec{d}^*(\vec{p}_s + e\vec{A}(t))e^{-\frac{i}{\hbar}S(\vec{p}_s,t,t')}dt' + c.c. \tag{1.51}$$

where α is a positive regularization constant used to deny $I(t,t')$ to diverge for $t = t'$. The factor $\left(\frac{\pi\mu\hbar}{\alpha+i\frac{(t-t')}{2}} \right)^{\frac{3}{2}}$ implies that the electrons recolliding at t longer than the laser optical cycle give lower contribution to the harmonics generation, in agreement with the quantum diffusion effect. The three integrations in (1.45) are thus reduced to a double integration that can be removed by applying the

same method as before. We can consider the action varying faster than other factors with respect to each variable and expand it in Taylor series around their respectively saddle points $(\vec{p}_s, t_s, t'_s)$. The saddle point approximation can be used to further simplify the Lewenstein integral (expression 1.45) by replacing the remaining integration in t' and t with few dominant contributions characterized by saddle point solutions t'_s and t_s:

- $\vec{\nabla}_{\vec{p}} S(\vec{p}, t, t')|_{\vec{p}_s} = 0$ is the first saddle point equation, implying that the electron recombines in the same position in which it was freed.

- $\hbar \frac{\partial}{\partial (t')} S(\vec{p}, t, t') = \frac{|\vec{p} + e\vec{A}(t')|^2}{2\mu} + I_p = 0$ establishes a relationship between ionization and recombination times together with the previous equation. If $I_p = 0$ electrons appear in the continuum with zero energy and canonical momentum is proportional to the vector potential at time t'. If $I_p > 0$ the equation is verified only for complex velocity (the electron in fact has just pass through the barrier and into the barrier the wave function is evanescent). In this case a complex ionization time appears, its imaginary part is negative and it gives rise to a real exponential with a value lower than 1. The initial kinetic energy is therefore negative, which is explained by the complex ionization time. The higher is I_p and so the imaginary part of the time the lower is the probability to cross the barrier.

- $\hbar \frac{\partial}{\partial (t)} [S(\vec{p}, t, t') - \omega t] = \frac{|\vec{p} + e\vec{A}(t)|^2}{2\mu} + I_p - \hbar\omega = 0$ or also $\frac{|\vec{p}_s + e\vec{A}(t)|^2}{2\mu} - \frac{|\vec{p} + e\vec{A}(t')|^2}{2\mu} = \hbar\omega$ express the conservation of energy by imposing that the emitted photon energy is the sum of the kinetic energy at recollision with the ionization energy. This condition selects the trajectories identified by $(\vec{p}_s, t_s, t'_s)$ that give their contribution to harmonics emission.

By solving the system of three equation we find the complex solutions $(\vec{p}_s, t, t')$; from these solutions one can determine the effective harmonic cutoff energy, that

is:

$$\omega_{cutoff} = \frac{1.32 I_p + 3.17 U_p}{\hbar} \tag{1.52}$$

The cutoff frequency is slightly different from that calculated with semiclassical model and this suggests that tunneling and quantum diffusion influence the cutoff energy. Instead of a sharp cut of the spectrum over the cut-off as predicted by the three step model, the Lewenstein model predicts an exponential decrease of harmonics intensity through the cutoff region.

Figure 1.5 shows a numerical solution of the saddle point equations with $I_p > 0$. In analogy with semiclassical model the Lewenstein model brings also to consider two categories of trajectories that give a predominant contribution to HHG: the long and short trajectories. The trajectories of the electrons that are accelerated in the continuum for a time longer then the laser optical cycle are neglected. We should also discard the unphysical solutions as the ones whose action assumes a negative imaginary part making the integrals in (1.45) divergent. Only the solutions with positive imaginary part of the action are acceptable. In the figure we observe the real part of t_s and t'_s. Imaginary and real parts of time could be interpreted as tunneling time and transit time in the continuum respectively. The time spent by the electron in the continuum changes very slightly with respect to the harmonic order among the *plateau*, this suggest that in first approximation the harmonic intensity can be considered a constant until the *cutoff*, whose intensity changes roughly.

1.3 The phase matching issue

In real experiments one does not deal with isolated atoms, but usually there is a large ensemble of atoms of molecule. Since the ionization of the gas induces non linear effects on laser pulse and the spatial evolution of the focused beam imposes different driving conditions along the medium, harmonics generated by atoms or molecule in different position are not in phase with each other. This
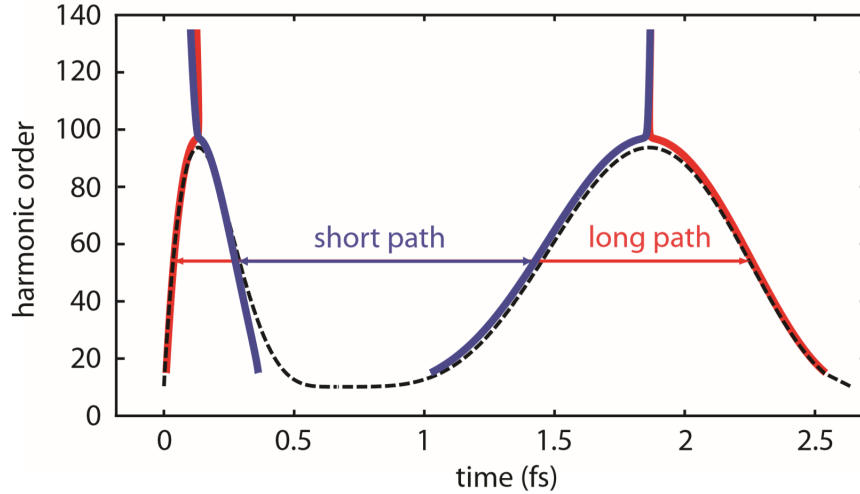
Figure 1.5: *Solution of the saddle point equations evaluated for $E = E_0 \cos(\omega_0 t)$, $E_0 = 7.2 \times 10^{10}$ V/m and $\lambda = 800$ nm. The curve corresponds to the ionization times t'_s on the left and to the recollision times t_s on the right, for short (blue line) and long (red line) trajectories. The dashed line represents the classical solutions.*

effect is known as phase mismatch. The final signal is a coherent (intended as optical coherence) sum of all single contributions. In adiabatic regime (when the laser intensity changes slower than the optical cycle) we can individuate two pairs of (t_i, t_r): one for short trajectories and one for long trajectories; contribution to harmonics from different kind of trajectories show different mismatch conditions. The emitted pulse is chirped because of the blue (if the emission occurs on rising edge) and red shift (if the emission occurs in the falling edge).

Phase matching conditions can affect dramatically the harmonic spectrum. Balcou and Saliéres proposed a geometrical method to calculate the focalization conditions favored by phase matching [1, 13]. We make the following hypothesis:

1. a sinusoidal oscillating electric field; depletion of the ground state neglected

2. the laser beam is gaussian and the propagation occurs along the z axis

3. the nonlinear medium is assumed isotropic and homogeneous

4. the chromatic dispersion of the medium is neglected

We call $\vec{k}_q$ the wave vector of the nonlinear polarization corresponding to the harmonic order q. The field generated by two different emitting points $\vec{r}_1$ and $\vec{r}_2$ sums constructively in the $\vec{k}_q$ direction if:

$$arg\left[P_q(\vec{r}_1)\exp\left(i\vec{k}_q \cdot (\vec{r}_2 - \vec{r}_1)\right)\right] = arg\left[P_q(\vec{r}_2)\right] \tag{1.53}$$

where P_q is non linear polarization component at the frequency $q\omega_0$. We get a perfect phase matching if

$$\Delta\vec{k} = 0 \tag{1.54}$$

In perturbative regime the phase matching condition is simply $\vec{k}_q = q\vec{k}_1$, where:

$$\vec{k}_1 = \frac{\omega_0}{c}\hat{e}_z + \vec{\nabla}\phi_{Gouy} \tag{1.55}$$

$$\phi_{Gouy} = arg\left[\frac{1}{b+2iz}\exp\left(-\frac{\omega_0 r^2}{c(b+2iz)}\right)\right] \tag{1.56}$$

ϕ_{Gouy} is a phase contribution due to the focalization, called Gouy phase. In non perturbative regime we must add another phase term and thus define an effective wave vector

$$\vec{K}(r,z) = \vec{\nabla}\phi_{dip}(r,z) = \vec{\nabla}\left(-\frac{1}{\hbar}S(\vec{p}_s, t_s, t'_s) + q\hbar\omega_0\right) \tag{1.57}$$

so phase matching condition becomes:

$$\vec{k}_q = q\vec{k}_1 + \vec{K} \tag{1.58}$$

On z axis, in the beam waist $(r = 0, z = 0)$ $q\vec{k}_1$ and $\vec{k}_q$ have the same direction and verse, but the amplitudes differ because of the term of phase due to focalization.
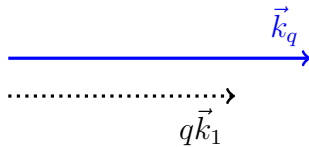
On z axis, after the beam waist $(r = 0, z > 0)$, effective wave vector $\vec{K}$ might compensate the offset produced by the focalization. In this case we have a perfect phase matching, called *collinear phase matching*, the XUV emission occurs along

the axes and it's characterized by spatial coherence.
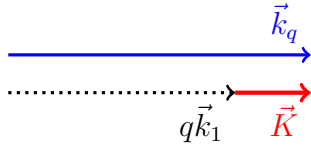
Before the waist $(z < 0)$, $\vec{K}$ increases the phase displacement on the z axis and gives a *non collinear phase matching* off axis $(r > 0)$ because the vectorial sum of $q\vec{k}_1$ and $\vec{K}$ is non parallel to the z axis. The q harmonic forms a ring around the axis and diverges even though the gaussian beam converges for $(z < 0)$.
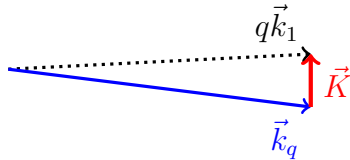
In order to optimize the overall emission it's important to minimize the phase displacement averaged on all interaction volume. Far from the waist the laser intensity decreases and so decreases also the harmonic emission of each atom or molecule. We can tune the distance between the gas jet and the laser focus to favour the phase matching, although the more far is the gas jet from the focus the lower is the laser intensity in the medium.

In figure 1.6 we can see the contributions of the Gouy and the dipole phase terms for the 45th harmonic in Neon on $r = 0$, by assuming a Gaussian beam propagating along z axis with a confocal parameter $b = 5$ mm, a peak intensity $I_0 = 6 \times 10^{14}$ W/cm^2, a duration of 150 fs, $\lambda = 800$ nm and a focus in $z = 0$, versus the position of the gas jet. We can observe that for $z \approx 3$ mm $(z > 0)$ the phase of polarization changes slowly with respect to the z direction, thus there is a good phase matching on axis. On the other hand for $z < 0$ the polarization phase varies faster along z axis and this implies that we have a good phase matching off axis. Figure 1.7 shows the typical generation efficiency trend of a plateau harmonic. For $\Delta z > 0$ one observes collinear phase matching, corresponding to on-axis harmonic emission, for $\Delta z < 0$ non collinear phase matching is present, corresponding to
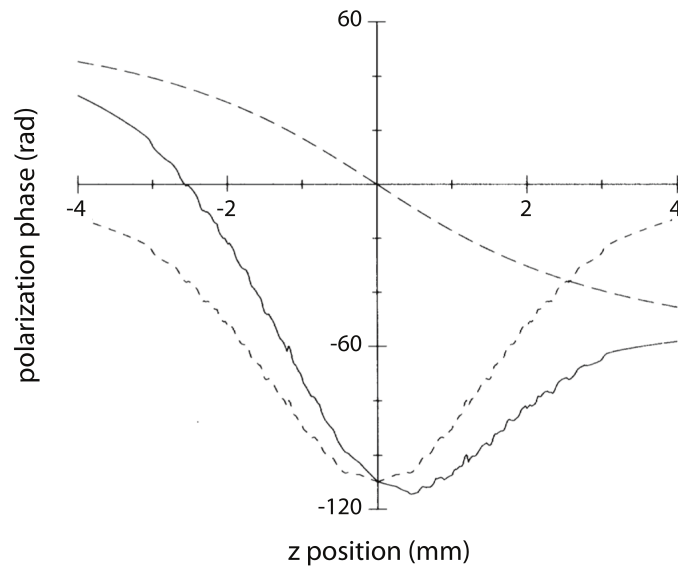
Figure 1.6: *Phase of the polarization on the propagation axis (solid line), term due to the propagation of the fundamental (long-dashed line) and dipole phase for a peak intensity $I_0 = 6x10^{14}$ W/cm^2 (small-dashed line). The laser propagates from the left to the right [1].*
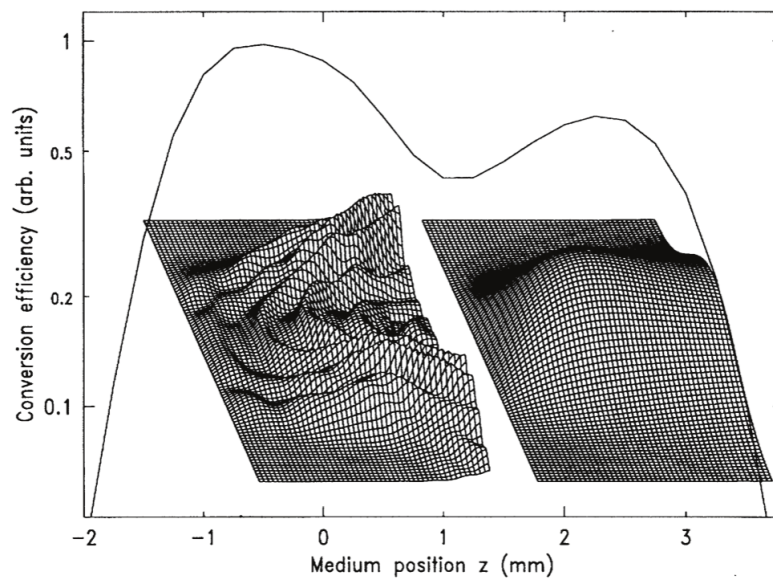
Figure 1.7: *Conversion efficiency of an harmonic of the plateau versus the distance between the gas jet and the beam waist. The radial distribution is also reported in two conditions: one corresponds to collinear phase matching, and the other to non collinear phase matching [1].*

the emission of an annular harmonic beam. We can understand it observing the radial distribution of radiation. We note that the harmonic generation intensity is higher when the focalization occurs after the laser jet. In non collinear phase matching the phase mismatch increases more slowly from the point in which there is the perfect phase matching. The presence of atomic phase dipole make the curve asymmetric respect to $z = 0$.

For each plateau harmonic there are two contributions that come from long and short trajectories. These lead to different dependence of the dipole phase on the intensity and so different vector $\vec{K}$ for long and short trajectories. Thus the phase matching condition changes according to the considered trajectories. A particular phase matching condition can be optimal for one trajectory type and not for the other. The long trajectories contribution, for example, is low in $\Delta z > 0$ and increases when the gas jet is on focus.

Chapter 2

Rotational dynamics in impulsively aligned molecules

HHG allows to investigate the structure and the dynamics of the molecules in gaseous phase with very high time resolution. Impulsive molecular alignment induced with an ultrafast and moderately intense laser pulse has led to high harmonic generation in aligned molecules that allows to obtain detailed information with respect to randomly oriented molecules.

This chapter is devoted to HHG in impulsively aligned molecules and is divided into two parts. The first one introduces the alignment theory in terms of rotational states of molecules and of the temporal evolution of their angular distribution in presence of an alignment laser pulse. The second part describes the implications of alignment on the molecular HHG and presents two imaging methods that exploit the harmonic emission in impulsively aligned molecules. The latter focuses on the features of the harmonic spectra with respect to the time delay between aligning and generating pulses (fractional rotational revivals) by explaining their connection with molecular orbitals and mentioning their possible applications.

2.1   Theory of impulsive molecular alignment

The fist evidence that a pulsed laser field can align a thermal ensemble of molecules, prior to their dissociative ionization, is provided by the experiments

conducted by Normand at al. [14]. There are two basic alignment techniques:

- *adiabatic alignment*, if the laser pulse duration (in the range of picosecond) is much longer than the rotational period of molecules (that is a characteristic time of the system);

- *impulsive alignment (or nonadiabatic alignment)*, if the laser pulse duration is much shorter than the rotational period of molecules.

In the measurements performed we used a nonadiabatic alignment induced by a pulse at $\lambda = 800 \, \text{nm}$ and a duration of about 60 fs.

A nonresonant laser field interacting with a molecule of non spherical symmetry creates an induced dipole moment that determines the rise of an anisotropy of molecular polarizability. The anisotropy creates a coherence within the $|J, M\rangle$ states generating rotational wave-packets that are a coherent superposition of field-free rotational states. Thus an intense laser pulse can create alignment of a thermal ensemble of molecules [15], prior to their dissociative ionization [16]. In the case of impulsive alignment a molecule evolves nonadiabatically from the initial field-free eigenstate to the rotational wave-packets and at the end of the pulse the rotational wavepacket arisen dephases and rephases periodically producing recurrent molecular alignment along the polarization axis of the laser electric field, under field-free conditions. It's important that the laser radiation is nonresonant with respect to the vibrational and electronic structure because such excitation can produce dissociation and ionization before alignment. The alignment in intense laser field can be easily understood classically, but the enhanced alignment after the pulse turn-off is a quantum phenomenon.

2.1.1 Schrödinger equation and rotational states in linear molecules

A molecule is an aggregate of N atoms held together by chemical bonds and is characterized by 3N degrees of freedom in the three-dimensional space whose

$3N - 6$ ($3N - 5$ for linear molecules where one rotational axis coincides with the molecular axis) are the vibrational normal modes (internal degrees of freedom), 3 are the translational degrees of freedom of the center of mass (external degrees of freedom) of the molecule and the remaining ones (2 for linear molecules and 3 for the others) are the rotational degrees of freedom of the molecule approximated as a rigid rotor. A more detailed description of the molecule as a rigid rotor is provided in appendix B. A linear molecule is characterized by only one rotation axis, that is orthogonal to the molecular axis, and has two rotational degrees of freedom θ and ϕ (the rotation around the molecular axis is not considered). The molecular hamiltonian can be partitioned in a sum of independent contributions (see appendix B): the motion of the center of mass, the rotations of the molecule thought as a rigid rotor and the vibrational normal modes (it is an approximation since the rotations interacts with vibrations). We suppose that the molecule is on its vibrational ground state since under a temperature of 300K the probability of finding a molecule on a vibrational excited state is about 10^{-5}. The calculation of rotational eigenstates in linear molecules consists in solving the Schrödinger equation related to the rotational part of the molecular hamiltonian under the approximation of rigid rotor:

$$H_{rot} \left| J, M \right\rangle = \mathcal{E}_{rot} \left| J, M \right\rangle \tag{2.1}$$

In the equation (2.1):

- H_{rot} is the rotational hamiltonian under field-free conditions expressed in spherical coordinates:

$$H_{rot} = \frac{\hat{J}^2}{2I} = -\frac{\hbar^2}{2I} \left[\frac{1}{\sin\theta} \frac{\partial}{\partial\theta} \left(\sin\theta \frac{\partial}{\partial\theta} \right) + \frac{1}{\sin^2\theta} \frac{\partial^2}{\partial\phi^2} \right] \tag{2.2}$$

  where $\hat{J}$ is the rotational angular momentum operator and I the moment of inertia;

- $|J, M\rangle$ are the rotational eigenstates that, for a linear rigid molecule, consist in the spherical harmonics:

$$|J, M\rangle = Y_{JM}(\theta, \phi) = (-1)^M \left[\frac{2J+1}{4\pi} \frac{(J-M)!}{(J+M)!} \right]^{1/2} P_J^M(\cos\theta) e^{iM\phi} \quad (2.3)$$

where $P_J^M(\cos\theta) = (-1)^{J+M} \frac{(J+M)!}{(J-M)!} \frac{(1-\cos^2\theta)^{-\frac{M}{2}}}{2^J J!} \frac{d^{J-M}}{d(\cos\theta)^{J-M}} (1-\cos^2\theta)^J$ is the Legendre polynomial with $|M| \leq J$.

- $\mathcal{E}_{rot}$ are the corresponding eigenvalues:

$$\mathcal{E}_{rot} = \frac{\hbar^2}{2I} J(J+1) \quad (2.4)$$

A linear molecule has only one moment of inertia, thus just one rotational constant is defined:

$$B = \frac{\hbar^2}{2I} \quad (2.5)$$

The rotational energy levels can then be written as

$$\mathcal{E}_{rot} = BJ(J+1) \quad (2.6)$$

The spherical harmonics are eigenfunctions of both rotational angular moment and its projection on a reference axis (e.g. z-axis):

$$\hat{J}^2 Y_{JM}(\theta, \phi) = \left[\hbar^2 J(J+1) \right] Y_{JM}(\theta, \phi) \quad (2.7)$$

$$\hat{J}_z Y_{JM}(\theta, \phi) = \left(\hbar M \right) Y_{JM}(\theta, \phi) \quad (2.8)$$

The eigenstates are characterized by two quantum numbers, J and M: J is a positive integer (J=0,1,2...) and defines the allowed values of the rotational angular momentum, whereas M is an integer such that $|M| \leq J$ ($M = 0, \pm 1, \pm 2, \cdots \pm J$) and represents the quantum number of the projection of the rotational angular momentum on a reference axis, i.e. M determines the allowed directions of the rotational angular momentum (see figure 2.1). Since the energy levels do not depend on the quantum number M, the rotational states are *degenerate*: the energies of different rotational eigenstates $|JM\rangle$ degenerate to the same energy. The rotational state $|JM\rangle$ is thus $(2J+1)$ times degenerate.
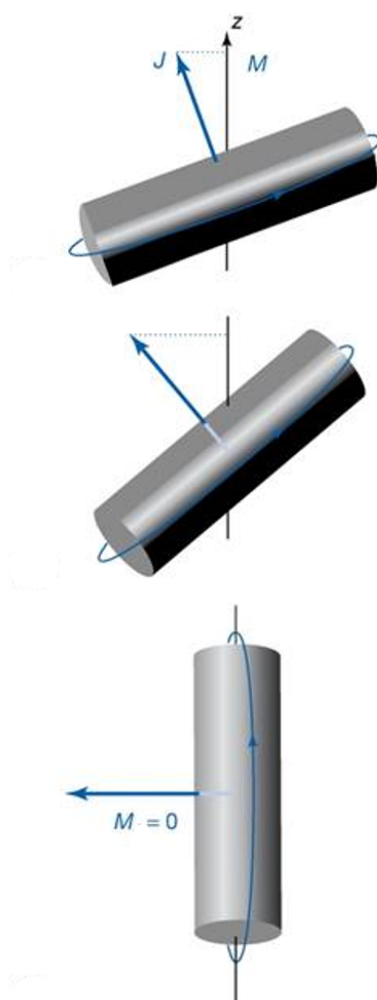
Figure 2.1: *The picture shows the quantum numbers J and M for different directions of rotation axis with respect to an arbitrary one for a linear rigid rotor.*

2.1.2 Rotational distribution in molecular gases: from pure to mixed rotational states

An isolated molecular gas under field-free conditions is a thermal ensemble characterized by a rotational temperature T. Owing to the small energy separation between two successive rotational levels,

$$\Delta E_{rot} = E_J - E_{J-1} = 2BJ \tag{2.9}$$

an ensemble of molecules is usually in a thermal distribution of $|J, M\rangle$ states and molecules are randomly oriented. The occupation probability of the state $|J, M\rangle$ is described by the Boltzmann distribution:

$$p(J, M) = \frac{1}{Z} \exp\left[-\frac{\hbar^2}{2I}\frac{J(J+1)}{K_b T}\right] \tag{2.10}$$

where K_b is the Boltzmann constant, T the rotational temperature and Z the *partition function* of the system:

$$Z = \sum_{J,M} \exp\left[-\frac{\hbar^2}{2I}\frac{J(J+1)}{K_b T}\right] = \sum_{J}(2J+1) \exp\left[-\frac{\hbar^2}{2I}\frac{J(J+1)}{K_b T}\right] \tag{2.11}$$

The rotational state of a single molecule is described by the function $|\Psi(t)\rangle = |J, M\rangle\, e^{-i\frac{\varepsilon_J}{\hbar}t}$, where $||J, M\rangle|^2 = |Y_{JM}(\theta, \phi)|^2$ represents the quantum probability density that the molecular axis of a molecule in the state identified by the quantum number J and M lies on a cone surface determined by an aperture equal to 2θ (see figure 2.2). This eigenfunction is an element of Hilbert space and evolves according to the time-dependent Schrödinger equation:

$$i\hbar\frac{\partial}{\partial t}|J, M\rangle\, e^{-i\frac{\varepsilon_J}{\hbar}t} = H_{rot}|J, M\rangle\, e^{-i\frac{\varepsilon_J}{\hbar}t} \tag{2.12}$$

In an hypothetic ensemble of quantum systems (in this case molecules) all prepared in the same way and all described by the same wave function $|\Psi(t)\rangle$, the state $|\Psi(t)\rangle$ is called *pure state*. A pure state is characterized by a perfect coherence, intended in its quantum meaning, and its evolution can be described by the time-dependent Schrödinger equation. However a molecular gas is a thermal ensemble
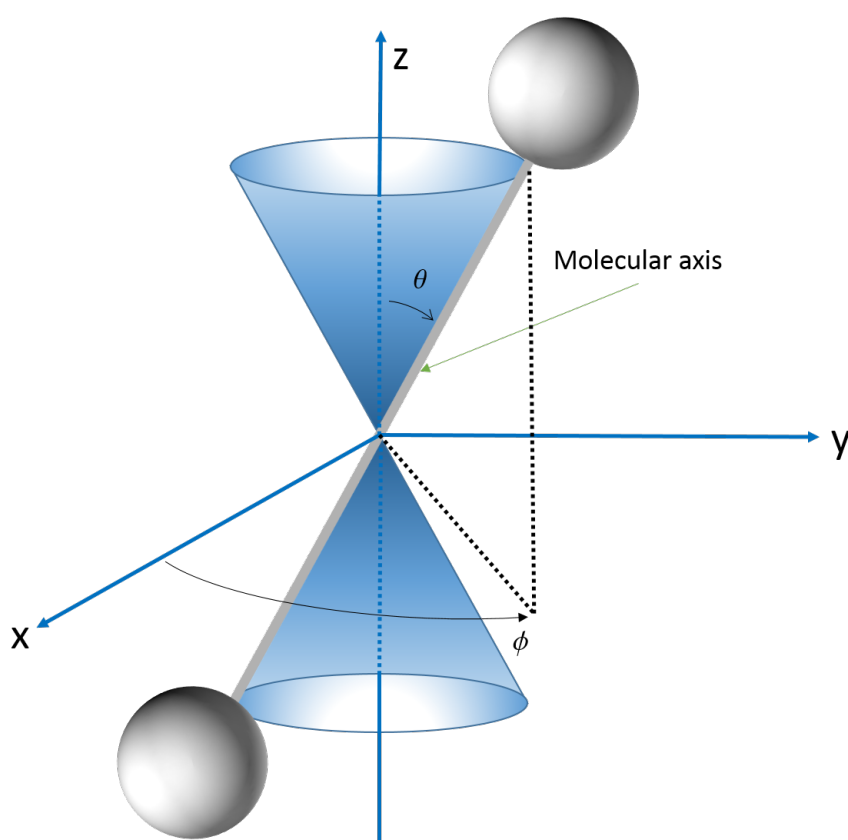
Figure 2.2: *Representation of the geometry for a molecule characterized by a state $|J, M\rangle$ with respect to a reference axis.*

of molecules characterized by the presence of a Boltzmann distribution of the states $|J, M\rangle$, thus we have an ensemble described by different wave functions each with a probability p(J,M), given by the equation (2.10). Such system is said to be in a *mixed state*. In order to describe a mixed state we have to use the density matrix formalism, where the density matrix operator ρ is defined as follows:

$$\rho = \sum_{J,M} p(J, M) |J, M\rangle \langle J, M| \tag{2.13}$$

where the sum is extended to all wave functions $|J, M\rangle$ that describe the entire system. The operator ρ introduced in (2.13) is an element of the Liouville space and evolves according to the Liouville equation:

$$i\hbar \frac{\partial \rho}{\partial t} = [H_{rot}, \rho] \tag{2.14}$$

The expectation value of such operator A for a mixed state is calculated by exploiting the density matrix formalism:

$$\langle A \rangle = \sum_{J,M} p(J, M) \langle J, M \,|\, A \,|\, J, M \rangle = Tr(\rho A) \tag{2.15}$$

where $Tr(\rho A)$ is the trace of the matrix (ρA) .

2.1.3 Theory of optical impulsive alignment in gases of linear molecules

The dynamics of a molecule interacting with an external electric field is described by a different Hamiltonian whose solutions have to be calculated by an appropriate theory [17].

We consider a single molecule subject to an intense pulsed-laser electric field linearly polarized

$$\vec{E}(t) = g(t)\vec{E}_0 \cos{(\omega t)} \tag{2.16}$$

with a gaussian temporal profile $g(t) = \exp{(-t/2\tau^2)}$ and a frequency oscillation ω. In order to obtain molecular impulsive alignment the pulse duration τ must

be much lower than the rotational period of the molecules τ_{rot} ($100\,\text{fs} \div 10\,\text{ps}$), $\tau \ll \tau_{rot}$, that can be expressed as

$$\tau_{rot} = \frac{h}{2B} \tag{2.17}$$

The total Hamiltonian of the molecule can be written under the dipole approximation as [17]

$$H = H_0 - \vec{\mu} \cdot \vec{E}(t) \tag{2.18}$$

where H_0 is the total molecular Hamiltonian in field-free conditions whose eigenfunctions are the rovibronic (rotationa-vibrational-electronic) wave functions, E(t) is the laser electric field and $\vec{\mu}$ the dipole moment operator. Owing to the potential energy due to the interaction between electric field and molecular dipole moment, the total hamiltonian cannot be partitioned, i.e. we cannot divide the rotations contribution from the vibrational and electronic ones. However we can approximate the total Hamiltonian to an effective one that acts just on rotational state within the lowest vibronic ground state [18]. The approximation is valid if the condition $|\omega - \omega_{nb}|\frac{\tau}{2\pi} \ll 1$ is fulfilled, where ω_{nb} is the resonance frequency of the transition between the vibrational and rotational levels of the molecule, i.e. if the laser electric field is nonresonant with the vibronic transition [17]. The dipole moment can be written as

$$\vec{\mu} = \vec{\mu_0} - \frac{1}{2}\underline{\underline{\alpha}} \cdot \vec{E}(t) \tag{2.19}$$

where $\vec{\mu_0}$ is the permanent dipole moment of the molecule and $\underline{\alpha}$ is the polarizability tensor:

$$\underline{\underline{\alpha}} = \begin{pmatrix} \alpha_{xx} & \alpha_{xy} & \alpha_{xz} \\ \alpha_{yx} & \alpha_{yy} & \alpha_{yz} \\ \alpha_{zx} & \alpha_{zy} & \alpha_{zz} \end{pmatrix}$$

For a linear molecule having the molecular axis along the z-axis the polarizability tensor is a diagonal matrix with $\alpha_{xx} = \alpha_{yy} = \alpha_\perp$ and $\alpha_{zz} = \alpha_\parallel$:

$$\underline{\underline{\alpha}} = \begin{pmatrix} \alpha_\perp & 0 & 0 \\ 0 & \alpha_\perp & 0 \\ 0 & 0 & \alpha_\parallel \end{pmatrix} \tag{2.20}$$

where $\alpha_\parallel$ and $\alpha_\perp$ are respectively the parallel and perpendicular components of the static polarizability with respect to the molecular axis. We will assume in the following that the molecule is non-polar, thus it has not a permanent dipole moment $(\vec{\mu_0} = 0)$, but only exhibits the dipole moment induced by the electric field. With these considerations and approximations and by considering electronic angular momentum equal to zero, we can write the effective Hamiltonian for a linear molecule subject to the electric field (2.16) as follows [17]:

$$H_{eff}(t) = B\hat{J}^2 - D\hat{J}^4 - \frac{1}{2}E^2(t)\left[(\alpha_\parallel \cos^2\theta + \alpha_\perp \sin^2\theta\right] \qquad (2.21)$$

where $\hat{J}$ is the dimensionless angular momentum operator defined as $\hat{J} = -i\nabla$, θ is the polar angle between the molecular axis and the polarization direction of the electric field and $D\hat{J}^4$ is the centrifugal correction. In order to calculate the temporal evolution of the rotational wave function, we have to solve the time-dependent Schrödinger equation corresponding to the Hamiltonian (2.21):

$$i\hbar\frac{\partial}{\partial t}\Psi(t) = H(t)\Psi(t) \qquad (2.22)$$

Let's define the dimensionless interaction parameters:

$$\begin{aligned}\beta_\parallel(t) &= \frac{\alpha_\parallel E^2(t)}{2B}\\ \beta_\perp(t) &= \frac{\alpha_\perp E^2(t)}{2B}\\ \Delta\beta(t) &= \beta_\parallel(t) - \beta_\perp(t)\end{aligned} \qquad (2.23)$$

where $\Delta\beta(t)$ determines the degree of anisotropy of the molecule, i.e. how susceptible is the molecule to the alignment by an external electric field. The solutions of the equation (2.22) depend on $\Delta\beta(t)$, $\Psi = \Psi(\Delta\beta(t))$, and can be expanded in a series of field-free rotor wave functions $|J, M\rangle \equiv Y_{JM}$ [17]:

$$\Psi(t) = \sum_J d_J(t)\,|J, M\rangle \qquad (2.24)$$

The problem to calculate the solutions of the time-dependent Schrödinger equation is reduced to find the expansion coefficients of the $\Psi(t)$. We have to substitute the

expression (2.24) into the equation (2.22). The all explicit calculations are given in appendix C. The result is a system of coupled differential equations in $d_J(t)$:

$$i\hbar\frac{\partial}{\partial t}d_J(t) = \left(BJ(J+1) - DJ^2(J+1)^2 - \frac{1}{2}E^2(t)\alpha_\perp\right)d_J(t) +$$
$$- \frac{1}{2}E^2(t)(\alpha_\parallel - \alpha_\perp)\sum_{J'}d_{J'}(t)\left\langle J,M\,\middle|\cos^2\theta\,\middle|\,J',M\right\rangle \tag{2.25}$$

where we adopted the substitution $\hat{J}^2\,|J,M\rangle = J(J+1)\,|J,M\rangle$. In order to simplify the formalism it is convenient to define the coefficients:

$$a_0(J,M) = \frac{2(J^2 - M^2 + J) - 1}{(2J-1)(2J+3)} = \frac{1}{3} + \frac{2}{3}\left(\frac{J(J+1) - 3M^2}{(2J+3)(2J-1)}\right) \tag{2.26}$$

$$a_{+2}(J,M) = \sqrt{\frac{(J-M+1)(J+M+1)(J-M+2)(J+M+2)}{(2J+1)(2J+3)^2(2J+5)}} \tag{2.27}$$

$$a_{-2}(J,M) = \sqrt{\frac{(J-M)(J+M)(J-M-1)(J+M-1)}{(2J+1)(2J-1)^2(2J-3)}} \tag{2.28}$$

By the calculations performed in appendix C we can affirm that the only nonzero matrix elements $(\cos^2\theta)_{JJ'}$ in (2.25) are:

$$\left\langle J,M\,\middle|\cos^2\theta\,\middle|\,J,M\right\rangle = \frac{1}{3} + \frac{2}{3}\left(\frac{J(J+1) - 3M^2}{(2J+3)(2J-1)}\right) \tag{2.29a}$$

$$\left\langle J,M\,\middle|\cos^2\theta\,\middle|\,J+2,M\right\rangle = \sqrt{\frac{(J-M+2)(J+M+2)(J-M+1)(J+M+1)}{(2J+5)(2J+3)^2(2J+1)}}$$
$$\tag{2.29b}$$

$$\left\langle J,M\,\middle|\cos^2\theta\,\middle|\,J-2,M\right\rangle = \sqrt{\frac{(J-M-1)(J+M-1)(J-M)(J+M)}{(2J-3)(2J-1)^2(2J+1)}}$$
$$\tag{2.29c}$$

We can notice that the matrix elements (2.29a), (2.29b) and (2.29c) are equal respectively to $a_0(J,M)$, $a_{-2}(J+2,M)$ and $a_{+2}(J-2,M)$. By these considerations and by using the interaction parameters (2.23) we can reduce the system of

equations (2.25) to

$$\frac{\partial}{\partial t}d_J(t) = \frac{B}{i\hbar}\left(J(J+1) - \frac{D}{B}J^2(J+1)^2 - \beta_\perp(t) - \Delta\beta(t)a_0(J,M)\right)d_J(t)+$$

$$- \frac{B}{i\hbar}\Delta\beta(t)a_{+2}(J-2,M)d_{J-2}(t)+$$

$$- \frac{B}{i\hbar}\Delta\beta(t)a_{-2}(J+2,M)d_{J+2}(t)$$

(2.30)

The solutions of the system (2.30) can be expressed in terms of the evolution matrix $U(t,t_0)$ [17]:

$$\vec{d}(\Delta\beta(t)) = U(t,t_0)\vec{d}(\Delta\beta(t_0))$$ (2.31)

where $\vec{d}$ is the vector whose components are the d_J. At this point by the calculation of the coefficient d_J we know the solutions (2.24) to the time-dependent Schrödinger equation (2.22). It is worth noting that a linearly polarized electric field, owing to the cylindrical symmetry of the problem, couples only the states of the same parity (i.e. with J's odd or even) and with the same M (i.e. $\Delta M = 0$). The term that determines the rotational states coupling depends just on the angle θ, thus the solutions $\Psi(t)$ don't depend on the azhimutal angle ϕ. The geometry of a linear molecule in presence of aligning linearly-polarized electric field is show in figure 2.3. By using the *rotating-wave approximation* we can eliminate the rapid oscillations of the electric field obtaining a time dependence due only to the pulse shape functions g(t) (i.e. $E(t) = \frac{1}{2}g(t)E_0$).

The alignment is realized by the electric field that excites some new rotational states ($\Delta J = 0, \pm 2$ and $\Delta M = 0$) establishing a phase relationship among them. A rotational wave-packet is characterized by a coherence among the rotational states that compose it, if their phases are related to each other. The probability density to find the molecular axis lying on the surface of a solid angle Ω with an aperture 2θ now depends on time and is $|\Psi(\theta,t)|^2$, whereas $|\Psi(\theta,t)|^2 d\Omega$ indicates the probability that the molecular axis lies within a solid angle $d\Omega = \sin\theta d\theta d\phi$, at the time t. Hence the probability to find, at time t, the molecular axis with re-
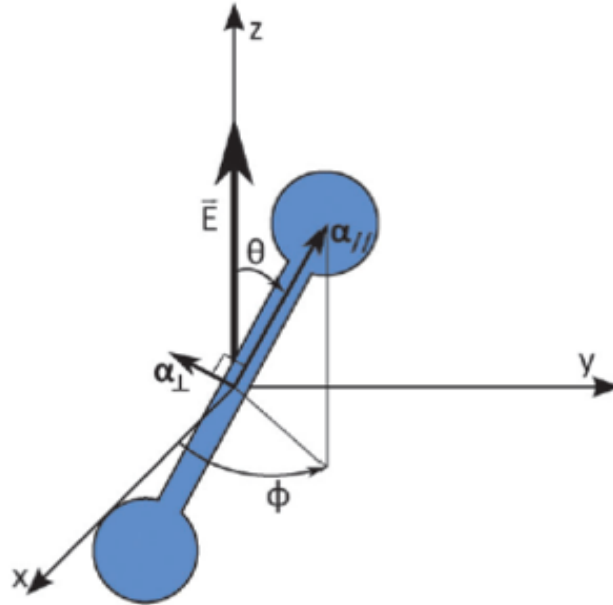
Figure 2.3: *Representation of a linear molecule aligned at an angle θ with respect to the z-axis by a linearly polarized electric field. $\alpha_\parallel$ and $\alpha_\perp$ are the parallel and perpendicular components of the nonlinear polarizability.*

spect to the polarization direction of the aligning pulse within an angle $d\theta$ centered around θ is

$$\int_0^{2\pi} d\phi |\Psi(\theta,t)|^2 \sin\theta d\theta = 2\pi |\Psi(\theta,t)|^2 \sin\theta d\theta \qquad (2.32)$$

where $2\pi \sin\theta |\Psi(\theta,t)|^2$ is the probability density to find the molecular axis, at time t, at an angle θ.

2.1.4   Alignment parameter and rotational revivals

The obtained $\Psi(t)$ is a rotational wave-packet constituted by a coherent superposition of the rotational states, whose phases depend on the aligning laser pulse and thus are related to each other. Since the rotational wave-packet contains a finite number of rotational states, the coherence among them is restored at specific time instants called *revivals*. The revivals occur whenever a precise phase relationship is established between the rotational states excited by the electric field. In particular the revivals occurring at fractions of rotational period of the molecule

are the *fractional revivals* (half revival $t = T_{rot}/2$, quarter revival $t = T_{rot}/4$, and so on.) and the one occurring every rotational period is called *full revival* (T_{rot}). The degree of alignment of a molecule is characterized by the expectation value of the square of cosine, $\langle \cos^2 \theta \rangle$, that is called *alignment parameter*. It can be defined as follows for a system described by the wave function $\Psi(\theta, t)$:

$$\langle \cos^2 \theta \rangle_{J,M} = 2\pi \int_0^\pi \cos^2 \theta |\Psi(\theta, t)|^2 \sin\theta d\theta \qquad (2.33)$$

For a single molecule that has been subject to the electric field the alignment parameter can be calculated as:

$$\begin{aligned}
\langle \cos^2 \theta \rangle_{J,M} &= \langle \Psi(t) | \cos^2 \theta | \Psi(t) \rangle = \\
&= \sum_J d_J^*(t) \langle J, M | \cos^2 \theta \sum_{J'} d_{J'}(t) | J', M \rangle = \\
&= \sum_{J,J'} d_J^*(t) d_{J'}(t) \langle J, M | \cos^2 \theta | J', M \rangle = \\
&= \sum_{J,J'} d_J^*(t) d_{J'}(t) \langle J, M | a_0(J') | J', M \rangle + \\
&\quad + \sum_{J,J'} d_J^*(t) d_{J'}(t) \langle J, M | a_{+2}(J') | J' + 2, M \rangle + \\
&\quad + \sum_{J,J'} d_J^*(t) d_{J'}(t) \langle J, M | a_{-2}(J') | J' - 2, M \rangle = \\
&= \sum_J |d_J(t)|^2 a_0(J) + \\
&\quad + \sum_J d_J^*(t) d_{J-2}(t) a_{+2}(J - 2) + \\
&\quad + \sum_J d_J^*(t) d_{J+2}(t) a_{-2}(J + 2)
\end{aligned} \qquad (2.34)$$

where the $d_J(t)$ is the solution of equation (2.25).

A thermal ensemble of molecules is characterized by a mixed state that is described by the matrix density. In absence of an aligning electric field the molecules are distributed isotropically and the rotational states have a casual phase relationship. If we calculate the alignment parameter for this quantum system we obtain $\langle \cos^2 \theta \rangle = 1/3$ (the calculations are performed in appendix D). The value found

corresponds to the worst alignment that can be obtained. A better alignment leads to an expectation value higher than 1/3. The density matrix of this system has all the matrix elements equal to zero except for those in the principal diagonal. If we now consider an ensemble of aligned molecules, the quantum system is a mixed state characterized by different coherent rotational wave-packets of the form of (2.24). Owing to the specific phase relationship between the rotational states, established by the electric field, the density matrix of the system presents nonzero out-of-diagonal matrix elements. The expectation value of $\cos^2\theta$ has to be calculated with the density matrix formalism:

$$
\begin{aligned}
\langle\cos^2\theta\rangle &= Tr(\rho\cos^2\theta) \\
&= Z^{-1}\sum_{J,M} e^{-\frac{BJ(J+1)}{k_B T}}\langle\cos^2\theta\rangle_{J,M} = \\
&= Z^{-1}\sum_{J} e^{-\frac{BJ(J+1)}{k_B T}}\sum_{M=-J}^{J}\langle\cos^2\theta\rangle_{J,M}
\end{aligned}
\tag{2.35}
$$

where $Z = \sum_J (2J+1)e^{-\frac{BJ(J+1)}{k_B T}}$ is the partition function, k_B the is Boltzmann constant, T is the rotational temperature, ρ is the density matrix, and $\langle\cos^2\theta\rangle_{J,M}$ is the cosine-square expectation value for a pure state represented by a rotational wave-packet excited starting from a rotational state J,M.

Let's consider e mixed state of molecules that are randomly aligned with an alignment parameter $\langle\cos^2\theta\rangle = 1/3$. When at t=0 the laser pulse interacts with the ensemble, the molecules experience a prompt alignment along the direction of pulse polarization and soon after they return to be randomly aligned. During the *fractional revival*, the *full revival* and their multiples the alignment is restored. The alignment recurrences are followed by *anti-alignment*. We call *alignment* the condition where the molecular axes are along the polarization direction of the pulse, whereas we call *anti-alignment* the condition where the molecular axes lie on a plane orthogonal to the pulse polarization direction. The alignment parameter ranges from 1/3 (isotropic or random alignment) to 1 (perfect aligned state) An example of the alignment parameter is showed in figure 2.4, where we can
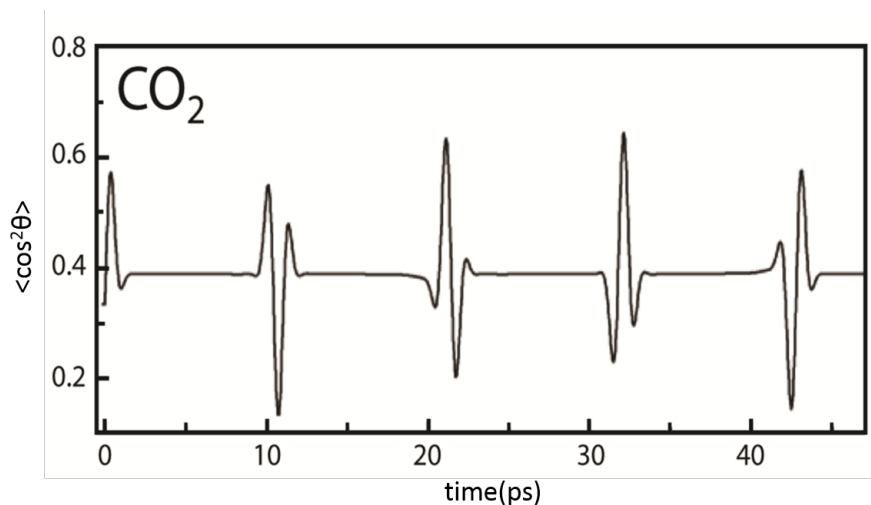
Figure 2.4: *Example of alignment parameter calculated for the CO_2 molecules. The duration of the aligning pulse is 25 fs and the peak intensity is 10^{14} W/cm^2.*

easily note the revivals that appear as peaks in the graph. An ensemble of aligned molecules exhibits an angular distribution, that represent the probability to find a molecule with the axis at an angle θ with respect the pulse polarization direction at time t, peaked about the direction of the aligning electric field. The presence of an angular distribution demonstrates that we can never completely align an ensemble along the polarization direction of the pulse whatever is its intensity.

The degree of alignment is influenced by some parameters as well as the rotational temperature T, in fact at fixed alignment pulse properties, the value of the alignment parameter decreases as the increasing of temperature. The intensity of the pulse is another parameter on which the degree of alignment depends: the higher is the intensity the higher is the number of the rotational states involved in the wave-packet. Since the rotational wave-packets excited depends on time by the expansion coefficient d_J, the alignment parameter is a function of time too. In figure 2.5 the temporal evolution of $\langle \cos^2 \theta \rangle$ is reported; we can observe that the alignment parameter oscillates around a specific value $(1/3)$ which represents the randomly aligned condition. The evolution is characterized by a sequence of maxima (*alignment* condition), minima (*anti-alignment* condition) and stationary
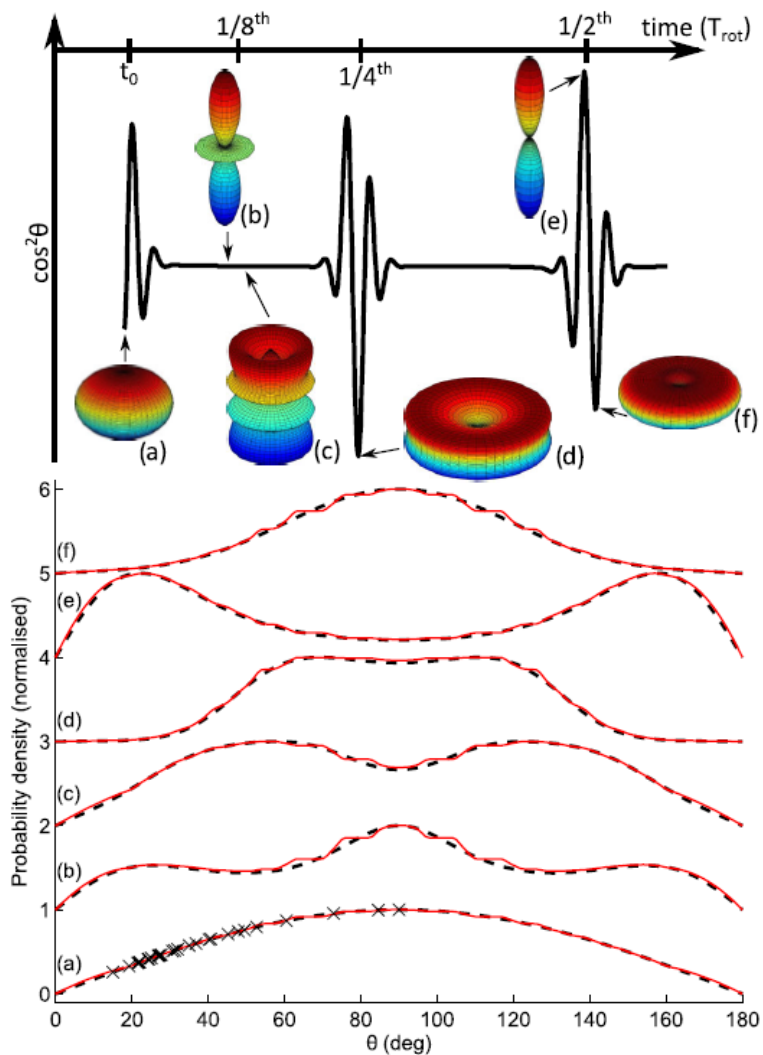
Figure 2.5: *At top the temporal evolution of alignment parameter for a molecular rotational wave-packet in units of T_{rot} with the illustrations of the corresponding probability density of alignment, at bottom is represented the angular shape of the rotational probability density. Figure reprinted from [2].*

regions (the rotational states are not in phase with one another). The appearance of sequences of alignment and anti-alignment occurs in correspondence of the revivals (fractions of rotational period). By observing the angular distribution at the revivals we note that there isn't, at any delay, a perfect alignment (or anti-alignment) along the polarization direction of the aligning electric field.

2.2   Alignment effect on HHG in molecules

HHG in molecules was studied both in isotropic distribution and in aligned conditions. The observations showed that the HHG is sensitive to the angle between the alignment direction and the driving pulse polarization, as well as to the spatial structure of the electronic wave-function [6]. As we have previously seen the HHG is a method used to generate attosecond pulses and to probe the matter with a high time resolution. In the latter case the recolliding electron wave-packet is used to probe the medium; in fact the HHG spectrum depends on the electron-core recollision probability that is strongly connected to the shape of the electron bound-state (i.e. orbital). We expected that in a medium of aligned molecules the recollision probability, and thus the HHG spectra, is influenced by the direction of the molecular axis with respect to the direction of the driving laser polarization. In particular the non-adiabatic alignment allows to probe a molecular sample during a rotational revival without an external electric field. For example it's possible to measure the angular distribution of molecular axes with respect to the polarization direction of the driving laser during a rotational revival. By controlling the alignment we can minimize or maximize the harmonic yield with respect to the angle θ, that can exhibit a suppression or an enhancement with respect to the non-aligned case. The dependence of HHG spectra on the alignment of the molecule can be exploited to extract more information, that could be used for HHG molecular spectroscopy and, more indirectly, for the orbital tomography. By investigating the evolution of the HHG signal with respect

to the angle between the aligning (pump) and the generation (probe) pulses, we are able to access to more information about the probed sample.

2.2.1   Harmonic emission from a gas of aligned molecules

The HHG process in molecules can be understood in terms of by the semi-classical three step model under the strong field limit: (i) tunnel ionization of the most weakly bound electron in proximity of the peak of the laser cycle (figure 2.6) from the outermost molecular orbital (HOMO); (ii) propagation in the continuum of the electron wave-packet accelerated by the oscillating electric field; (iii) recombination of the ionized electron that can be approximated as a plane wave ($\psi_c \approx \exp\left(-i\vec{k} \cdot \vec{r}\right)$). Both the ionization and the recombination processes in a molecule strongly depend on the angle θ between the polarization direction of the driven laser pulse and the molecular axis as well as on the structure of the HOMO orbital. In case of HHG from a diatomic molecule, the harmonic emission may be seen as the overlap between emissions from the two atomic sites. These two emissions may interfere. The interference condition is specific for the molecule and depends on the symmetry of the orbital from which the electron is ionized and on the interatomic distance [7]. The dependence on θ results from the projection of the interatomic distance along the propagation direction of the recombining electron with a De Broglie wavelength λ_B [19]. By acquiring many HHG spectra at different time delay between the alignment pulse and the driving laser pulse, we obtain the harmonic yields with respect the degree of alignment in molecules. The molecular alignment influences the macroscopic harmonic emission by a modulation of the harmonic intensity, that thus acquires a dependence on the orientation of the molecules [20]. The modulation observed can be attributed to different conditions of interference between the contribution to the emission from the emission centers of the molecules. This modulation appears either in the harmonic spectrum at a fixed delay between aligning and driving pulses (and thus at a fixed θ) or in a particular harmonic yield as a function of the delay (each time delay
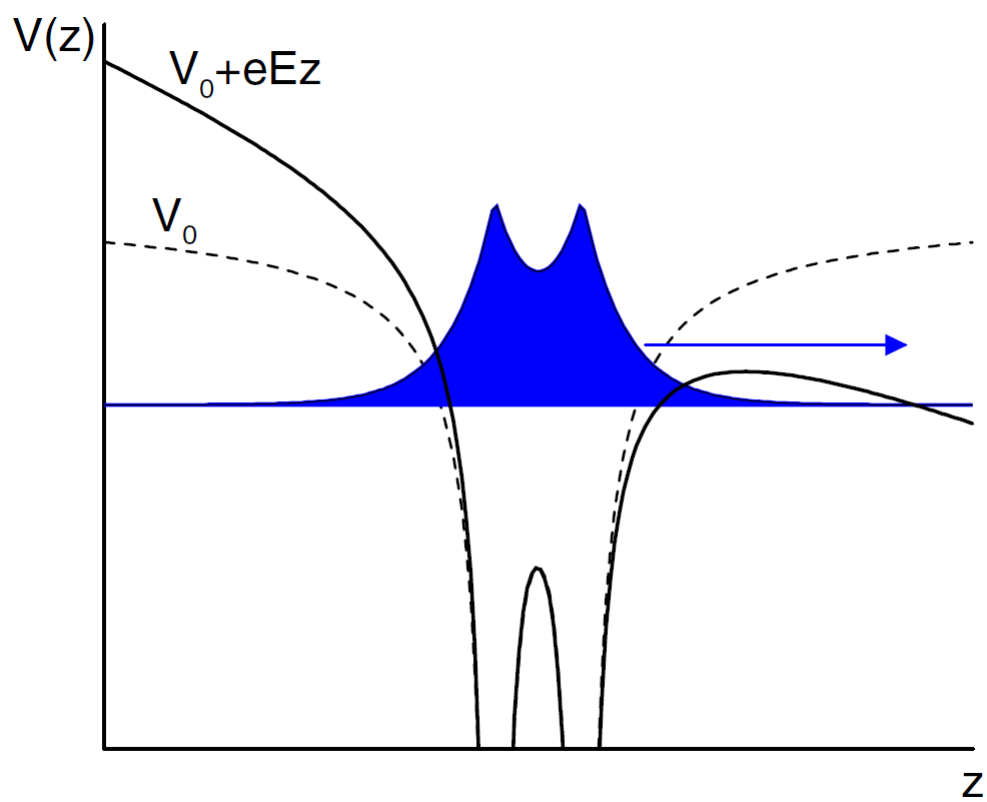
Figure 2.6: *Schematic representation of tunnel ionization from a diatomic molecule subject to a strong electric field with strength E and directed along the negative z-axis. Figure reprinted from [19]*

correspond to a specific angle θ between the polarization directions of aligning and generating beams). In particular the harmonic yield with respect to the time delay between the aligning and the driving pulses is characterized by a shape that can completely change between two different harmonic orders. In figures 2.7 and 2.9(b) we can see an intuitive demonstration of dependence of the harmonic yield on the molecular alignment by a comparison among the harmonic emission with and without the alignment pulse by a representation of the time delay evolution of the ratio of intensity with and without alignment. In the first case the alignment is adiabatic since the pulse duration is longer than the rotational period of molecule, whereas in the latter the alignment is non-adiabatic (impulsive alignment). Different harmonic yields can exhibit different time evolutions. Figure 2.8 shows an intensity modulation of two harmonic yields in impulsively aligned CO_2 molecules, owing to the half-revival, in comparison with the time evolution of $\langle \cos^2 \theta \rangle$. We can note that the time evolution of the harmonic yields follow in one case the alignment parameter evolution, whereas in the other case is inverted with respect to the alignment parameter. Moreover the evolution of the angular distribution of the impulsively aligned molecules is reported; this indicates that it's impossible to have a perfect alignment along the direction of the aligning pulse ($\langle \cos^2 \theta \rangle$=1). An intensity modulation of HHG spectra can be observed also at a fixed time delay in the correspondent HHG spectrum as shown in figure 2.9(a), where we can see a suppression around the 33rd harmonic. The depression is visible also in figure 2.9(b) where is represented the ratio of the intensity with and without the pump pulse. It's worth noting that the ratio increases out of the minimum and exceeds the unity at higher order of harmonics: this suggests that the alignment produces suppression of such harmonic yield and enhancement of others. The effect of alignment in harmonic emission increases if the rotational temperature decreases [21]. The features of harmonic emission is strongly connected to the HHG process that is significantly influenced by the orientation of the
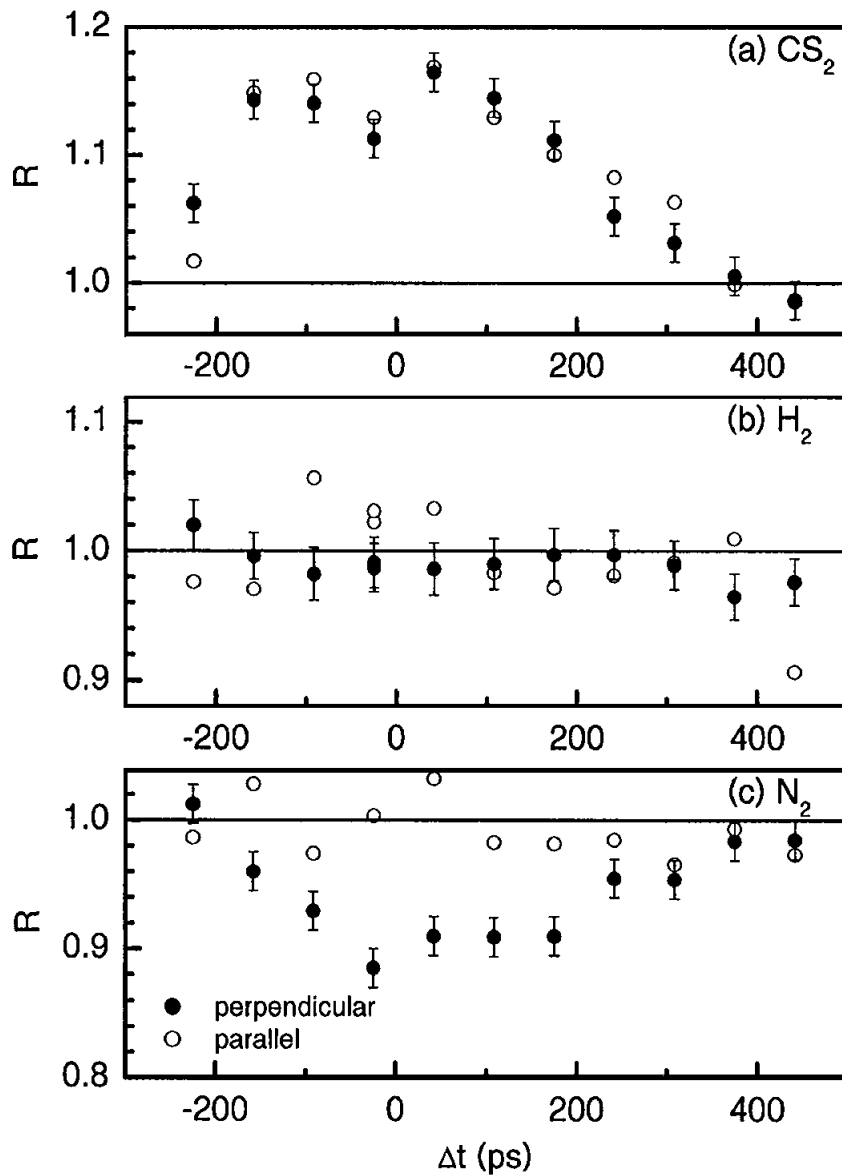
Figure 2.7: *Ratio R of the harmonic intensity of the 9th harmonic with and without the aligning pulse as a function of the delay Δt between the aligning and generation pulse. The molecules are aligned adiabatically by an aligning pulse with a duration of 300 ps and the harmonics generation is obtained by a 70-fs pulse. The full circle represents the perpendicular laser polarizations and the empty circle represents the parallel laser polarizations. The samples are (a) CS_2, (b) H_2 and (c) N_2. Figure reprinted from [21].*
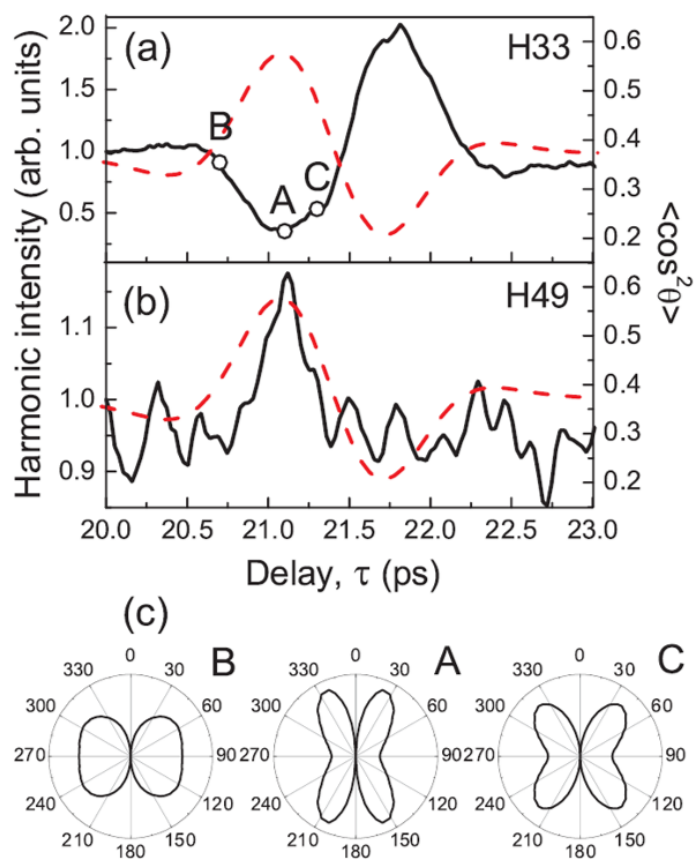
Figure 2.8: *Modulation of the harmonic yield in impulsively aligned CO_2 molecules due to half-revival of rotational wave packet (a) for the 33rd and (b) 49th harmonic order. Aligning and generating pulses have parallel polarization. Pump pulse: energy $200\,\mu J$, duration $60\,fs$. Probe pulse: intensity $2 \times 10^{14}\,W/cm^2$, duration $30\,fs$. Dashed curve in (a) and (b) displays the calculated temporal evolution of the corresponding $\langle \cos^2 \theta \rangle$. (c) Polar plot of the angular distribution for different pump-probe delays: $\tau = 20.7, 21.1, and 21.3$ ps. Figure reprinted from [7].*
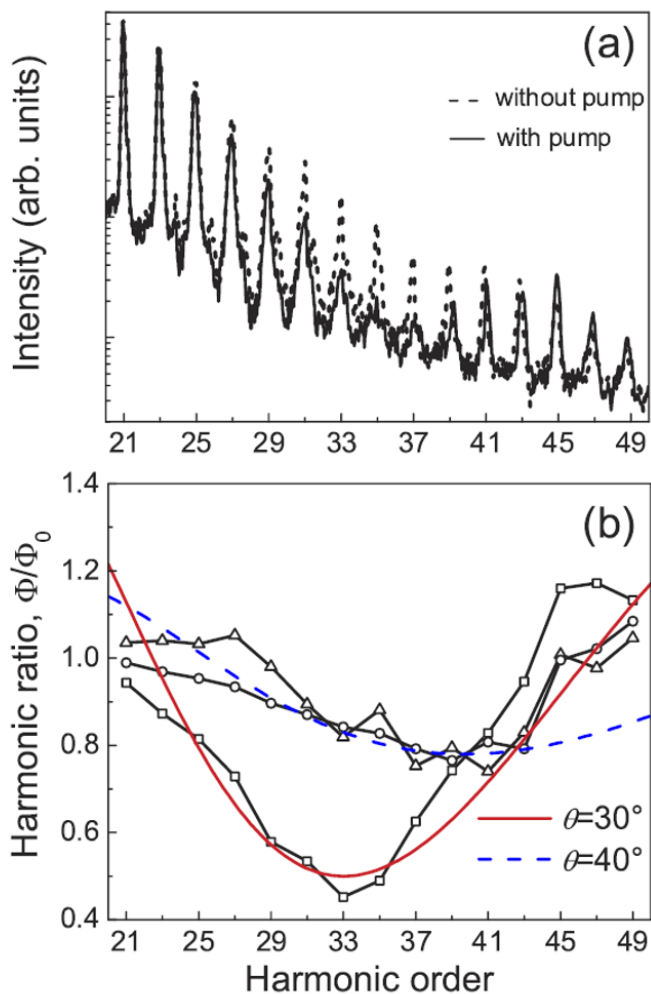
Figure 2.9: *(a) Harmonic spectra generated by 30 fs pulses with (solid curve) and without (dashed curve) aligning beam (pump and probe pulses with parallel polarization), measured for a pump-probe delay of 21.1 ps. (b) Ratio $\phi = \phi_0$ between the harmonic intensities measured with (ϕ) and without (ϕ_0) the pump pulse, measured at three pump-probe delays of 20.7 ps (circles), 21.1 ps (squares), and 21.3 ps (triangles). The lines shows the modulation in harmonic yield. A vertical offset term added for θ=30°(solid red online curve) and θ=40°(dashed blue online curve). Figure reprinted from [7].*

molecules. The phenomena of the revival reversal among different harmonic yields and the suppression of the harmonic emission at certain angles are consequences of the destructive quantum interference (or two-center destructive interference) at the recombination step, where the atoms are approximated as point emitters. The modulation of the harmonic yield can be written as [7]

$$I(q,\theta) = I_0(\theta) \left[1 \pm \cos\left(\frac{2\pi R \cos\theta}{\lambda_B(q)} \right) \right] \qquad (2.36)$$

where the signs $\pm$ represent the symmetric and the antisymmetric orbitals respectively, θ is the angle between the laser polarization direction and the molecular axis, R is the interatomic distance, $\lambda_B(q) = h/\sqrt{2m_e(qh\nu - I_p)}$ is the De-Broglie wavelength of the electron responsible for the emission of the q-th harmonic and q is an integer. If the modal alignment angle increases, the harmonic order that fulfills the interference condition increases too. The interference condition depends also by the symmetry of the HOMO orbitals, that can be represented by the superposition of atomic orbitals (LCAO: appendix A). If the combination is antisymmetric

$$\psi_{mol}(\theta) = \phi_0\left(\vec{r} + \frac{\vec{R}}{2} \right) - \phi_0\left(\vec{r} - \frac{\vec{R}}{2} \right) \qquad (2.37)$$

where $\vec{R}$ is the interatomic distance and θ is the angle between the molecular axis and the driving laser polarization direction. The recombination dipole matrix in velocity form among the continuum state and the bound state $\psi_{mol}(\theta)$ is given by:

$$\left\langle \psi_{mol}(\theta) \left| \hat{\vec{d}} \right| e^{i\vec{k}\cdot\vec{r}} \right\rangle = 2i\vec{k}\sin\left(\frac{kR}{2}\cos\theta \right) \left\langle \phi_0(\vec{r}) \left| e^{i\vec{k}\cdot\vec{r}} \right\rangle \qquad (2.38)$$

where $(\vec{k})$ define the direction of the re-colliding electron and thus the driving electric field polarization direction. The interference is destructive if:

$$R\cos\theta = n\lambda_B(q) \qquad (2.39)$$

where $\lambda_B(q)$ is the De-Broglie wavelength of an electron responsible for the emission of the n-th harmonic and n is an integer. If the combination of atomic orbitals

is symmetric $\psi_{mol}(\theta) = \phi_0\left(\vec{r} + \frac{\vec{R}}{2}\right) - \phi_0\left(\vec{r} - \frac{\vec{R}}{2}\right)$, the quantum interference condition becomes:

$$R\cos\theta = \left(n - \frac{1}{2}\right)\lambda_e(q) \tag{2.40}$$

The destructive interference corresponds to a crossing of the zero by the dipole matrix element; the dipole change the sign and this fact corresponds to a phase jump of π. This phenomenon reflects on the harmonic emission from a gas of aligned molecules by the appearance of minima, whose position is predicted by the formula (2.40) [22, 23]. The spectral features are due to the destructive interference between the different atomic centers in the molecule and appears as minima in the harmonic spectrum. The phase of the harmonic emission also depends on the molecular angular distribution [21]. The intensity of a such harmonic is the result of the contributions from all the possible angles of the molecules [21]. For instance the macroscopic harmonic emission in aligned CO_2 molecules is characterized by the phenomenon of *cutoff recession* far from the rotational revivals; in fact the macroscopic emission can be regarded as the sum among the microscopic emissions from molecules with different orientation. It has been observed that there is a phase jump near to π between the contributions of the CO_2 molecules oriented at small angles ($<40°$) and the CO_2 molecules oriented at large angles ($>40°$) for high photon energy emissions ($>50\,$eV). The molecular distribution far from rotational revivals is random-like, thus the XUV spectrum from CO_2 exhibits a partial suppression of the emission above $50\,$eV.

2.2.2 Exploitation of alignment in HHG molecular spectroscopy and tomography (overview)

The impulsive alignment can be exploited to increase the amount of information that can be extracted from HHG molecular spectroscopy: this alignment allows to probe the molecular sample during a rotational revival under field-free conditions [24]. The modulation of the HHG spectrum, produced by the align-

ment, is characteristic of the molecular geometry and of the orbitals that take part to the harmonic emission [6]. The information about the molecular structure and dynamics are encoded in the modulation of the harmonic spectrum. The study of these features could allow to reconstruct the structure of the outermost molecular orbitals (HOMOs). The amount of information that we can extract from the analysis of the HHG spectra depends on the extension of the cutoff; in this case it could be useful to work with high laser wavelength (e.g. in the mid-IR). Moreover a longer wavelength allow to obtain an higher spatial resolution due to the shorter De-Broglie wavelength one can achieve.

A molecule exposed to a strong laser field can be tunnel ionized from more than one orbital simultaneously, creating an electron-hole wave-packet (for instance in aligned N_2 the tunnel ionization occurs both from the highest occupied molecular orbital, HOMO, and the lower-lying orbital, HOMO-1). The evolution of the wave-packet between ionization and recombination may be encoded as a dependence of the harmonic spectral shape on the laser intensity. Such dependence can be sometimes observed as a destructive interference in the harmonic emission for different generation channels. Alignment can be exploited to characterize the harmonic emission in order to individuate such channels. This allow us to access to the dynamics of the wave-packet with attosecond temporal resolution [25]. The tunnel ionization from several outermost orbitals simultaneously may occur owing to a small energy separation among them. The influence of alignment in this phenomenon is connected to the angle dependence of the total dipole moment $\vec{D}(\theta, q\omega_0)$ of the qth harmonic. Owing to the different geometries of the contributing outermost orbitals, their ionization probability ratio is strongly dependent on the angle θ and is maximum at a certain value of θ. It's possible to exploit this fact to disentangle the orbital contribution to HHG of aligned molecules [25].

The idea of tomography is based on the possibility to reconstruct the function $\vec{r}\psi_0(\vec{r})$, where the $\psi_0(\vec{r})$ is the molecular orbital, by measuring the HHG spectrum

$\mathcal{E}_{XUV}(\omega)$. In fact remembering that

$$\mathcal{E}_{XUV}(\omega) \propto \omega(t)b(\vec{k}) \left\langle \psi_0(\vec{r}) \left| \hat{\vec{d}} \right| e^{i\vec{k}(\omega)\cdot\vec{r}} \right\rangle \quad for \ \omega = \frac{k^2}{2} + I_P, \quad (2.41)$$

the measure of HHG spectra in molecules allows one to access to the dipole matrix element $\left\langle \psi_0(\vec{r}) \left| \hat{\vec{d}} \right| e^{i\vec{k}(\omega)\cdot\vec{r}} \right\rangle$ by knowing the coefficient $b(\vec{k})$, since the dipole moment matrix appears as the Fourier transform of the function $\vec{r}\psi_0(\vec{r})$ [6] :

$$\left\langle \psi_0(\vec{r}) \left| \hat{\vec{d}} \right| e^{i\vec{k}(\omega)\cdot\vec{r}} \right\rangle = \int \vec{r}\psi_0(\vec{r})e^{i\vec{k}(\omega)\cdot\vec{r}}d\vec{k} \quad (2.42)$$

The $b(\vec{k})$ is the wave-packets amplitude of the ionized electron in the continuum. The impulsive alignment allows to acquire harmonic spectra in a molecular gas at different angles between the polarization direction of the driving laser and the molecular axis. By making a scan over a set of different angles we obtain $\mathcal{E}_{XUV}(\omega, \theta)$ with the assumption that all molecules are aligned along the polarization direction of the generating electric field and that the measured macroscopic emission is equivalent to a single molecule signal. If we measure also the phase of the complex harmonic signal, we can completely reconstruct the HOMO orbital of the investigated molecules.

2.3   Fractional revivals in HHG from molecules

The revivals are the instants of time, corresponding to such delay between aligning and generating pulses, in which the rotational wave-packet rephases giving an alignment (angular distribution centered about θ=0°with respect the polarization direction of the aligning pulse) followed by an anti-alignment (angular distribution centered about θ=90°with respect the polarization direction of the aligning pulse) condition. The rephasing is periodical with time and occurs at instants equal to the rotational period of the molecule T_{rot} (*full* revival), or fractions of it (*fractional* revivals), and to their integer multiples. The fractional revivals appear in the HHG spectra as intensity modulations that are clearly visible in the harmonic yields scanned along the rotational revival. Their positions

and nature are determined by the symmetry of the molecule and by the excited rotational states (JM). The low-order fractional revivals can be clearly seen in the $\langle \cos^2 \theta \rangle$ with respect to the time delay. The fractional revivals in some cases follow the trend of the alignment parameter, but in other cases the harmonic yield is anticorrelated with the $\langle \cos^2 \theta \rangle$. This fact is connected to the internuclear distance and to the symmetry and shape of the molecular orbitals. However in the $\langle \cos^2 \theta \rangle$ appear only fractional revivals up to 1/4, higher order fractional revivals are not predicted by this function. The fact that high-order fractional revivals appear in the harmonic yield and not in the time evolution of $\langle \cos^2 \theta \rangle$ may be attributed the angular distribution of the molecules in the gas [2]. Indeed, if $\Psi(t, \theta, \phi)$ is a rotational wave packet in a molecule excited by short laser pulse and $\rho(t, \theta, \phi)d\Omega = |\Psi(t, \theta, \phi)|^2 d\Omega$ is the probability to find the molecular axis lying within a solid angle $d\Omega = \sin\theta d\theta d\phi$, and F is a physical quantity measured exploiting the interaction between a probe laser beam with an impulsively aligned molecular sample, we observe a convolution of the quantity with the molecular distribution:

$$S(t, \alpha) = \int_0^{2\pi} d\phi \int_0^{\pi} d\theta \sin\theta \rho(t, \theta, \phi) F_\alpha[\theta_L(\theta, \phi)] \qquad (2.43)$$

where α is the angle between the polarization directions of the pump and probe pulses and θ_L is the angle between the molecular axis and the polarization on the generating electric field. By the point of view of the angular distribution, the observable F acts as a filter, tunable by changing the probe angle α, on the molecular distribution, and thus the harmonic yield shows some complex features that don't appear in the $\langle \cos^2 \theta \rangle$. The fractional revivals in the harmonic yield can be described by cosine moments $\langle \cos^N \theta \rangle$; in particular cosine moments up to N=8 can well describe the time positions of the higher-order harmonic [26].

2.3.1   Role of molecular orbitals in the appearance of the fractional revivals

The total molecular wave function can be factorized in a product of wave functions:

$$\Psi_{mol} = \psi_{el}\psi_{rot}\psi_{vib}\psi_{spin} \qquad (2.44)$$

The symmetry of Ψ_{mol} is fixed and is antisymmetric, the ψ_{vib} corresponds to the ground state at room temperature thus is symmetric, hence the rotational wave function symmetry is connected to the symmetry of the remaining two wave functions, ψ_{el} and ψ_{spin} in order to obtain an antisymmetric total wave function. The symmetry of the rotational wave function is determined by the quantum number J. In particular if J is even the rotational wave function is symmetric, if J is odd the rotational wave function is antisymmetric. This fact means that, if the symmetry of the spin wave function is known, the symmetry of the electronic wave function influences the J population of the rotational wave functions; they can be all odd, all even or a fraction odd and a fraction even. The J parity reflects on the nature of the revivals that can be partially suppressed if the J population is a mix of odd J and even J. For example in CO_2 the HOMO orbital is antisymmetric and the spin wave function is symmetric (the nuclei spin is zero), thus only even J are populated, since the rotational wave function have to be antisymmetric. For N_2 the populated J are 1/3 odd and 2/3 even. The symmetry of the molecular orbitals are involved also in the quantum interference condition between the different contributions in the molecule. For such molecules that can be approximated to a diatomic homo-nuclear molecule, the phenomenon can be treated with the two-center interference according to which the harmonic amplitude can be written in two different forms depending on whether the HOMO is symmetric or antisymmetric. In the case that the molecular orbital is antisymmetric, as well as for CO_2, the harmonic amplitude is expressed as [26]:

$$H(\theta) = A \sin\left(\frac{\pi R}{\lambda_B}\cos\theta\right) \qquad (2.45)$$

where A is constant parameter, R is the internuclear distance, θ is the angle between the probe polarization direction and the molecular axis. Since we have not a perfect alignment, the harmonic yield is obtained by an integration over the molecular distribution of molecules:

$$I(t) = \left| \int_0^{\pi/2} H(\theta)\rho(\theta,t) \sin\theta d\theta \right|^2 + C \qquad (2.46)$$

Owing to the antisymmetry of the ionization matrix element, the integral extends up to $\pi/2$. It's worth noting that the rotational angular distribution ρ doesn't depend on the azimuthal angle ϕ if the pump and probe electric fields have parallel polarization direction, since the angular distribution has a cylindrical symmetry with respect to the polarization direction of the aligning pulse. Two-center interference model well describes the HHG in particular linear molecules as CO_2, but is affected by some limitations as well as the assumption that it's possible to consider the only electronic part of the time-dependent dipole moment, neglecting the rotations and assuming a fixed orientation of molecules or an average of the electronic dipole over a distribution of aligned molecules [27]. In order to gain the analytical expression of the time-dependent harmonic emission (that we observe experimentally) we should adopt a more general theoretical model. The HHG spectrum is the Fourier transform of the component of the dipole moment along the polarization direction of the probe pulse $\hat{n}$:

$$\langle \Psi(t) \,|\, \vec{\mu} \cdot \hat{n} \,|\, \Psi(t) \rangle \qquad (2.47)$$

where Ψ is a rotational-electronic wave packet that combines the rotational wave packet and the dynamics of the continuum electron [27].

The highest order revivals are strongly sensitive to the shape of the spatial filter (equation (2.43)) which is represented by the HHG signal that reflects the structure of the molecular orbitals. Figure 2.10 shows the sensitivity of high-order fractional revivals to the shape of molecular orbitals. The angular filter is tunable by varying the angle α. Indeed, up to quarter revival HOMO and HOMO-1 seems
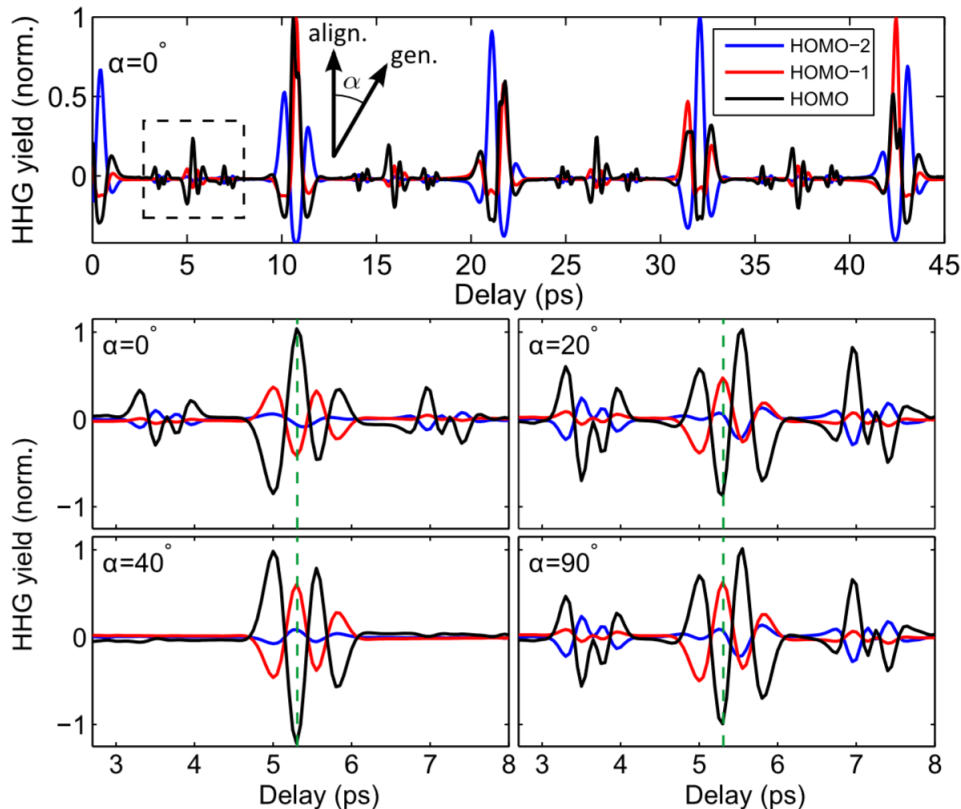
Figure 2.10: *Harmonic yield of the 31st harmonic of 800 nm pulse from three orbitals of aligned CO_2: HOMO, HOMO-1, HOMO-2. The evolution over a rotational period is represented for $\alpha=0°$, whereas the evolution over the 1/8 revival is showed for $\alpha=0°$, 20°40°and 90°. Figure reported from [2].*

to be similar, whereas the structure of 1/8 revival changes from one to another. We also observe that such high-order fractional revival can be visible in one orbital and not visible in others at a certain angle α, as well as the 1/12 revival that doesn't appear in HOMO-1 orbital at $\alpha = 40°$.

2.3.2   Applications

The observation of the fractional revivals in HHG from impulsively aligned molecules is a new probe technique that can have different applications:

- By extracting the electronic dipole elements from the HHG signal it's possible to access to the continuum electron dynamics [26]. This is possible

thanks to the high sensitivity of HHG to the rotational wave packets dynamics. Every fractional revival correspond to a particular rotational expectation value (cosine moment) that is connected to the continuum electronic dynamics. We can extract information on the attosecond electronic motions that is encoded on the rotational fractional revivals structure.

- The fractional revivals in HHG can give information on the rotational wave packets excited by an aligning laser pulse.

- High-order fractional revivals is sensitive to the molecular orbitals, thus it can be exploited as probe of the contributing orbitals to HHG.

- The observable convoluted with the angular distribution can be use to gain information on the molecular distribution or on the observable itself as recollision cross section, high harmonic dipole and multichannel contributions to the HHG process.

Chapter 3

Experimental setup

This chapter aims to present the laboratory setup and the instruments used to carry out the experiments in this thesis work. The first section will provide a description of the laser source, that is a near-IR ($1400\,\mathrm{nm} \div 1800\,\mathrm{nm}$) tunable parametric source pumped by a Ti:Sapphire laser. Then I will describe the apparatus used to perform experiments in vacuum in order to avoid the strong absorbtion of XUV and soft X-ray radiation in air; it consists in a generation chamber and an XUV spectrometer. The last section describes in brief the experiment and the method adopted to acquire the measures analyzed in this work.

3.1 Laser source

As previously mentioned the HHG process requires a laser source able to provide ultrashort and intense laser pulses in order to induce the tunnel ionization of the outermost electron in atoms or molecules. Moreover according to the cutoff law (1.21) the spectral extension of the XUV burst depends on the ponderomotive energy that is proportional to the square of generating laser wavelength $U_p \propto \lambda^2$: the higher is the wavelength λ the higher is the cut off energy. This fact implies that the generation of attosecond pulses needs a low fundamental frequency. The increase of the wavelength, however, produces a reduction of the harmonics generation efficiency at constant intensity. In fact the harmonic emission yield
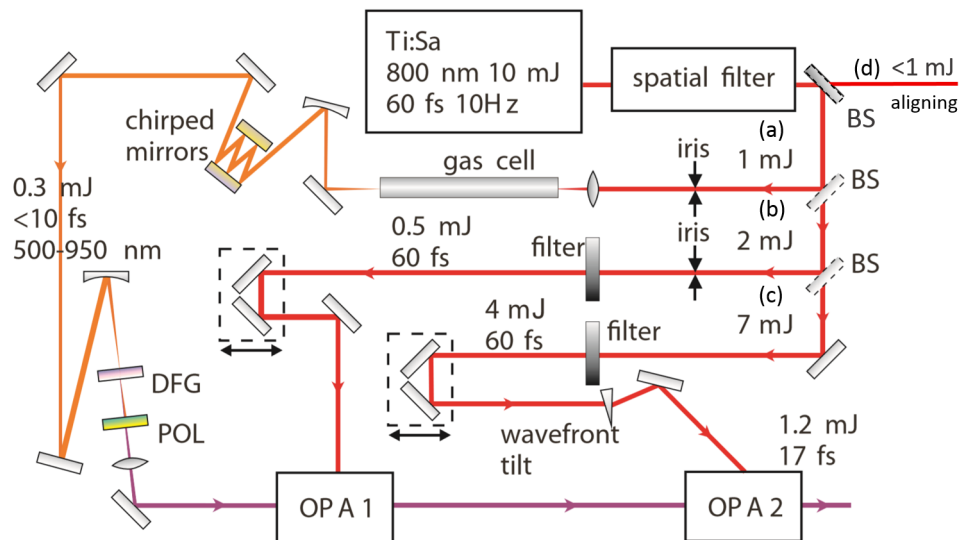
Figure 3.1: *Experimental setup of the laser source for the generation of high-energy-self-phase-stabilized-IR pulses. (a) A fraction of the 800 nm pump beam with energy of 1 mJ is used for the DFG which provides the seed of the OPA. (b) A fraction of the pump beam with 2 mJ energy is used to pump the first OPA stage. (c) A third fraction of the 800 nm beam with an energy of 7 mJ is used as the pump of the second OPA stage. (d) The splitted beam of less than 1 mJ is used for the alignment of the molecules emitting high order harmonics. The figure is reproduced by [3]*

decreases according to the law $\eta(\lambda) \propto \lambda^{-5}$ at constant intensity [28, 29]. Hence there is a trade-off with respect to the wavelength: we can obtain a higher harmonic cutoff reducing the efficiency or vice versa a higher efficiency with a less extended harmonic cutoff.

For acquiring the measures during the experiment we used a laser source developed by Vozzi et. al [30, 3] that is a parametric source with passive intra-pulse CEP stabilization, tunable between 1350 nm and 1800 nm with a pulse duration ranging between 17 and 25 fs, according to the central wavelength. The pump is an amplified Ti:sapphire laser that produces pulses with a duration of 60 fs, a maximum energy of 120 mJ and with a repetition rate of 10 Hz. The central wavelength of the pumping laser spectrum is $\lambda = 800$ nm. A schematic representation of the laser source for HHG is shown in figure 3.1.

A fraction of the Ti:Sapphire laser beam passes through a spatial filter in

order to improve the spatial beam properties. After the filter the pulse energy is about 10 mJ. At first the beam is splitted in two parts: one with energy less than 1 mJ will become the aligning beam that will be exploited for impulsive alignment of molecules undergoing high-order harmonic emission; the remaining fraction of the beam is used to pump the parametric source. The pump beam is splitted again by a second beam splitter in two parts, one of which with an energy of 1 mJ is focused through an iris in a krypton-filled gas cell in order to broaden the pulse bandwidth obtaining a so called *supercontinuum*. Typically the supercontinuum spectral band is in the range of 600 nm ÷ 950 nm. Owing to the dispersion into the gas cell, the pulse at the output is chirped and thus a compensation of the dispersion is required. A set of chirped mirrors perform a dispersion compensation after which the pulse has an energy of 0.3 mJ and a duration of 10 fs. Afterwards the pulse is focused into a β-barium borate (BBO) crystal of thickness 400 μm for the difference frequency generation (DFG) between the spectral tails of the high-energy supercontinuum. The DFG is a second order nonlinear process according to which two incoming frequencies ω_1 and ω_2 such that $\omega_1 < \omega_2$ generate a new frequency $\omega_3 = \omega_2 - \omega_1$ by an energy transfer to the difference frequency. This process allows one to obtain at the output of the nonlinear crystal a near-IR pulse with a spectrum extending between 1.3 and 2.2 microns and with a stable Carrier-Envelope Phase (CEP). The phase stabilization is an important requirement for the attosecond pulse generation through the HHG process [5, 31]. The electric field of the pump pulse is polarized parallel to the working plane along the extraordinary axis of the crystal whereas the difference frequency electric field is polarized along the ordinary axis perpendicular to the working plane, therefore a *type II* phase matching condition is fulfilled. The crystal is positioned far from the focus of the pump beam in order to keep the intensity below the threshold of third order nonlinear phenomena.

Figure 3.2 shows the setup of the DFG. To increase the output pulse energy
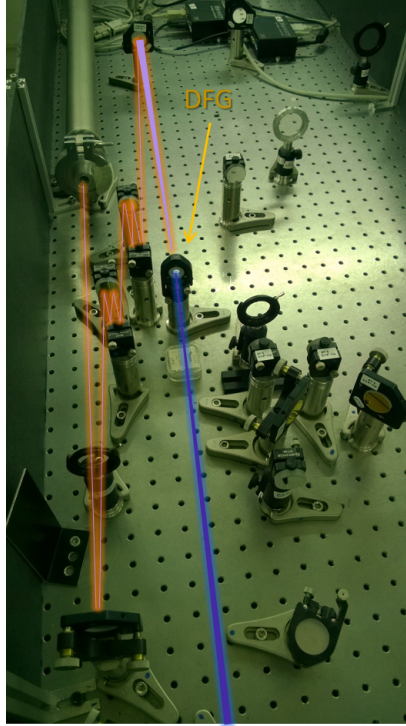
Figure 3.2: *Setup for DFG.*

a two-stage optical parametric amplifier (OPA) is used. The second beam exiting from the second beam splitter is divided by a third beam splitter in two pulses, both passing through irises in order to tune the pulse energy, that are respectively the *pump* of the fist stage (0.5 mJ) and the *pump* of the second stage (4 mJ) of the OPA. The parametric amplification doesn't change the absolute phase of the pulse, thus the CEP stabilization of the signal is preserved [3]. With the type II phase-matching configuration we are able to tune the spectral gain bandwidth by changing the angle between the incident beam and the OPA crystal. Since we are interested in a few-cycle pulse duration, type II configuration is preferred to type I, in fact the pulse obtained with the type II is shorter without any compressor stage after the amplification. The optimal output pulse features correspond to an energy of 1.2 mJ and a duration of 17 fs, slightly longer than the *transform limited* duration of 16 fs.
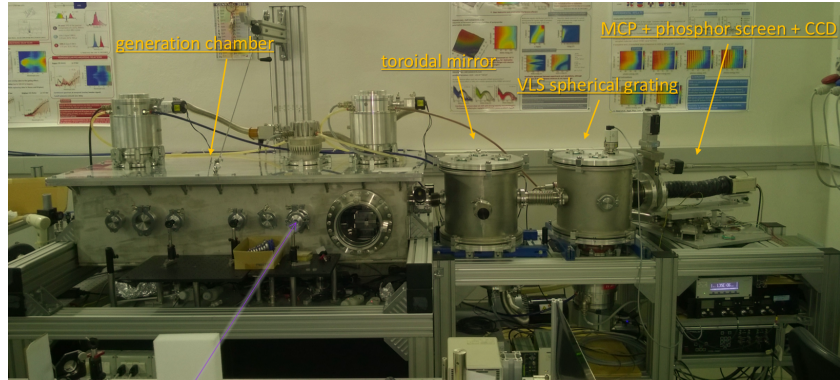
Figure 3.3: *Picture of the generation chamber and the detection system: on the left the vacuum chamber, in the middle the XUV spectrometer with a variable line spacing (VLS) spherical grating and on the right the CCD camera.*

3.2   Generation chamber and XUV spectrometer

When XUV radiation propagates in air it experiences a strong absorption. For this reason high harmonics radiation is generated by focusing the laser pulses on a gas jet positioned into a vacuum chamber. The laser jet comes from a pulsed electromagnetic valve with opening rate of $10\,\mathrm{Hz}$, synchronized with the laser pulses, and with a nozzle of diameter $500\,\mu\mathrm{m}$. The gas at the output of the valve experiences a supersonic expansion in the vacuum, thus the molecules are rotationally cooled and the intermolecular collisions can be neglected. The rotational temperature of the gas-jet molecules in the thesis experiments conditions is about $70\,\mathrm{K}$. The valve can be moved along three orthogonal axes.

Figure 3.3 shows an image of the generation chamber together with the XUV spectrometer and the CCD camera; in figure 3.4 we can see a zoom on the vacuum camera. The generation chamber is coupled with a flat field *XUV spectrometer*, that consists of two grazing incidence optical elements (see figure 3.5):

toroidal mirror : this component allows the compensation of the astigmatism and produces a stigmatic beam by focusing the radiation also in the direction perpendicular to the grating dispersion plane (sagittal plane) [32]. Moreover it improves the grating efficiency making it able to better collects
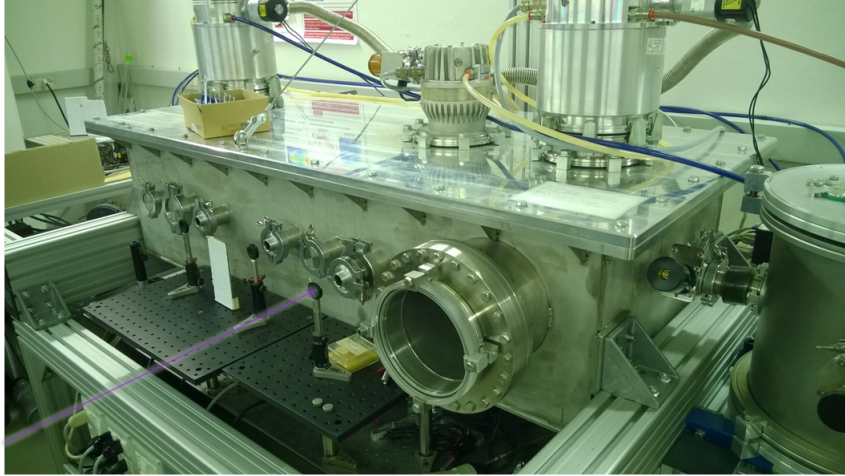
Figure 3.4: *Picture of the vacuum chamber.*

the harmonics radiation (see figure 3.6).

grating : this allows to disperse the radiation spectral components and focus
them on different spatial points of the detector in order to view the signal
for each frequency. In a spherical grating the light is focused on a cylindri-
cal surface (spectral focal plane), called Rowland cylinder, with a diameter
equal to the grating radius. In order to obtain a wide spectrum several
acquisitions are needed by moving the detector along the Rowland circle.
In our experiments we used a *spherical varied line spacing* (SVLS) grat-
ing [33, 34] where the spacing between lines is variable. The SVLS allows
to focus the diffracted rays along an almost flat focal surface, thus with a
curvature higher than the Rowland circle, at near normal incidence to the
detector. With a proper choice of line spacing distribution, the spectral
focal plane can become almost straight, well fitting the detector plane. In
this way we can obtain a wider spectrum for a single acquisition. We can
observe a different spectral range depending on the detector position. The
detector can move continuously.
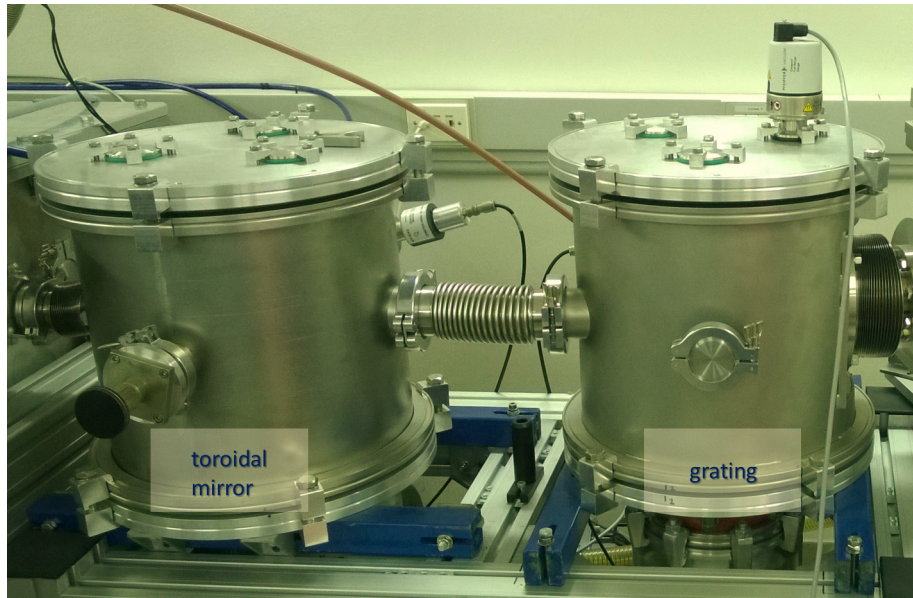
Figure 3.5: *Picture of the XUV spectrometer: on the left the toroidal mirror and on the right the grating.*
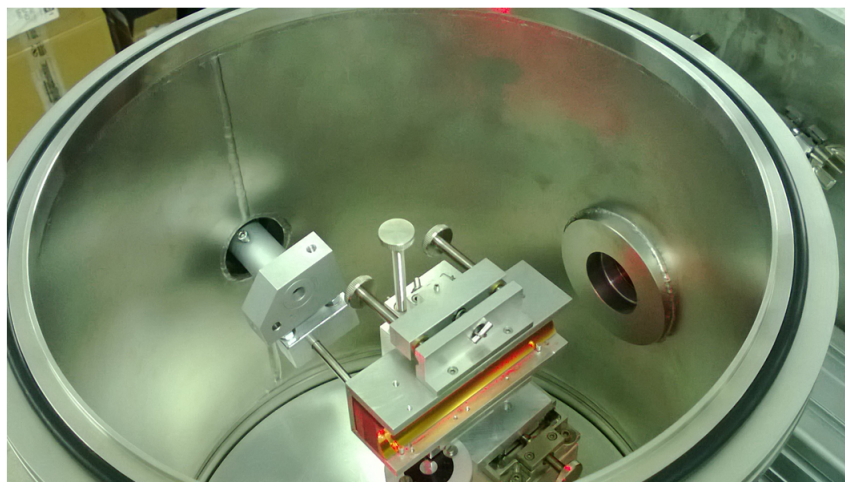
Figure 3.6: *XUV spectrometer detail: the toroidal mirror.*
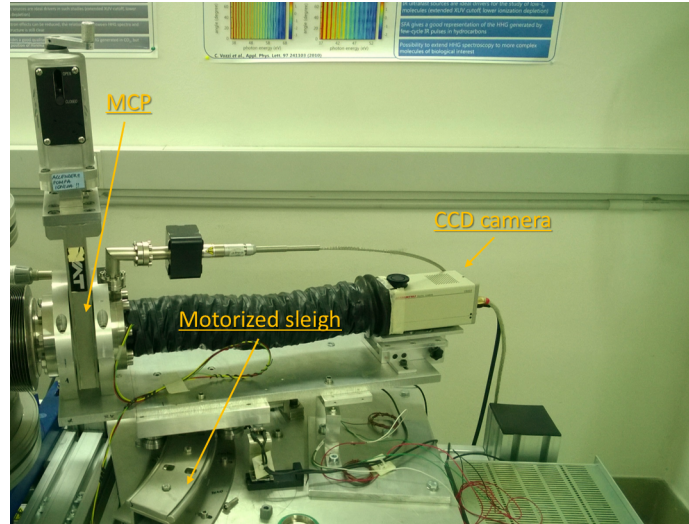
Figure 3.7: *Picture of the detector: from the left to the right we can see the MCP and the CCD camera.*

The detector position is chosen according to the experimental requirements and its motion can be remotely controlled by a motorized stage. When the radiation reaches the detector the impinging photons are converted into electrons by a magnesium fluoride photocathode ($M_g F_2$). The obtained signal is amplified by a micro-channel plate (MCP) with a voltage of 900 V. Then the electronic signal is converted again in an optical signal by accelerating electrons onto a phosphor screen. In the end a CCD camera acquires the final image allowing to display it on the screen. Figure 3.7 shows a detector picture.

3.3 Revival scanning and alignement

The data analysis presented in this thesis work regards the measures of the HHG signal emitted by CO_2 and N_2O molecules during a revival period. A scheme of the experimental setup for the acquisitions is reported in figure 3.8. The pulse at 1450 nm is the driving pulse whereas the pulse at 800 nm is the aligning one. In order to perform the scanning with the aligning pulse polarization parallel to that of the generating one, we introduce a $\lambda/2$ plate at 45°along the aligning path for rotating its polarization by 90°. It's possible to get measures also at
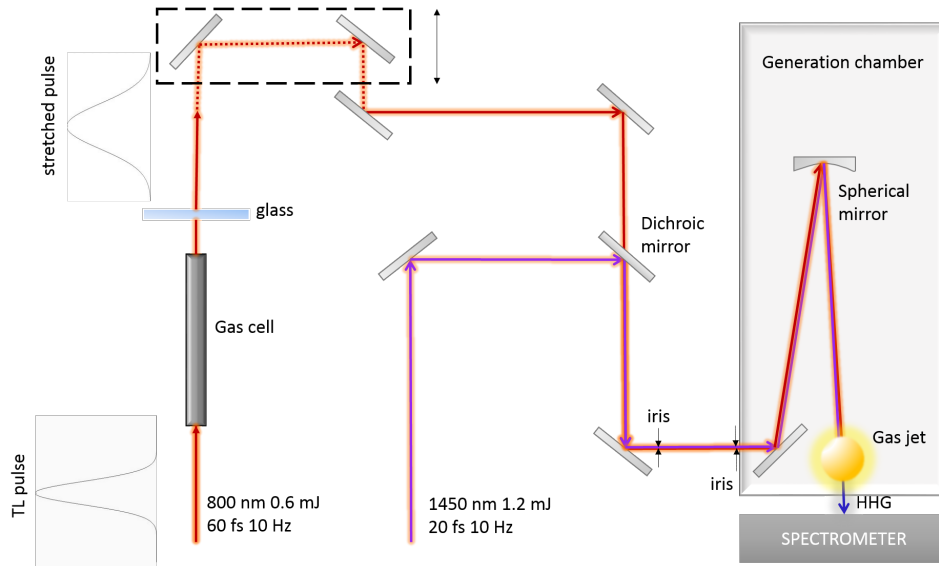
Figure 3.8: *Schematic representation of the acquisition setup.*

different angles between the polarization directions of the aligning and generating pulses. Since we are interested in the harmonics signal generated by the near-IR pulse, the aligning intensity should be low enough to avoid high harmonic generation by the 800 nm pulse. For this purpose, before entering the chamber, the 800 nm pulse is focused into an argon-filled gas cell in order to improve its spatial properties and create new frequencies, thereby broadening the spectrum. After the filamentetion the pulse passes through a glass plate in order to introduce a pulse chirp. The dispersion increases the pulse duration and the peak intensity decreases. By broadening the pulse spectrum, the dispersion effect on the pulse duration is more important because there are more frequencies with different group velocity. After the filamentation chamber, the pulse propagates along a variable delay line. A dichroic beam combiner allows to bring into the chamber the two beams with collinear configuration. The two-color beam is focused on the gas get by a spherical mirror.

We acquired HHG signal at different time delay between aligning and generation pulses by changing the optical path of the 800 nm beam through a motorized stage. In the end we have a HHG spectrum for each time delay, thus we can reconstruct

the intensity signal with respect to the temporal delay for each harmonic.

Chapter 4

Fractional rotational revivals in HHG from impulsively aligned molecules

The experimental activity is focused on the observation of the rotational fractional revivals in HHG from aligned molecules of N_2O and CO_2. The supporting theory has been discussed in the previous chapters. In particular we have pointed out that the harmonic emission is sensitive to the angle formed between the aligning and generating pulses, that we can control with a non-adiabatic alignment in order to probe the molecules under field-free condition. The obtained high harmonic spectra encode the information about the structure and the symmetries of the molecular orbitals by the appearance of particular features. CO_2 and N_2O are two linear molecules, thus we can apply the theory of impulsive alignment in gases of linear molecules discussed before in order to describe the evolution of
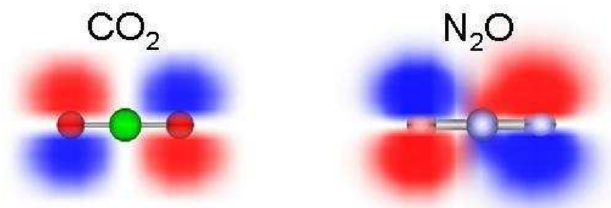
Figure 4.1: *Representation of the Highest Occupied Molecular Orbital (HOMO) for CO_2 and N_2O.*

the rotational states when they interact with an aligning laser beam. However the two molecules have different orbital symmetries. The CO_2 molecule has the carbon atom in the middle, and the oxygen atoms at the extremes; its HOMO is antisymmetric (π_g) and presents two nodal planes, one parallel with the molecular axis and one another orthogonal. The rotational period for CO_2 is T_{rot}=42.8 ps. The N_2O is not a symmetric molecule, indeed the oxygen atom is external and there are one nitrogen atom in the middle and one at the other edge. Hence the HOMO orbital has not a defined symmetry, even though it look likes to a π_g symmetry. However the average contribution of the HOMO orbital from an ensemble of N_2O molecules to the HHG spectra is the same as CO_2. N_2O is characterized by a rotational period T_{rot}=39.8 ps. Figure 4.1 shows the shape of the HOMO orbital for the two molecule.

The chapter provides at first a description of the data acquisition and in the second part presents the results of data analysis according to the theory. The high order fractional revivals are compared to the half revival for each sample analyzed in this thesis work. The behaviour of HHG signal around a delay equal to $T_0/2$ is well known and studied in the literature, as opposed to the high order fractional revivals.

4.1   HHG spectra acquisition

The data were acquired by using the setup described in chapter 3. For both the two sets of measures the molecules were aligned by a 800 nm laser pulse with a duration of 60 fs, much shorter then the rotational periods of the CO_2 (T_{rot}=42.8 ps) and N_2O (T_{rot}=39.8 ps), thus a non-adiabatic alignment was adopted. The molecules were then exposed to 1450 nm laser pulse characterized by a duration of about 20 fs. The aligning pulse has a duration longer than the ionizing pulse in order to keep its intensity low and avoid harmonic generation. The HHG-photons detection system was set with MCP voltages equal to 900 V

and $4.5\,\text{kV}$, CCD gain equal to 1. The valve baking pressure was carefully chosen in order to both maximize the HHG signal and prevent molecules clusterization. The valve baking pressure used for the CO_2 was equal to $5\,\text{bar}$, whereas that used for the N_2O was equal to $4\,\text{bar}$.

The synchronization between aligning and driving pulses is recognized by the occurrence of a prompt alignment that influences the HHG signal. Since we are interested into the fractional revivals within a rotational period, the scanning was limited to a suitable range of time delays. We performed a scanning along the revival for every fractional revivals we were interested to. A certain number of HHG spectra, that depends on measures, were acquired at each time delay between the aligning and the generating pulses starting from an initial time delay τ_0 by steps of stage that vary according to the measure. In all scans the polarization of the aligning pulse is parallel with the polarization of the generating one: the molecular axes are aligned along the polarization direction of the probe respect to which the angular distribution of the molecules is characterized by a cylindrical symmetry, thus doesn't depends on the azimuthal angle ϕ. Two sets of fractional revivals scans, for CO_2 and N_2O, were acquired. The acquired data where then compared

Carbon dioxide (CO_2)

For the CO_2 we considered the 1/8, expected around the delay $\tau = T_{rot}/8 = 5.35\,\text{ps}$, and the 1/16, expected around the delay $\tau = T_{rot}/16 = 2.675\,\text{ps}$. The 1/8 revival scan consists of 40 acquisitions, for each of which 6 spectra were acquired with a single-spectrum integration time equal to $5\,\text{s}$ (this is useful to increase the signal-noise ratio), separated by a step equal to $25\,\text{fs}$ from an initial delay $\tau_0 = 4.7\,\text{ps}$. The obtained data, integrated along the direction orthogonal to the detector spectral plane, are shown in figure 4.2. We can clearly see the harmonic intensity modulation with respect to the variation of the delay. The 1/16 revival scan, as well as for the 1/8, consists of 40 acquisitions starting from $\tau_0 = 2.1\,\text{ps}$

Figure 4.2: *Time evolution of the HHG radiation from aligned CO_2 molecules scanned along the 1/8 revival, normalized to the maximum of each harmonic within the revival. The data are smoothed in order to make the view of the graph clearer.*
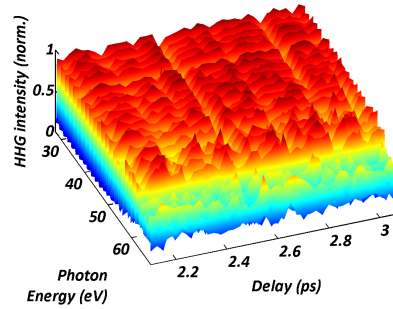
Figure 4.3: *Time evolution of the HHG radiation from aligned CO_2 molecules scanned along the 1/16 revival, normalized to the maximum of each harmonic within the revival. The data are smoothed in order to make the view of the graph clearer.*

separated by a step of 25 fs, each of one was obtained by integrating 6 spectra for 5 s. The data acquired are reported in figure 4.3. In this case the harmonic intensity modulation is weakly visible, but it is clearer after an elaboration of the data. Such sets of data are compared to the half revival, expected around the $\tau = T_{rot}/2 = 21.4$ ps. The half revival scan consists in 60 acquisitions starting from $\tau_0 = 19.5$ ps separated by a step of 50 fs, with 5 spectra per acquisition and an integration time per spectrum of 3 s. The result is a very clear modulation that we can see in figure 4.4.

Figure 4.4: *Time evolution of the HHG radiation from aligned CO_2 molecules scanned along the 1/2 revival, normalized to the maximum of each harmonic within the revival. The data are smoothed in order to make the view of the graph clearer.*
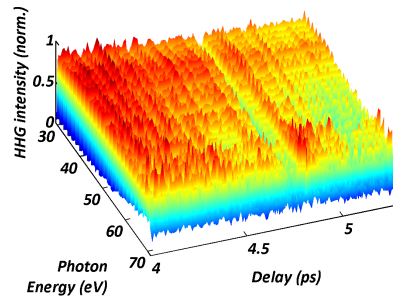
Figure 4.5: *Time evolution of the HHG radiation from aligned $N2O$ molecules scanned along the 1/8 revival, normalized to the maximum of each harmonic within the revival. The data are smoothed in order to make the view of the graph clearer.*

Nitrogen dioxide (N_2O)

In aligned molecules N_2O gas we checked the 1/8, 1/4 and 1/6 revivals. For the 1/8 revival, expected around the delay $\tau = T_{rot}/8 = 4.975$ ps, we performed a scan of 100 acquisitions separated by a step of 10 fs starting from the delay $\tau_0 = 4$ ps, with 6 spectra per acquisition and an integration time per spectrum equal to 5 s. The spectra acquired are represented in figure 4.5. A fast modulation is visible in the raw data representation. We then scanned the 1/4 revival, expected around the delay $\tau = T_{rot}/4 = 9.95$ ps, on 120 acquisitions starting from a initial delay equal to $\tau_0 = 8.255$ ps, with 2 spectra per acquisition and an integration time per spectrum equal to 5 s. The scan is reported in figure 4.6: these spectra also need an elaboration to make the intensity modulation observable, however we can
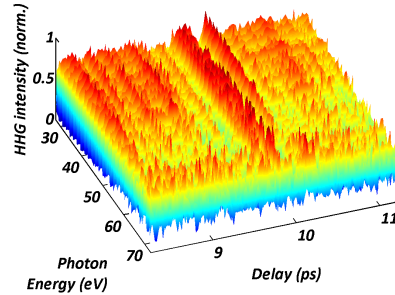
Figure 4.6: *Time evolution of the HHG radiation from aligned N2O molecules scanned along the 1/4 revival, normalized to the maximum of each harmonic within the revival. The data are smoothed in order to make the view of the graph clearer.*
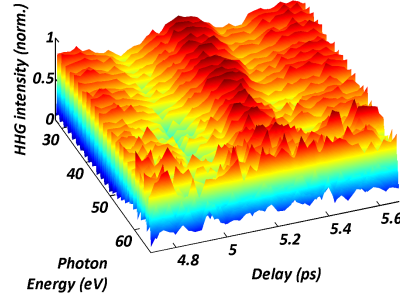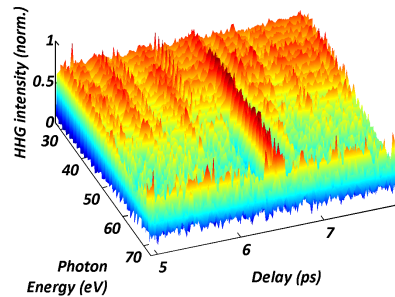

Figure 4.7: *Time evolution of the HHG radiation from aligned N2O molecules scanned along the 1/6 revival, normalized to the maximum of each harmonic within the revival. The data are smoothed in order to make the view of the graph clearer.*

catch a glimpse of an hole in correspondence of $\tau = T_{rot}/4$. The 1/6 revival was scanned with the same parameters used for the 1/4, thus 120 acquisitions with step of 25 fs, 2 spectra per acquisition and an integration time per spectrum equal to 5 s, starting from the time delay $\tau_0 = 4.92$ ps, since we expect it around the delay $\tau = T_{rot}/6 = 6.633$ ps. The scanning results are shown in figure 4.7. In this case we distinguish more clearly the intensity modulation. For a comparison with the fractional revivals, an half revival scan is reported in figure 4.8. The half revival for N_2O is expected around the delay $\tau = T_{rot}/2 = 19.9$ ps. The scan consists of 60 acquisitions separated by a step equal to 50 fs from an initial delay equal to $\tau_0 = 18.5$ ps, with 3 spectra for acquisition and an integration time for spectrum equal to 5 s.
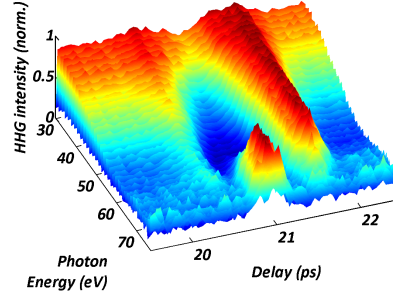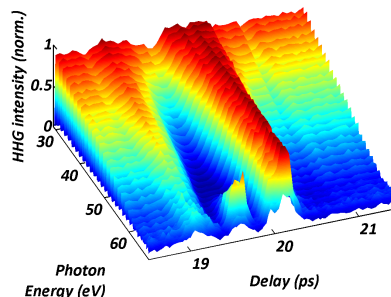
Figure 4.8: *Time evolution of the HHG radiation from aligned $N2O$ molecules scanned along the 1/2 revival, normalized to the maximum of each harmonic within the revival. The data are smoothed in order to make the view of the graph clearer.*

4.2 Data analysis

The raw data presented in the first paragraph were later analyzed by a Matlab script that I wrote. In particular the script performs a search of the minima between the harmonics in the spectrum with the most extended cutoff and then, for each HHG spectrum acquired during the revival scan, integrates each harmonic within its two neighboring minima obtaining a temporal trace as a function of the harmonic order. This procedure allows to increase the signal-to-noise ratio. Hence the harmonic yield for each time delay is normalized to the maximum yield within the revival scan with the aim of a better rendering of the plots. The obtained spectra are smoothed on three points with respect to both the time delay axis and the photon energy axis in order to reduce the noise in the measures. We would like to observe high-order fractional revivals in N_2O and CO_2 and investigate if the shape of the modulation related to a particular fractional revival changes when one moves from lower harmonic orders towards higher ones. A comparison among the various harmonic orders is presented for each set of acquisitions.

Carbon dioxide CO_2

At first we present the results for the half revival of the CO_2. Figure 4.9 shows a 2D plot of spectra with respect to the time delay and the harmonic order of

Figure 4.9: *2D plot in linear scale of the HHG emission from aligned CO_2 molecules along the half revival, normalized to the maximum of each harmonic within the revival. In the axes it is reported the time delay between pump and probe and the harmonic order of the fundamental photon energy, equal to $E_0 = 0.853$ eV. The data are smoothed in order to make the view of the graph clearer. Pump and probe have parallel polarizations.*

the fundamental photon energy $E_0 = 0.853$ eV and it's three-dimensional view. It is worth noting the formation of an "island" in the HHG signal during the scan. This is due to the two center interference, discussed in chapter 2, that occurs when the molecular axes are aligned along the polarization direction of the probe electric field. The suppression of the HHG signal, i.e. the formation of the island, is followed by an enhancement that represents the condition of anti-alignment (θ=90°) of the molecular axes, according to the antisymmetry of the CO_2 HOMO orbital. Now we consider three harmonic orders:one at the low-harmonic side of the spectrum, the other in the middle and the last one in the proximity of the cutoff. In figure 4.10 we can se that the shape of the half revival changes drastically from the lower harmonic order to the highest harmonic order until to reverse its trend with respect to the time delay. The harmonic orders considered are the 41st, 69th, 95th of the fundamental one. The graph in (a) consists of all visible normalized harmonic yields separated by a constant chosen arbitrarily, whereas (b) and (c) compare the selected harmonics. Such behaviour is well known and isn't a new information got with this experimental work. The results for the scan along the 1/8 revival are reported in the figures 4.11 and 4.12. By observing the waterfall we note the intensity modulation for the 1/8 revival remains constant among the different harmonic orders. However it seems that by moving towards

(a)

(b)

(c)

Figure 4.10: *Harmonic yield with respect to the time delay between pump and probe from aligned CO_2 molecules along the half revival, normalized to the maximum of each harmonic within the revival:(a) waterfall of harmonic yields in which harmonic order increase from the bottom to the top, the normalized harmonic yields are spaced by a constant quantity; (b) comparison of the red colored harmonic in the waterfall; (c) superposition of the three underlined harmonics. The fundamental photon energy is equal to $E_0 = 0.853$ eV. The data are smoothed in order to make the view of the graph clearer. Pump and probe have parallel polarizations.*
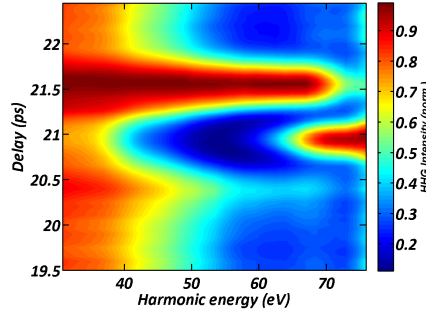
Figure 4.11: *2D plot in linear scale of the HHG emission from aligned CO_2 molecules along the 1/8 revival, normalized to the maximum of each harmonic within the revival. In the axes it is reported the time delay between pump and probe and the harmonic order of the fundamental photon energy, equal to $E_0 = 0.853\,eV$. The data are smoothed in order to make the view of the graph clearer. Pump and probe have parallel polarizations.*

higher harmonics the peak of the modulation decrease and the right hole begins larger. A comparison between the 33rd, 55th and 71st harmonic orders of the driving laser frequency shows a little enlargement of the minimum at about $5.4\,\mathrm{ps}$, in particularly in the 71st harmonic. This observation is supported by the pcolor graph that in this case shows clearer the variation of the modulation. The results of the 1/16, reported in the figure 4.13 and figure 4.14, appear more noisy with respect to the other revivals, but we can observe a weak modification of the modulation shape in the waterfall of the harmonic yield and in the superposed yields of the 33rd, 57th and 71st harmonics. Indeed the minima at $2.5\,\mathrm{ps}$ and $2.7\,\mathrm{ps}$ become deeper by moving towards the 71st harmonic. In this case too the pcolor plot confirms such evolution of the minima, in particularly in the three-dimensional view, even thought it may be a noise effect. In impulsively aligned CO_2 gas the half revival experiences an inversion of its shape from lower harmonics to higher harmonics. The high order fractional revivals exhibit a modification of the modulation shape with respect to the harmonic order, but we can't observe their behaviour at higher harmonics as well as in the half revival because for the higher order fractions of the rotational period the cutoff is shifted towards lower harmonics.
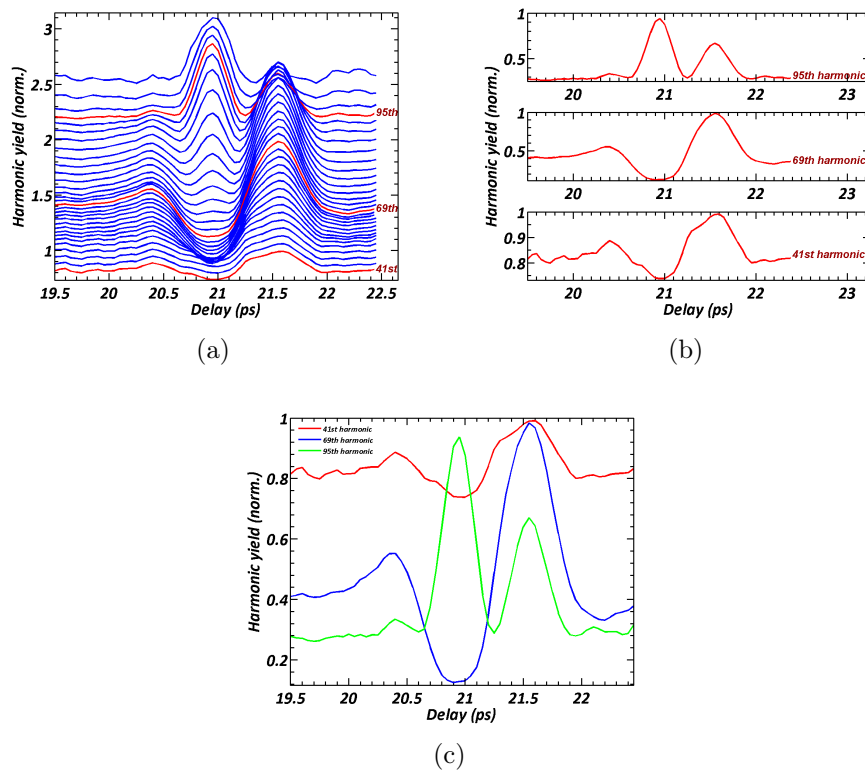
(a)

(b)

(c)

Figure 4.12: *Harmonic yield with respect to the time delay between pump and probe from aligned CO_2 molecules along the 1/8 revival, normalized to the maximum of each harmonic within the revival:(a) waterfall of harmonic yields in which harmonic order increase from the bottom to the top, the normalized harmonic yields are spaced by a constant quantity; (b) comparison of the red colored harmonic in the waterfall; (c) superposition of the three underlined harmonics. The fundamental photon energy is equal to $E_0 = 0.853\,eV$. The data are smoothed in order to make the view of the graph clearer. Pump and probe have parallel polarizations.*

Figure 4.13: *2D plot in linear scale of the HHG emission from aligned CO_2 molecules along the 1/16 revival, normalized to the maximum of each harmonic within the revival. In the axes it is reported the time delay between pump and probe and the harmonic order of the fundamental photon energy, equal to $E_0 = 0.853\,eV$. The data are smoothed in order to make the view of the graph clearer. Pump and probe have parallel polarizations.*
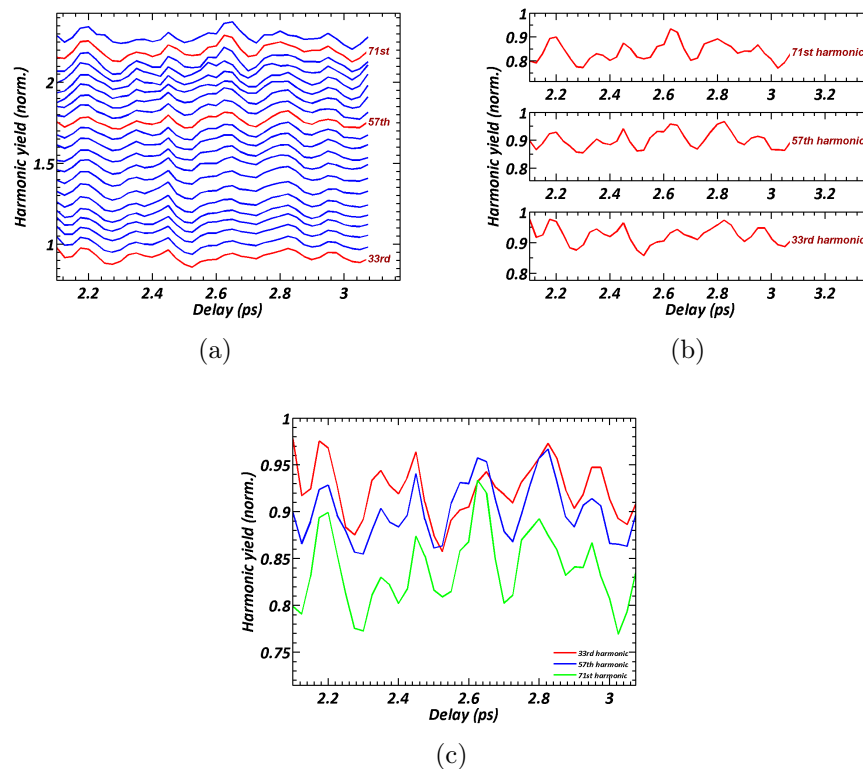
Figure 4.14: *Harmonic yield with respect to the time delay between pump and probe from aligned CO_2 molecules along the 1/16 revival, normalized to the maximum of each harmonic within the revival:(a) waterfall of harmonic yields in which harmonic order increase from the bottom to the top, the normalized harmonic yields are spaced by a constant quantity; (b) comparison of the red colored harmonic in the waterfall; (c) superposition of the three underlined harmonics. The fundamental photon energy is equal to $E_0 = 0.853$ eV. The data are smoothed in order to make the view of the graph clearer. Pump and probe have parallel polarizations.*
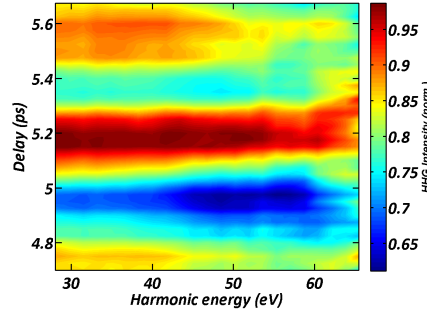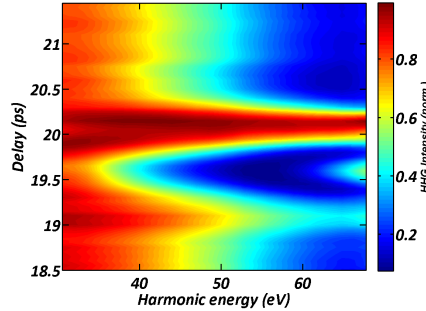
Figure 4.15: *2D plot in linear scale of the HHG emission from aligned N_2O molecules along the half revival, normalized to the maximum of each harmonic within the revival. In the axes it is reported the time delay between pump and probe and the harmonic order of the fundamental photon energy, equal to $E_0 = 0.853\,eV$. The data are smoothed in order to make the view of the graph clearer. Pump and probe have parallel polarizations.*

Nitrogen dioxide (N_2O)

As for the carbon dioxide, we fists presents the results of the half revival scan for the N_2O. In the figure 4.15 it is clear that the modulation changes drastically from the lower harmonics to the higher ones, as it happens for the CO_2, and an island appears too. The trend of the waterfall of harmonics and the comparison among the 43rd, 65th and 89th harmonics in figure 4.16 confirm the behaviour well described by the 2D plot. Owing to the cutoff more shifted towards lower harmonics then the CO_2 cut-off, the half of N_2O doesn't exhibit an inversion of the modulation. However we observe that the minimum at 19.5 ps that we can see for the 43rd and 89th harmonics is substituted by a maximum in the 89th harmonic. We analyze now the results of the 1/8 revival scan. In the figures 4.17 and 4.18 we observe a more clear modulation related to the 1/8 revival with respect to what seen for the CO_2. The plots unequivocally show a dramatic signal decay due to a progressive misalignment of the laser. From the superposition of the three harmonics we note that the 77th harmonic has a more pronounced minimum at 4.75 ps and experiences the formation of a maximum at 4.8 ps, not present in the 35th and 55th harmonics, and a minimum at 4.97 ps. In the waterfall we can see the transformation of the modulation from the bottom
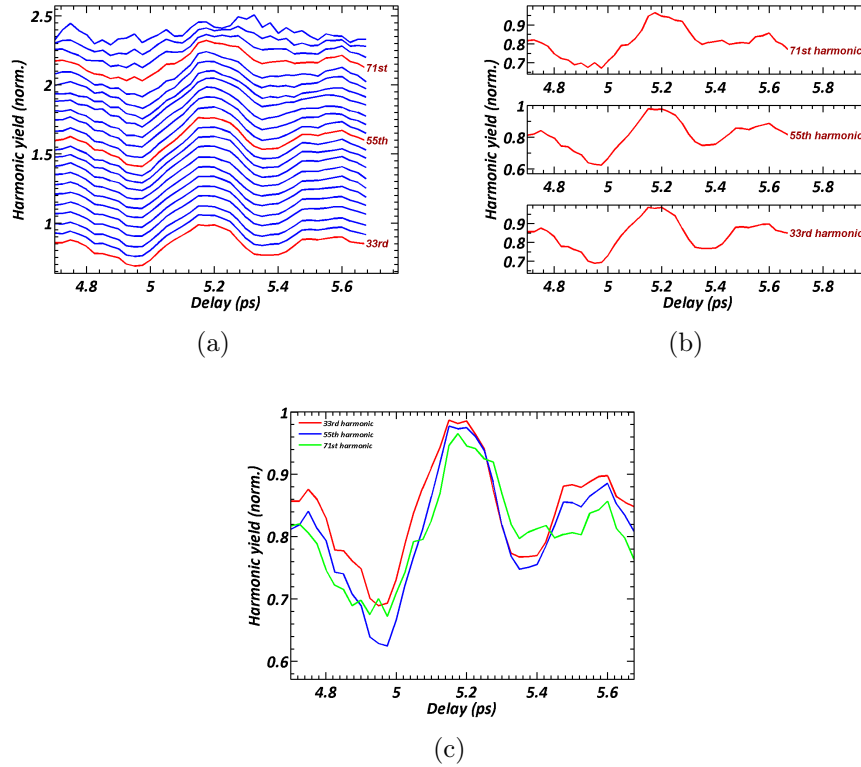
(a)

(b)

(c)

Figure 4.16: *Harmonic yield with respect to the time delay between pump and probe from aligned $N2O$ molecules along the half revival, normalized to the maximum of each harmonic within the revival:(a) waterfall of harmonic yields in which harmonic order increase from the bottom to the top, the normalized harmonic yields are spaced by a constant quantity; (b) comparison of the red colored harmonic in the waterfall; (c) superposition of the three underlined harmonics. The fundamental photon energy is equal to $E_0 = 0.853$ eV. The data are smoothed in order to make the view of the graph clearer. Pump and probe have parallel polarizations.*
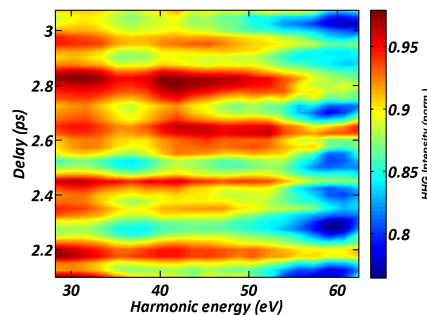
Figure 4.17: *2D in linear scale of the HHG emission from aligned N_2O molecules along the 1/8 revival, normalized to the maximum of each harmonic within the revival. In the axes it is reported the time delay between pump and probe and the harmonic order of the fundamental photon energy, equal to $E_0 = 0.853$ eV. The data are smoothed in order to make the view of the graph clearer. Pump and probe have parallel polarizations.*

(low harmonics) to the top (high harmonics). In the impulsively aligned N_2O gas the 1/4 revival is also visible as reported in figure 4.19. We can appreciate the variations of the shape of the 1/4 revival in figure 4.20 where both the comparison of the 33rd, 63rd and 83rd harmonics and the waterfall that reports all harmonic orders exhibit a strong shape modification. The structure constituted by two maxima and one minimum in the 33th harmonic is replaced by the structure with one maximum and one minimum of the 83th harmonic. It is worth noting that the modulation exhibit a weak inversion for high harmonics in correspondence of the delay $\tau = 10.2$. In the end we focalize the attention on the 1/6 revival, whose results are shown in figure 4.21 where we clearly identify a modulation of the HHG signal. The comparison in figure 4.22 among the harmonics 35th,59th and 79th together with the waterfall exhibits a weak modulation for the lower harmonic orders and a strong modulation for higher harmonic orders as well as the 79th that is characterized by a very pronounced maximum at 6.5 ps followed by a minimum and another maximum.

(a)

(b)

(c)
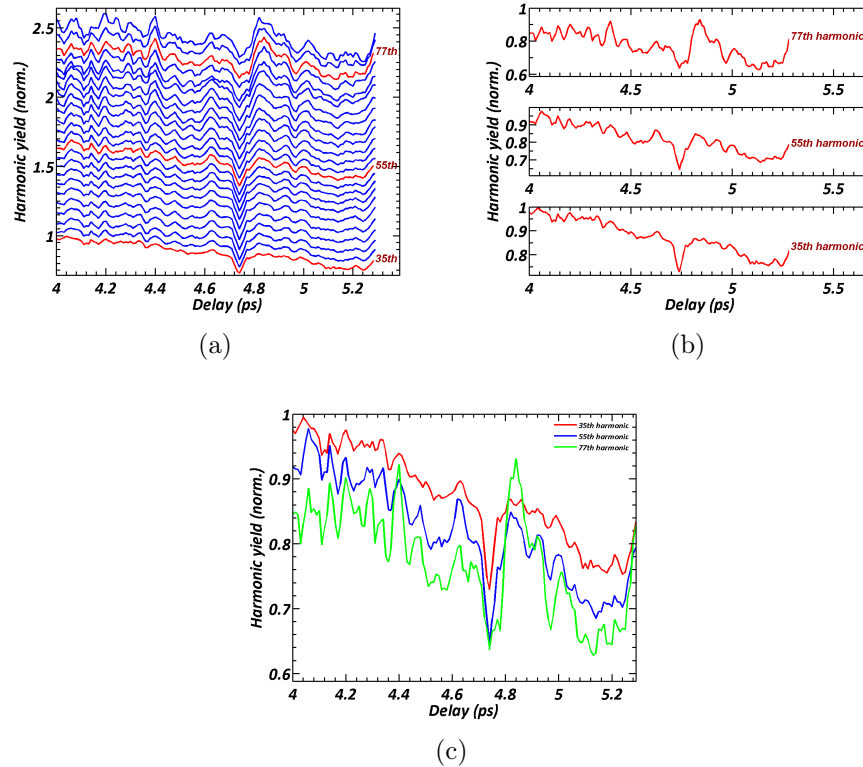
Figure 4.18: *Harmonic yield with respect to the time delay between pump and probe from aligned $N2O$ molecules along the 1/8 revival, normalized to the maximum of each harmonic within the revival:(a) waterfall of harmonic yields in which harmonic order increase from the bottom to the top, the normalized harmonic yields are spaced by a constant quantity; (b) comparison of the red colored harmonic in the waterfall; (c) superposition of the three underlined harmonics. The fundamental photon energy is equal to $E_0 = 0.853$ eV. The data are smoothed in order to make the view of the graph clearer. Pump and probe have parallel polarizations.*
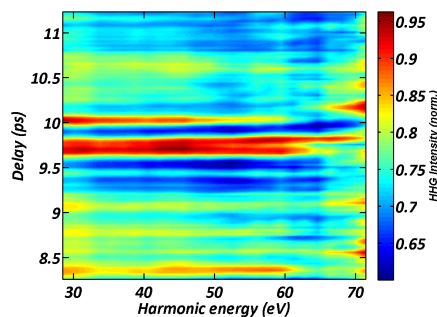
Figure 4.19: *2D plot in linear scale of the HHG emission from aligned N_2O molecules along the 1/4 revival, normalized to the maximum of each harmonic within the revival. In the axes it is reported the time delay between pump and probe and the harmonic order of the fundamental photon energy, equal to $E_0 = 0.853$ eV. The data are smoothed in order to make the view of the graph clearer. Pump and probe have parallel polarizations.*

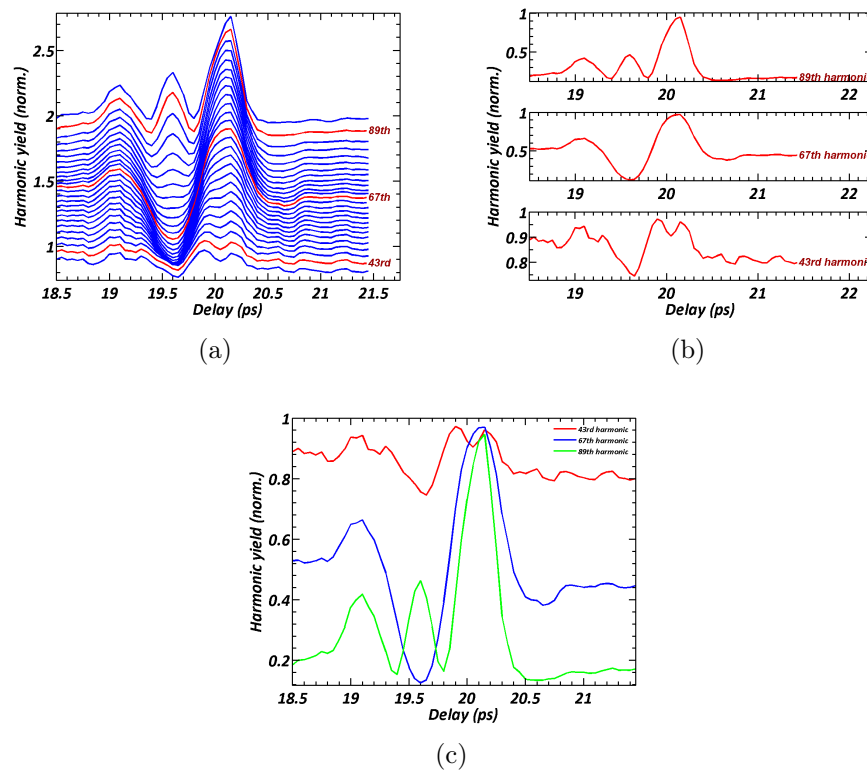(a)   (b)

(c)
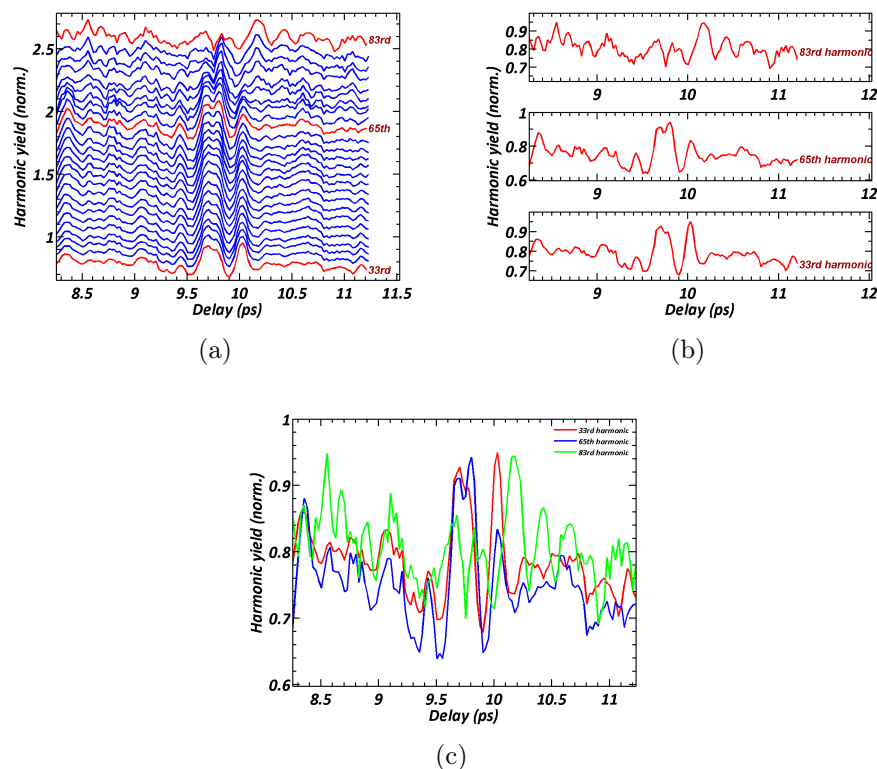
Figure 4.20: *Harmonic yield with respect to the time delay between pump and probe from aligned $N2O$ molecules along the 1/4 revival, normalized to the maximum of each harmonic within the revival:(a) waterfall of harmonic yields in which harmonic order increase from the bottom to the top, the normalized harmonic yields are spaced by a constant quantity; (b) comparison of the red colored harmonic in the waterfall; (c) superposition of the three underlined harmonics. The fundamental photon energy is equal to $E_0 = 0.853$ eV. The data are smoothed in order to make the view of the graph clearer. Pump and probe have parallel polarizations.*
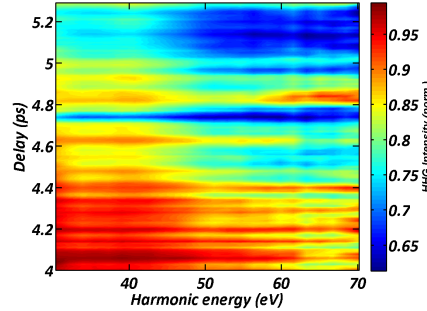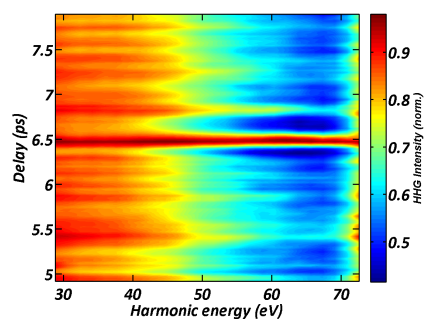

Figure 4.21: *2D plot in linear scale of the HHG emission from aligned N_2O molecules along the 1/6 revival, normalized to the maximum of each harmonic within the revival. In the axes it is reported the time delay between pump and probe and the harmonic order of the fundamental photon energy, equal to $E_0 = 0.853$ eV. The data are smoothed in order to make the view of the graph clearer. Pump and probe have parallel polarizations.*

(a)

(b)

(c)
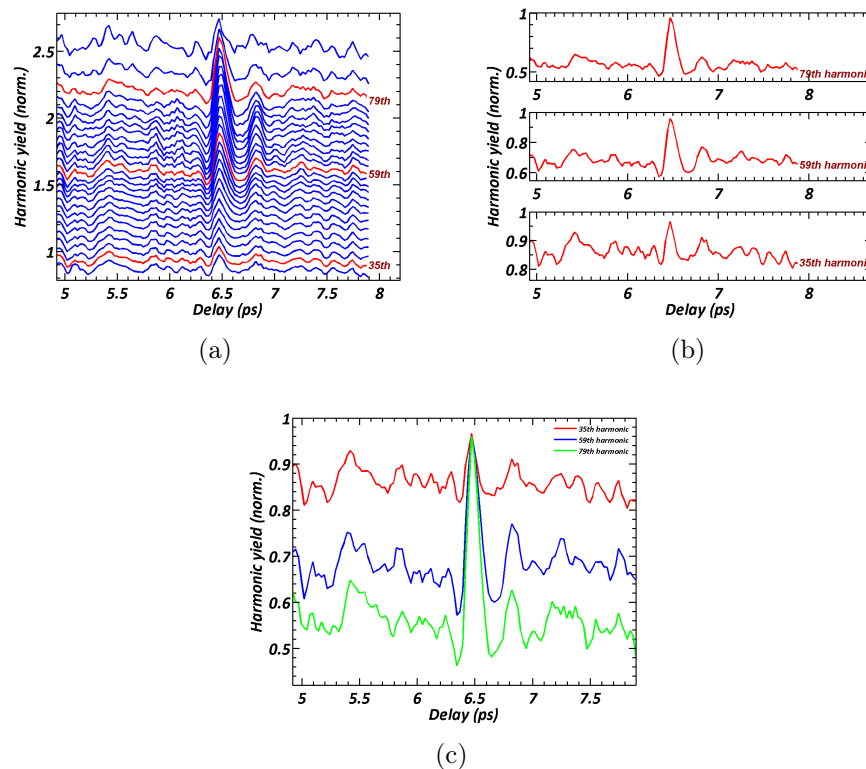
Figure 4.22: *Harmonic yield with respect to the time delay between pump and probe from aligned $N2O$ molecules along the 1/6 revival, normalized to the maximum of each harmonic within the revival:(a) waterfall of harmonic yields in which harmonic order increase from the bottom to the top, the normalized harmonic yields are spaced by a constant quantity; (b) comparison of the red colored harmonic in the waterfall; (c) superposition of the three underlined harmonics. The fundamental photon energy is equal to $E_0 = 0.853$ eV. The data are smoothed in order to make the view of the graph clearer. Pump and probe have parallel polarizations.*

4.3   Conclusions

The half revival behaviour with respect to the harmonic order is well known and connected to the orbital symmetry of the investigated molecules. In addition in both CO_2 and N_2O the higher-order fractional revivals present a change in their structure moving from low harmonics to high harmonics. In CO_2 the $1/8$ and $1/16$ revivals are visible and exhibit weak variations, whereas the $1/8$, $1/4$ and $1/6$ revivals visible in N_2O experience clearer modifications of their shape with increasing harmonic order.

We checked the appearance of the fractional revivals in the harmonic emission from impulsively aligned gases of CO_2 and N_2O, discussed their behaviour and observed that their shape is sensitive to the harmonic orders. All the sets of analyzed spectra experience a variation of the revival shape, independently on the fractional revival nature, with respect to the increasing of the harmonic order. This fact may lead to new spectroscopic information based on the observation of the high-order fractional revivals in the HHG spectra. We saw the importance of the molecular orbitals (HOMO) in the appearance of fractional revivals in HHG emission from impulsively aligned molecule; the changes of the intensity modulation among different harmonic orders paves the way to possible applications in the molecular orbital tomography and spectroscopy. Few works are present in literature about such argument and the existing ones [26, 2] regard the study of fractional revivals in harmonic emission generated by a $800\,\mathrm{nm}$ probe pulse. For these measures we used a $1450\,\mathrm{nm}$ generating pulse in order to extend the cutoff and thus observe more harmonic orders. The availability of more harmonics allows to observe the revival shape modifications within a higher spectral range. It's the first time that the fractional revivals are observed in harmonic emission generated by a mid-IR laser pulse. More investigations are needed about the nature of the observed modulations of the high-order fractional revivals in order to establish if such variations encode some information, depending on the harmonic order, about

the property and the symmetry of the molecular orbitals, as in the case of the half revival.

A very interesting aspect is that the high order fractional revivals could be more sensitive to multi-orbital contribution in HHG, since high harmonics can be produced also by lower-energy orbitals than HOMO. In fact, as we discussed in the section 2.3.1, the fractional revival shape changes with respect to the symmetry of the orbital that contributes to the harmonic emission [2]. Moreover, the possibility to correlate each fractional revival to a specific dipole moment element allows to extract information about the attosecond electronic motions and could be exploit to explore the role of the multiple orbitals [26]. Hence the structure of the fractional revivals can provide information not only about the rotational coherence, but also on the high harmonic dipole and the multichannel contribution to the harmonic emission.

Appendix A

Molecular orbitals

The problem of calculation of molecular orbitals consists in solving the time-dependent Schrödinger equation for a molecule:

$$i\hbar\frac{\partial}{\partial t}\ket{\Psi_{mol}(\vec{r},\vec{R},t)} = H_{mol}\ket{\Psi_{mol}(\vec{r},\vec{R},t)} \qquad (A.1)$$

where $\vec{r}$ is the vector of the all electrons coordinates and $\vec{R}$ is the vector of the all nuclei coordinates. By defining $\vec{R}_\alpha$ the position of the α-th nucleus ($\alpha = 1 \div N$) with atomic number z_α and $\vec{r}_i$ the position of the i-th electron ($i = 1 \div \mathcal{N}$), we can write the explicit expression of H_{mol}:

$$H_{mol} = -\frac{\hbar^2}{2}\sum_{\alpha=1}^{N}\frac{1}{M_\alpha}\nabla_\alpha^2 +$$

$$-\frac{\hbar^2}{2m_e}\sum_{i=1}^{\mathcal{N}}\nabla_i^2 +$$

$$+\sum_{\alpha<\beta}\frac{z_\alpha z_\beta e^2}{4\pi\epsilon_0|\vec{R}_\alpha - \vec{R}_\beta|} +$$

$$+\sum_{i<j}\frac{e^2}{4\pi\epsilon_0|\vec{r}_i - \vec{r}_j|} +$$

$$-\sum_{\alpha,i}\frac{z_\alpha e^2}{4\pi\epsilon_0|\vec{R}_\alpha - \vec{r}_i|}$$

where the addends are respectively the total kinetic energy of the nuclei, the total kinetic energy of the electrons, the total repulsive potential energy arising

from the interaction between the nuclei, the total repulsive potential energy arising from the interaction between the electrons and the total attractive potential energy arising from the interaction between the nuclei and the electrons. Since equation A.1 has not analytical solutions we use some approximations in order to simplify and thus solve the Schrödinger equation:

- **Born-Oppenheimer (BO) approximation**: since the electrons mass is much smaller than the mass of the nuclei ($m_N/m_e \simeq 2000$), the two dynamics occur in a different timescale thus the nuclei problem can be treated separately from the electron problem and the total wave function can be factorized into two terms:

$$|\Psi_{mol}(\vec{r}, \vec{R})\rangle = |\Psi_{el,\vec{R}}(\vec{r})\rangle \, |\Phi_N(\vec{R})\rangle \tag{A.2}$$

where $|\psi_{el,\vec{R}}(\vec{r})\rangle$ is the electronic wave function at a fixed nuclei configuration and $|\Phi_N(\vec{R})\rangle$ is the nuclear wave function. We can solve first the electrons problem by considering the nuclei as stationary and then the nuclei problem by using an effective potential energy given by the sum of the nuclei interaction potential energy to the energy configuration of electrons.

- **Orbital approximation**: by neglecting the electron-electron interaction we can factorize the molecular electronic eigenfunction in

$$|\Psi_{el}(\vec{r})\rangle = |\psi_1(\vec{r}_1)\rangle \, |\psi_2(\vec{r}_2)\rangle \, |\psi_3(\vec{r}_3)\rangle \ldots |\psi_{\mathcal{N}}(\vec{r}_{\mathcal{N}})\rangle \tag{A.3}$$

where $|\psi_i(\vec{r}_i)\rangle$ is the *molecular orbital*. The $|\Psi_{el}(\vec{r})\rangle$ is the molecular electronic eigenfunction and describes the all electrons population. The orbital is a one-electron function, thus very different from the eigenfunction because describes the spatial distribution of one electron. The molecular orbitals are delocalized on the molecule.

- **LCAO (Linear Combination of Atomic Orbital) approximation**: a generic molecular orbital can be written as a linear combination of atomic

orbitals

$$|\psi_i(\vec{r}_i)\rangle = \sum_j c_{ij} |\phi_j(\vec{r}_j)\rangle \tag{A.4}$$

In equation A.4 the outermost atomic orbitals are characterized by higher values of the coefficients c_{ij} because they most contribute to the bond, instead the core atomic orbitals give no contribution to the bond, thus the corresponding coefficients are zero.

We can write the Hamiltonian in terms of K and V that are the kinetic energy operator and the potential energy operator respectively:

$$H_{mol} = K_{el} + V_{el,el}(\vec{r}) + V_{el,N}(\vec{r}, \vec{R}) + K_N + V_{N,N}(\vec{R})$$

The eigenvalues equation becomes:

$$\left(K_{el} + V_{el,el}(\vec{r}) + V_{el,N}(\vec{r}, \vec{R}) \right) |\Psi_{el,\vec{R}}(\vec{r})\rangle |\Phi_N(\vec{R})\rangle +$$
$$+ \left(K_N + V_{N,N}(\vec{R}) \right) |\Psi_{el,\vec{R}}(\vec{r})\rangle |\Phi_N(\vec{R})\rangle = \mathcal{E}_{mol} |\Psi_{el,\vec{R}}(\vec{r})\rangle |\Phi_N(\vec{R})\rangle$$

We can solve separately the electrons problem by exploiting the BO approximation: electronic part depends parametrically on the set of nuclei coordinates $\vec{R}$. For every nuclei configuration we suppose that the Schrödinger equation is verified:

$$\left(K_{el} + V_{el,el}(\vec{r}) + V_{el,N}(\vec{r}, \vec{R}) \right) |\Psi_{el,\vec{R}}(\vec{r})\rangle = \mathcal{E}_{el,\vec{R}} |\Psi_{el,\vec{R}}(\vec{r})\rangle \tag{A.5}$$

From (A.5) we extract the $|\Psi_{el,\vec{R}}(\vec{r})\rangle$ and the $\mathcal{E}_{el,\vec{R}}$ for a such configuration of nuclei position. If we repeat the computation for a range of the set $\vec{R}$, we obtain electronic eigenvalues as function of nuclei position $\mathcal{E}_{el,\vec{R}}(\vec{R})$:

$$\mathcal{E}_{el,\vec{R}}(\vec{R}) |\Psi_{el,\vec{R}}(\vec{r})\rangle |\Phi_N(\vec{R})\rangle + \left(K_N + V_{N,N}(\vec{R}) \right) |\Psi_{el,\vec{R}}(\vec{r})\rangle |\Phi_N(\vec{R})\rangle =$$
$$\mathcal{E}_{mol} |\Psi_{el,\vec{R}}(\vec{r})\rangle |\Phi_N(\vec{R})\rangle \tag{A.6}$$

By multiplying the (A.6) for $\left\langle \Psi_{el,\vec{R}}(\vec{r}) \right|$ the eigenvalues equation for a molecule becomes:

$$-\hbar^2 \sum_\alpha \frac{1}{2M_\alpha} \nabla_\alpha^2 |\Phi_N(\vec{R})\rangle + V_{BO}(\vec{R}) |\Phi_N(\vec{R})\rangle = \mathcal{E}_{mol} |\Phi_N(\vec{R})\rangle$$

where $V_{BO}(\vec{R}) = V_{N,N}(\vec{R}) + \mathcal{E}_{el,\vec{R}}(\vec{R})$ is the effective potential that takes into account the presence of the electrons in the Schrödinger equation for the nuclei and $\mathcal{E}^g_{el,\vec{R}}(\vec{R})$ are the electronic eigenvalues depending on the nuclei configuation; an electronic transition produces variations in BO-potential. The effective potential, called *Potential Energy Surface* (PES), exhibits a minimum at the interatomic distance corresponding to the equilibrium distance of atoms. The molecular orbital can be calculated by exploiting the Hartree-Fock (HF) method, also known as self-consistent-field method. We compute first the atomic orbitals for each component of molecule with the HF method and then we combine them, each centered on their respective nucleus, by exploiting the LCAO theory. The atomic eigenfunction is a multi-electronic wave function and can be approximated by an antisymmetrized product of atomic orbitals. The HF method assumes that the electron-electron interaction $V_{el,el} = \sum_{i<j} \frac{e^2}{4\pi\epsilon_0 |\vec{r}_i - \vec{r}_j|}$ can be replaced by $\sum_i V_{el,i}(\vec{r}_i)$, where $V_{el,i}(\vec{r}_i)$ is the potential felt by the i-th electron and exerted on it by the mean field created by others. HF method is not the only one used for calculating molecular orbitals.

In LCAO theory the atomic orbitals represent a basis for the construction of molecular orbitals. The molecular orbitals contain the information about the symmetry of the molecule. Let's consider for simplicity a omonuclear diatomic molecule with only one orbital per atom, ϕ_A and ϕ_B. There are two possible combinations of these atomic orbitals, one at lower energy and one at higher energy. The molecular orbital at lower energy is called bonding and the one at higher energy is called anti-bonding (identified by *). A molecule with more than two atoms has more bonding and anti-bonding orbitals. These orbitals are characterized by the following symmetry properties:

- **Symmetry with respect to molecular axis:**

    $\sigma(m_l = 0)$: no nodal plane containing the internuclear axis (cylindrical symmetry)

$\pi(m_l = \pm 1)$: one nodal plane containing the internuclear axis

$\delta(m_l = \pm 2)$: two nodal plane containing the internuclear axis

- **Inversion symmetry with respect to the center of the molecule:**

  gerade(even): if an infinitesimal element of the molecular orbital doesn't change its sign under an inversion with respect to the inversion center of molecule;

  ungerade(odd): if an infinitesimal element of the molecular orbital changes its sign under an inversion with respect to the inversion center of molecule.

We can note that the orbital σ is always gerade and the orbital σ^* is always ungerate. The inversion center coincides with the center of molecule and is the point in which the π-rotational axis and the orthogonal reflection plane intersect the molecular axis. In molecules we don't find orbitals with spherical symmetry that is typical of atoms, thus we can't define the quantum number l because the angular momentum is not conserved. The projection along molecular axis of the angular momentum, instead, is conserved and thus m_l is a good quantum number. Two of the all bound and anti-bound orbitals of a molecule are more important than others:

HOMO: Highest Occupied Molecular Orbital

LUMO: Lowest Unoccupied Molecular Orbital

The HOMO orbital is very important because defines the properties of the bound and its energy determines the effective potential in which occurs the nuclear motion. The LOMO orbital determines the behaviour of molecule interacting with an external electric field. If the LUMO behaviour is the same of figure A.1, an excitation produces the molecular dissociation since potential energy decreases by increasing the internuclear distance d.
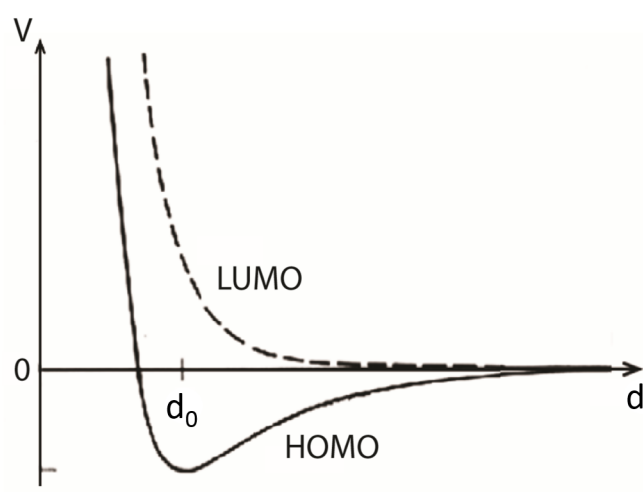
Figure A.1: *Potential Energy Surface of the HOMO orbitals (solid line) and of the LUMO orbitals (dashed line). The minimum at distance d_0 is the equilibrium internuclear distance.*

Appendix B

Rigid rotor molecule

As seen in appendix A, by exploiting the Born-Oppenheimer approximation we can reduce the molecular Hamiltonian to the nuclear dynamics since electronic dynamics is taken into account by the electrons eigenvalues at various nuclei position, included in the effective potential exerted on the nuclei. If N is the number of nuclei, the molecule has 3N degrees of freedom whose 3N-6 (3N-5 for linear molecules that don't have the rotation along the molecular axis) are the internal degrees of freedom and the remaining ones are the cartesian coordinates in the laboratory frame. The internal 3N-6 coordinates are called vibrational normal mode and can describe the system if we choose a reference frame that moves and rotates together with the molecule. The molecular Hamiltonian can be partitioned as follows:

$$H_{mol} = H_{CM} + H_{rot} + H_{vib} \tag{B.1}$$

where $H_{CM} = -\frac{\hbar^2}{2\mu}\nabla^2_{\vec{R}}$ is the Hamiltonian of the center of mass, with μ reduced mass, H_{rot} is the rotational Hamiltonian and $H_{vib} = K_{vib} + V_{vib}$ is the vibrational Hamiltonian, with K_{vib} and V_{vib} vibrational kinetic energy and vibrational potential energy operators respectively. The effective potential V_{BO} introduced in Appendix A can be approximated around the minimum by a parabolic potential V_{vib}. The nuclei oscillate around the equilibrium position like the harmonic

oscillator, thus the energy associated to the vibrational states is:

$$\mathcal{E}_{vib} = \hbar\omega_0\left(\nu + \frac{1}{2}\right) \qquad \nu = 0, 1, 2... \tag{B.2}$$

where ω_0 is the characteristic oscillation frequency of the molecule and ν is the vibrational quantum number.

The others 6 (5 for linear molecule) degrees of freedom divide into 3 translational coordinates of the center of mass and 3 (2 for linear molecule) rotational degrees of freedom.

The molecule with all its masses, that occupy specific positions, is considered as a rigid body. However the rigid body is an approximation because rotations interact with vibrations and this fact is taken into account by a correction term due to the Coriolis forces, that is neglected in this treatment. The molecule can rotate around one or more of its axes, as well as a rigid rotor, in the three-dimensional space with a rotational angular momentum:

$$\vec{J} = I\vec{\omega} \tag{B.3}$$

In (B.3) $I = \sum_i m_i r_i^2$ is the moment of inertia, where the m_i are point mass and the r_i are the distances of the masses from the rotational axis, and $\vec{\omega}$ is the angular velocity. A more general definition of the rotational angular momentum is needed if the rotational axis is not known:

$$\vec{J} = \underline{\underline{I}}\vec{\omega} \tag{B.4}$$

where $\underline{I}$ is the tensor of inertia. A tensor can be always reduced to its principal axes, thus the tensor of inertia can be decomposed in the moments of inertia around the three principal axes of the molecule: I_A, I_B, I_C (conventionally $I_A < I_B < I_C$, see figure B.1). The kinetic energy operator reduced to the three principal axes is:

$$K_{rot} = \frac{J_A^2}{2I_A} + \frac{J_B^2}{2I_B} + \frac{J_C^2}{2I_C} \tag{B.5}$$
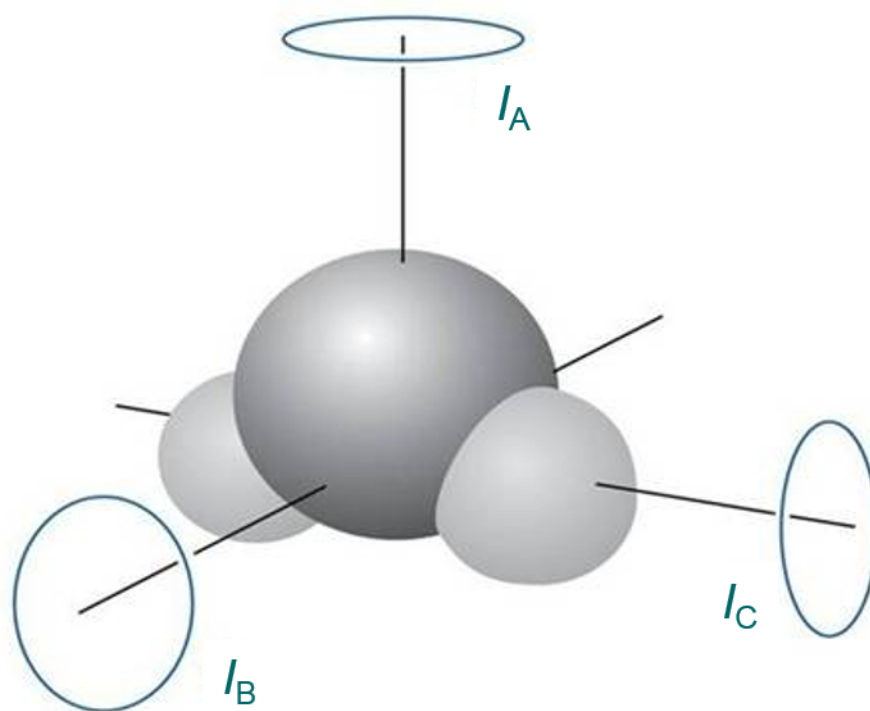
Figure B.1: *The rigid rotor molecule with its three moments of inertia; conventionally $I_A < I_B < I_C$.*
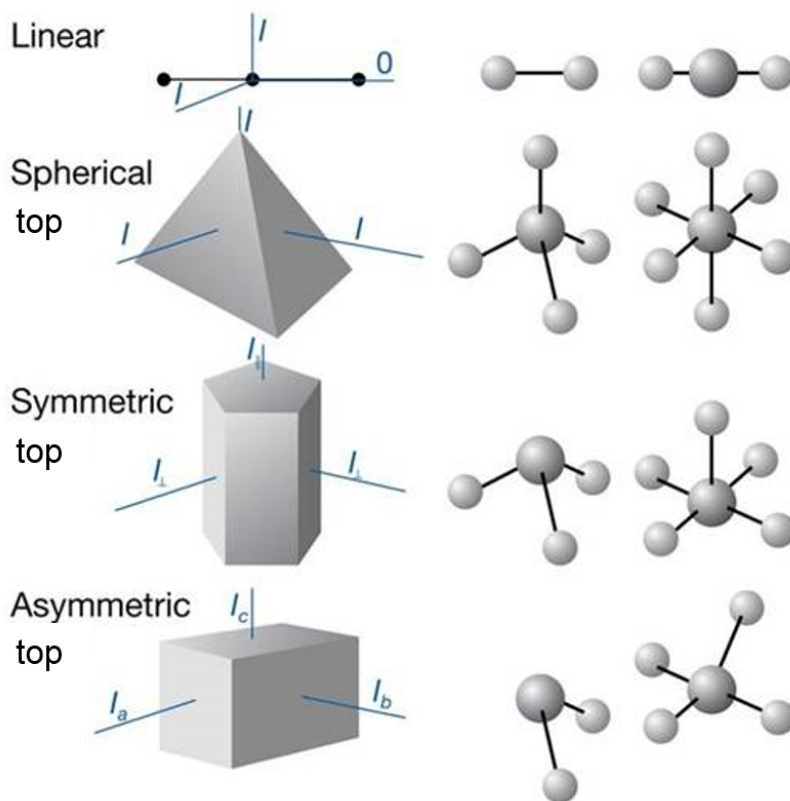
Figure B.2: *Molecules symmetry classification. Examples of linear molecules are CO, CO_2, N_2O, for spherical top are CH_4, SF_6, for symmetric top NH_3 and for asymmetric top H_2O. The symmetric top represented is oblate.*

Let's now define the rotational constants:

$$
\begin{aligned}
A &= \frac{\hbar^2}{2I_A} \\
B &= \frac{\hbar^2}{2I_B} \\
C &= \frac{\hbar^2}{2I_C}
\end{aligned}
\tag{B.6}
$$

The molecules can be divided into three classes depending on the values of the moments of inertia (figure B.2):

- *Spherical top*, if all three moments of inertia are equal and nonzero $I_A = I_B = I_C$; molecules with this symmetry has not permanent dipole moment and has an isotropic polarizability, thus no pure rotational transition can be observed.

- *Linear*, if the molecules have just one moment of inertia, conventionally chosen equal to $I_B = \mu r_0^2$, that corresponds to a rotation axis perpendicular to the molecular axis.

- *Symmetric top*, if only two moments of inertia are equal, but distinct from the third; we can distinguish two rotor types having this symmetry:

  oblate, if $I_A = I_B < I_C$

  prolate, if $I_A < I_B = I_C$

- *Asymmetric top*, if all three moments of inertia are different $I_A \neq I_B \neq I_C$; by defining the asymmetry parameter

$$k = \frac{2B - A - C}{A - C} \tag{B.7}$$

  we divide molecules in those close to the oblate limit for k>0 and those close to the prolate limit for k<0.

The kinetic energy of a linear rigid rotor is given by

$$K_{rot} = \frac{1}{2} I \omega^2 \tag{B.8}$$

In a linear molecule that we approximate as a rigid rotor, characterized by a rotational angular momentum $\hat{\vec{J}}$ and an angular quantum number J, the rotational Hamiltonian can be written as

$$H_{rot} = \frac{\hat{J}^2}{2I} \tag{B.9}$$

and the rotational energy level as:

$$\mathcal{E}_{rot} = \frac{\hbar^2}{2I} J(J + 1) = BJ(J + 1) \tag{B.10}$$

A linear molecule has two rotational degrees of freedom that correspond to the spherical coordinates θ and ϕ. By considering that $\hat{\vec{J}} = -i\hbar \vec{\nabla}$ and by expressing
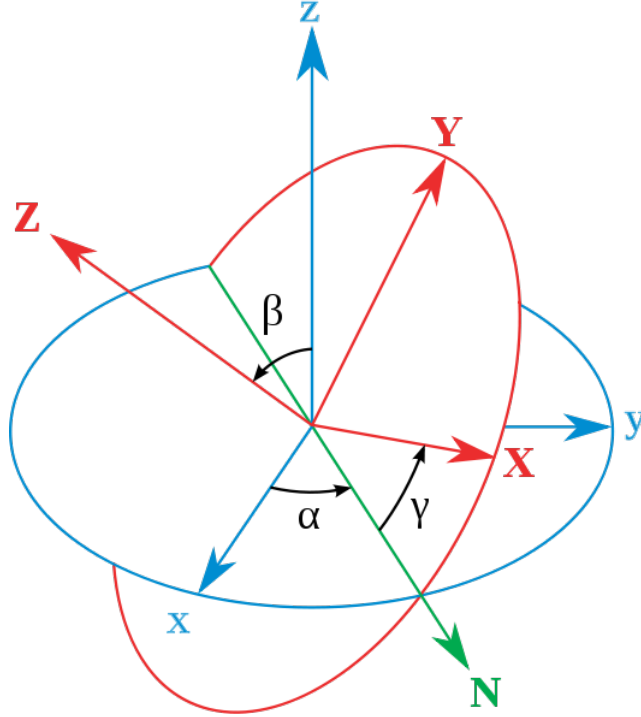
Figure B.3: *Euler angles representing rotations about z, N and Z. The xyz original system is shown in blue, the XYZ rotated system is shown in red, the line of nodes N is shown in green.*

the Laplace operator ∇^2 in terms of the spherical coordinates (only its angular part) we obtain:

$$H_{rot} = -\frac{\hbar^2}{2I}\left[\frac{1}{\sin\theta}\frac{\partial}{\partial\theta}\left(\sin\theta\frac{\partial}{\partial\theta}\right) + \frac{1}{\sin^2\theta}\frac{\partial^2}{\partial\phi^2}\right] \tag{B.11}$$

Usually in spectroscopy the energy levels are expressed in $\mathcal{F}_{cm^{-1}}$

$$\mathcal{F}_{cm^{-1}} = \frac{\mathcal{E}_{rot}}{hc} = \frac{\hbar h J(J+1)}{2\pi hcI} = \frac{\hbar}{4\pi cI}J(J+1)$$

If we define the rotational constant in cm^{-1} $\tilde{B} = B/hc$ the energy level can be written as

$$\mathcal{F}_{cm^{-1}} = \tilde{B}J(J+1) \tag{B.12}$$

A molecule characterized by a non linear symmetry has 3 rotational degrees of freedom and the three coordinates are called Euler angles α,β,γ. Every reference frame rotation can be considered as a sequence of three rotations (figure B.3):

- $\alpha \in (0, 2\pi)$: represents a rotation around the z axis,

- $\beta \in (0, \pi))$: represents a rotation around the x' axis,

- $\gamma \in (0, 2\pi)$: represents a rotation around the z" axis.

Appendix C

Calculation of rotational states in impulsive aligned molecules

The Schrödinger equation for a single molecule subject to a nonresonant electric field is:

$$i\hbar\frac{\partial}{\partial t}\Psi(t) = H(t)\Psi(t) \tag{C.1}$$

where the Hamiltonian H(t) is the effective Hamiltonian introduced in chapter 2 [17]:

$$H(t) = B\hat{J}^2 - D\hat{J}^4 - \frac{1}{2}E^2(t)\left[\alpha_\parallel \cos^2\theta + \alpha_\perp \sin^2\theta\right] =$$
$$= B\hat{J}^2 - D\hat{J}^4 - \frac{1}{2}E^2(t)\left[(\alpha_\parallel - \alpha_\perp)\cos^2\theta + \alpha_\perp\right] \tag{C.2}$$

In the equation (C.2) $\hat{\vec{J}}$ is the dimensionless angular momentum operator defined as $\hat{\vec{J}} = -i\vec{\nabla}$, $B = \frac{\hbar^2}{2I}$ is the rotational constant, E(t) is the electric field with gaussian temporal profile ($E(t) = g(t)E_0\cos(\omega t)$), $\alpha_\parallel$ and $\alpha_\perp$ are respectively the parallel and perpendicular components of the static polarizability with respect to the molecular axis, θ is the polar angle between the molecular axis and the polarization direction of the electric field and $D\hat{J}^4$ is the centrifugal correction (figure C.1). Let's define the dimensionless interaction parameters:

$$\beta_\parallel(t) = \frac{\alpha_\parallel E^2(t)}{2B}$$
$$\beta_\perp(t) = \frac{\alpha_\perp E^2(t)}{2B} \tag{C.3}$$
$$\Delta\beta(t) = \beta_\parallel(t) - \beta_\perp(t)$$

103
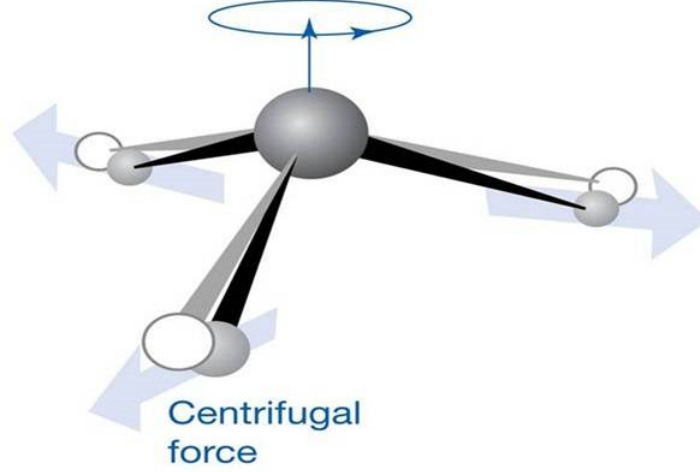
Figure C.1: *Schematic representation of the effect of the centrifugal force due to the rotation.*

where $\Delta\beta(t)$ determines the degree of anisotropy of the molecule, i.e. how susceptible is the molecule to alignment by the external electric field. The solutions of the equation (2.22) depend on $\Delta\beta(t)$, $\Psi = \Psi(\Delta\beta(t))$, and can be expanded in a series of field-free rotor wave functions $|J, M\rangle$:

$$\Psi(t) = \sum_{J} d_J(t) |J, M\rangle \tag{C.4}$$

where the $|J, M\rangle$ are defined as:

$$|J, M\rangle = Y_{JM}(\theta, \phi) = (-1)^M \left[\frac{2J+1}{4\pi} \frac{(J-M)!}{(J+M)!} \right]^{1/2} P_J^M(\cos\theta) e^{iM\phi} \tag{C.5}$$

The problem to calculate the solutions of the time-dependent Schrödinger equation is reduced to find the expansion coefficients of the $\Psi(t)$. We have to substitute the expression (C.4) to the equation (C.1).

$$i\hbar \frac{\partial}{\partial t} \Psi(t) = \left[B\hat{J}^2 - D\hat{J}^4 - \frac{1}{2} E^2(t) \left((\alpha_\| - \alpha_\perp) \cos^2\theta + \alpha_\perp \right) \right] \Psi(t) \tag{C.6}$$

Now we substitute $\Psi(t)$ with the expression (C.4)

$$i\hbar \frac{\partial}{\partial t} \left(\sum_{J'} d_{J'}(t) |J', M\rangle \right) = \left[B\hat{J}^2 - D\hat{J}^4 - \frac{1}{2} E^2(t) \left((\alpha_\| - \alpha_\perp) \cos^2\theta + \alpha_\perp \right) \right] \times$$

$$\times \left(\sum_{J'} d_{J'}(t) |J', M\rangle \right)$$

$$\Downarrow$$

$$i\hbar\frac{\partial}{\partial t}\left(\sum_{J'}d_{J'}(t)\,|J',M\rangle\right)=\left(B\hat{J}^2-D\hat{J}^4-\frac{1}{2}E^2(t)\alpha_\perp\right)\left(\sum_{J'}d_{J'}(t)\,|J',M\rangle\right)+$$

$$-\frac{1}{2}E^2(t)\Big(\left(\alpha_\parallel-\alpha_\perp\right)\cos^2\theta\Big)\left(\sum_{J'}d_{J'}(t)\,|J',M\rangle\right)$$

$$\Downarrow$$

$$i\hbar\sum_{J'}\frac{\partial}{\partial t}d_{J'}(t)\,|J',M\rangle=\sum_{J'}d_{J'}(t)\left(B\hat{J}^2-D\hat{J}^4-\frac{1}{2}E^2(t)\alpha_\perp\right)|J',M\rangle+$$

$$-\frac{1}{2}E^2(t)(\alpha_\parallel-\alpha_\perp)\sum_{J'}d_{J'}(t)\cos^2\theta\,|J',M\rangle$$

By multiplying both of the members for $\langle J,M|$ we obtain:

$$i\hbar\sum_{J'}\frac{\partial}{\partial t}d_{J'}(t)\,\langle J,M\,|\,J',M\rangle=\sum_{J'}d_{J'}(t)\left\langle J,M\,\Big|\,B\hat{J}^2\,\Big|\,J',M\right\rangle+$$

$$-\sum_{J'}d_{J'}(t)\left\langle J,M\,\Big|\,D\hat{J}^4\,\Big|\,J',M\right\rangle+$$

$$-\frac{1}{2}E^2(t)\alpha_\perp\sum_{J'}d_{J'}(t)\,\langle J,M\,|\,J',M\rangle+$$

$$-\frac{1}{2}E^2(t)(\alpha_\parallel-\alpha_\perp)\sum_{J'}d_{J'}(t)\left\langle J,M\,\big|\,\cos^2\theta\,\big|\,J',M\right\rangle$$

We remember that:

$$B\hat{J}^2\,|J,M\rangle=BJ(J+1)\,|J,M\rangle \tag{C.7}$$

$$D\hat{J}^4\,|J,M\rangle=DJ^2(J+1)^2\,|J,M\rangle \tag{C.8}$$

The $|J,M\rangle$ constitutes an orthonormal basis on which the solutions $\Psi(t)$ are projected, thus their scalar product is equal to the Kronecker Delta:

$$\langle J,M\,|\,J',M\rangle=\delta_{JJ'} \tag{C.9}$$

Hence we obtain:

$$i\hbar\frac{\partial}{\partial t}d_J(t)=\left(BJ(J+1)-DJ^2(J+1)^2-\frac{1}{2}E^2(t)\alpha_\perp\right)d_J(t)+$$

$$-\frac{1}{2}E^2(t)(\alpha_\parallel-\alpha_\perp)\sum_{J'}d_{J'}(t)\left\langle J,M\,\big|\,\cos^2\theta\,\big|\,J',M\right\rangle \tag{C.10}$$

By considering the following recurrence relations for Legendre polynomials

$$(2J+1)\cos\theta P_J^M(\cos\theta) = (J+M)P_{J-1}^M(\cos\theta) + (J-M+1)P_{J+1}^M(\cos\theta) \quad \text{(C.11)}$$

and that

$$|J-1,M\rangle = (-1)^M \left[\frac{2J-1}{4\pi}\frac{(J-1-M)!}{(J-1+M)!}\right]^{1/2} P_{J-1}^M(\cos\theta)e^{iM\phi} \quad \text{(C.12)}$$

$$\Downarrow$$

$$(-1)^M P_{J-1}^M(\cos\theta)e^{iM\phi} = \left[\frac{4\pi}{2J-1}\frac{(J-1+M)!}{(J-1-M)!}\right]^{1/2} |J-1,M\rangle \quad \text{(C.13)}$$

$$|J+1,M\rangle = (-1)^M \left[\frac{2J+3}{4\pi}\frac{(J+1-M)!}{(J+1+M)!}\right]^{1/2} P_{J+1}^M(\cos\theta)e^{iM\phi} \quad \text{(C.14)}$$

$$\Downarrow$$

$$(-1)^M P_{J+1}^M(\cos\theta)e^{iM\phi} = \left[\frac{4\pi}{2J+3}\frac{(J+1+M)!}{(J+1-M)!}\right]^{1/2} |J+1,M\rangle \quad \text{(C.15)}$$

we can find:

$$\cos\theta\,|J,M\rangle = (-1)^M \left[\frac{2J+1}{4\pi}\frac{(J-M)!}{(J+M)!}\right]^{1/2} \cos\theta P_J^M(\cos\theta)e^{iM\phi}$$

$$\Downarrow$$

$$\cos\theta\,|J,M\rangle = (-1)^M e^{iM\phi} \left[\frac{2J+1}{4\pi}\frac{(J-M)!}{(J+M)!}\frac{(J+M)^2}{(2J+1)^2}\right]^{1/2} P_{J-1}^M(\cos\theta) +$$

$$+ (-1)^M e^{iM\phi} \left[\frac{2J+1}{4\pi}\frac{(J-M)!}{(J+M)!}\frac{(J-M+1)^2}{(2J+1)^2}\right]^{1/2} P_{J+1}^M(\cos\theta)$$

$$\Downarrow$$

$$\cos\theta\,|J,M\rangle = \left[\frac{2J+1}{4\pi}\frac{(J-M)!}{(J+M)!}\frac{(J+M)^2}{(2J+1)^2}\right]^{1/2} \times$$

$$\times \left[\frac{4\pi}{2J-1}\frac{(J-1+M)!}{(J-1-M)!}\right]^{1/2} |J-1,M\rangle +$$

$$+ \left[\frac{2J+1}{4\pi}\frac{(J-M)!}{(J+M)!}\frac{(J-M+1)^2}{(2J+1)^2}\right]^{1/2} \times$$

$$\times \left[\frac{4\pi}{2J+3}\frac{(J+1+M)!}{(J+1-M)!}\right]^{1/2} |J+1,M\rangle$$

By making some simplifications we have that:

$$
\cos\theta\,|J,M\rangle = \left[\frac{(J-M)(J+M)}{(2J+1)(2J-1)}\right]^{1/2}|J-1,M\rangle + \\
+ \left[\frac{(J-M+1)(J+1+M)}{(2J+1)(2J+3)}\right]^{1/2}|J+1,M\rangle \tag{C.16}
$$

Now we calculate:

$$
\cos^2\theta\,|J,M\rangle = \cos\theta\Big(\cos\theta\,|J,M\rangle\Big) = \cos\theta\Bigg(\sqrt{\frac{(J-M)(J+M)}{(2J+1)(2J-1)}}\,|J-1,M\rangle + \\
+ \sqrt{\frac{(J-M+1)(J+1+M)}{(2J+1)(2J+3)}}\,|J+1,M\rangle\Bigg)
$$

$$\Downarrow$$

$$
\cos^2\theta\,|J,M\rangle = \sqrt{\frac{(J-M)(J+M)}{(2J+1)(2J-1)}}\Bigg(\sqrt{\frac{(J-1-M)(J-1+M)}{(2J-1)(2J-3)}}\,|J-2,M\rangle + \\
+ \sqrt{\frac{(J-M)(J+M)}{(2J-1)(2J+1)}}\,|J,M\rangle\Bigg) + \\
+ \sqrt{\frac{(J-M+1)(J+1+M)}{(2J+1)(2J+3)}}\times \\
\times\Bigg(\sqrt{\frac{(J-M+1)(J+1+M)}{(2J+3)(2J+1)}}\,|J,M\rangle + \\
+ \sqrt{\frac{(J-M+2)(J+2+M)}{(2J+3)(2J+5)}}\,|J+2,M\rangle\Bigg)
$$

$$\Downarrow$$

$$
\cos^2\theta\,|J,M\rangle = \sqrt{\frac{(J-M)(J+M)(J-M-1)(J+M-1)}{(2J+1)(2J-1)^2(2J-3)}}\,|J-2,M\rangle + \\
+ \left(\frac{(J-M)(J+M)}{(2J+1)(2J-1)} + \frac{(J-M+1)(J+M+1)}{(2J+3)(2J+1)}\right)|J,M\rangle + \\
+ \sqrt{\frac{(J-M+1)(J+M+1)(J-M+2)(J+M+2)}{(2J+1)(2J+3)^2(2J+5)}}\,|J+2,M\rangle
$$

We can factorize the second term in (C) as follows:

$$\frac{(J-M)(J+M)}{(2J+1)(2J-1)} + \frac{(J-M+1)(J+M+1)}{(2J+3)(2J+1)} =$$
$$= \frac{(J^2-M^2)(2J+3) + (J^2+2J+1-M^2)(2J-1)}{(2J+1)(2J-1)(2J+3)} =$$
$$= \frac{(J^2-M^2+J^2+2J+1-M^2)(2J+1) - 2(2J+1)}{(2J+1)(2J-1)(2J+3)} =$$
$$= \frac{2J^2-2M^2+2J-1}{(2J-1)(2J+3)}$$

We finally rewrite the expression of $\cos^2\theta\,|J,M\rangle$ as

$$\cos^2\theta\,|J,M\rangle = a_0(J,M)\,|J,M\rangle + a_{+2}(J,M)\,|J+2,M\rangle + a_{-2}(J,M)\,|J-2,M\rangle \tag{C.17}$$

where we have defined the following coefficients:

$$a_0(J,M) = \frac{2(J^2-M^2+J)-1}{(2J-1)(2J+3)} = \frac{1}{3} + \frac{2}{3}\left(\frac{J(J+1)-3M^2}{(2J+3)(2J-1)}\right) \tag{C.18}$$

$$a_{+2}(J,M) = \sqrt{\frac{(J-M+1)(J+M+1)(J-M+2)(J+M+2)}{(2J+1)(2J+3)^2(2J+5)}} \tag{C.19}$$

$$a_{-2}(J,M) = \sqrt{\frac{(J-M)(J+M)(J-M-1)(J+M-1)}{(2J+1)(2J-1)^2(2J-3)}} \tag{C.20}$$

Let's consider also that:

$$a_{+2}(J-2,M) = \sqrt{\frac{(J-M-1)(J+M-1)(J-M)(J+M)}{(2J-3)(2J-1)^2(2J+1)}}$$

$$a_{-2}(J+2,M) = \sqrt{\frac{(J-M+2)(J+M+2)(J-M+1)(J+M+1)}{(2J+5)(2J+3)^2(2J+1)}}$$

From the calculations we can notice that the operator $\cos^2\theta$ applied to a state $|J,M\rangle$ produces a sum of three states $|J,M\rangle$, $|J+2,M\rangle$ and $|J-2,M\rangle$ multiplied for appropriate coefficients, which are functions of the quantum numbers J and

M. By using these results we can rewrite the system of equations (C.10) as:

$$
\begin{aligned}
\frac{\partial}{\partial t} d_J(t) = &\frac{1}{i\hbar} \left(BJ(J+1) - DJ^2(J+1)^2 - \frac{1}{2}E^2(t)\alpha_\perp \right) d_J(t) + \\
&- \frac{1}{2}E^2(t)(\alpha_\parallel - \alpha_\perp) \sum_{J'} d_{J'}(t) a_0(J', M) \langle J, M \,|\, J', M \rangle + \\
&- \frac{1}{2}E^2(t)(\alpha_\parallel - \alpha_\perp) \sum_{J'} d_{J'}(t) a_{+2}(J', M) \langle J, M \,|\, J'+2, M \rangle + \\
&- \frac{1}{2}E^2(t)(\alpha_\parallel - \alpha_\perp) \sum_{J'} d_{J'}(t) a_{-2}(J', M) \langle J, M \,|\, J'-2, M \rangle
\end{aligned}
\tag{C.21}
$$

Since $\langle J, M \,|\, J', M \rangle = \delta_{JJ'}$, $\langle J, M \,|\, J'+2, M \rangle = \delta_{J(J'+2)}$ and $\langle J, M \,|\, J'-2, M \rangle = \delta_{J(J'-2)}$, the only nonzero matrix elements are respectively $J' = J$, $J' = J-2$ and $J' = J+2$:

$$
\begin{aligned}
\frac{\partial}{\partial t} d_J(t) = &\frac{B}{i\hbar} \left(J(J+1) - \frac{D}{B}J^2(J+1)^2 - \beta_\perp(t) - \Delta\beta(t) a_0(J, M) \right) d_J(t) + \\
&- \frac{B}{i\hbar} \Delta\beta(t) a_{+2}(J-2, M) d_{J-2}(t) + \\
&- \frac{B}{i\hbar} \Delta\beta(t) a_{-2}(J+2, M) d_{J+2}(t)
\end{aligned}
\tag{C.22}
$$

Finally the system of coupled differential equations can be written in the form:

$$
\dot{d_J}(t) = k_{-2}(t, J, M) d_{J-2}(t) + k_0(t, J, M) d_J(t) + k_{+2}(t, J, M) d_{J+2}(t) \tag{C.23}
$$

where we have defined:

$$
k_{-2}(t, J, M) = -\frac{B}{i\hbar} \Delta\beta(t) a_{+2}(J-2, M) \tag{C.24}
$$

$$
k_0(t, J, M) = \frac{B}{i\hbar} \left(J(J+1) - \frac{D}{B}J^2(J+1)^2 - \beta_\perp(t) - \Delta\beta(t) a_0(J, M) \right) \tag{C.25}
$$

$$
k_{+2}(t, J, M) = -\frac{B}{i\hbar} \Delta\beta(t) a_{-2}(J+2, M) \tag{C.26}
$$

We can write a temporal evolution matrix where rows are the starting state and columns the arrival state:

$$
\begin{bmatrix}
k_0(t,0) & 0 & k_{+2}(t,2) & 0 & 0 \\
0 & k_0(t,1) & 0 & k_{+2}(t,1) & 0 \\
k_{-2}(t,2) & 0 & k_0(t,2) & 0 & k_{+2}(t,2) \\
0 & k_{-2}(t,3) & 0 & k_0(t,3) & 0 \\
0 & 0 & k_{-2}(t,4) & 0 & k_0(t,4)
\end{bmatrix}
$$

Appendix D

Alignment parameter calculation for an anisotropic distribution

As affirmed in paragraph 2.1.2, in order to describe a thermal ensemble of molecules, each one characterized by a rotational state $|J, M\rangle$, we have to exploit the density matrix formalism. Let's remember that the density matrix is defined as

$$\rho = \sum_{J,M} p(J, M) |J, M\rangle \langle J, M| \tag{D.1}$$

We can calculate the expectation value of $\cos^2 \theta$ (alignment parameter) for a non-aligned thermal ensemble of molecules as

$$
\begin{aligned}
\langle \cos^2 \theta \rangle =& Tr(\rho \cos^2 \theta) = \\
=& \sum_{J,M} \langle J, M| \left(\sum_{J',M'} p(J', M') |J', M'\rangle \langle J', M'| \cos^2 \theta \right) |J, M\rangle = \\
=& \sum_{J,M} \sum_{J',M'} p(J', M') \langle J, M \,|\, J', M'\rangle \langle J', M'| \cos^2 \theta \,|J, M\rangle = \\
=& \sum_{J,M} p(J, M) \langle J, M \,|\, \cos^2 \theta \,|\, J, M \rangle = \\
=& \sum_{J,M} \frac{e^{-\frac{B(J(J+1))}{k_B T}}}{\sum_{J,M} e^{-\frac{B(J(J+1))}{k_B T}}} \Big(a_0(J) \langle J, M \,|\, J, M \rangle + \\
& + a_{-2}(J) \langle J, M \,|\, J-2, M \rangle + a_{+2}(J) \langle J, M \,|\, J+2, M \rangle \Big) = \\
=& \sum_{J,M} \frac{e^{-\frac{B(J(J+1))}{k_B T}}}{\sum_{J,M} e^{-\frac{B(J(J+1))}{k_B T}}} a_0(J)
\end{aligned}
$$

By remembering that

$$a_0(J) = \frac{2(J^2 - M^2 + J) - 1}{(2J - 1)(2J + 3)} \tag{D.2}$$

$$\sum_M 1 = \sum_{M=-J}^{J} 1 = (2J + 1), \quad M = -J \div J \tag{D.3}$$

we can write

$$\langle \cos^2 \theta \rangle = \sum_{J,M} \frac{e^{-\frac{B(J(J+1))}{k_B T}}}{\sum_{J,M} e^{-\frac{B(J(J+1))}{k_B T}}} \frac{2(J^2 - M^2 + J) - 1}{(2J - 1)(2J + 3)} =$$

$$= \frac{1}{\sum_{J,M} e^{-\frac{B(J(J+1))}{k_B T}}} \sum_{J,M} e^{-\frac{B(J(J+1))}{k_B T}} \frac{2J(J + 1) - 1}{(2J - 1)(2J + 3)} +$$

$$- \frac{1}{\sum_{J,M} e^{-\frac{B(J(J+1))}{k_B T}}} \sum_{J,M} e^{-\frac{B(J(J+1))}{k_B T}} \frac{2M^2}{(2J - 1)(2J + 3)} =$$

$$= \frac{1}{\sum_{J}(2J + 1)e^{-\frac{B(J(J+1))}{k_B T}}} \sum_{J}(2J + 1)e^{-\frac{B(J(J+1))}{k_B T}} \frac{2J(J + 1) - 1}{(2J - 1)(2J + 3)} +$$

$$- \frac{1}{\sum_{J}(2J + 1)e^{-\frac{B(J(J+1))}{k_B T}}} \sum_{J} e^{-\frac{B(J(J+1))}{k_B T}} \frac{2}{(2J - 1)(2J + 3)} \sum_M M^2$$

Now we consider that

$$\sum_M M^2 = \sum_{M=-J}^{J} M^2 = \sum_{M=-J}^{0} M^2 + \sum_{M=0}^{J} M^2 = 2\sum_{M=1}^{J} M^2 = 2\frac{J(J + 1)(2J + 1)}{6} \tag{D.4}$$

thus we obtain

$$
\begin{aligned}
\langle \cos^2 \theta \rangle = & \frac{1}{\sum_J (2J+1) e^{-\frac{B(J(J+1))}{k_B T}}} \sum_J (2J+1) e^{-\frac{B(J(J+1))}{k_B T}} \frac{2J(J+1)-1}{(2J-1)(2J+3)} + \\
& - \frac{1}{\sum_J (2J+1) e^{-\frac{B(J(J+1))}{k_B T}}} \sum_J e^{-\frac{B(J(J+1))}{k_B T}} \frac{2J(J+1)(2J+1)}{3(2J-1)(2J+3)} = \\
= & \frac{1}{\sum_J (2J+1) e^{-\frac{B(J(J+1))}{k_B T}}} \sum_J (2J+1) e^{-\frac{B(J(J+1))}{k_B T}} \frac{2J(J+1)-1}{(2J-1)(2J+3)} + \\
& - \frac{1}{\sum_J (2J+1) e^{-\frac{B(J(J+1))}{k_B T}}} \sum_J (2J+1) e^{-\frac{B(J(J+1))}{k_B T}} \frac{2J(J+1)}{3(2J-1)(2J+3)} = \\
= & \frac{1}{\sum_J (2J+1) e^{-\frac{B(J(J+1))}{k_B T}}} \sum_J (2J+1) e^{-\frac{B(J(J+1))}{k_B T}} \left(\frac{2J(J+1)-1}{(2J-1)(2J+3)} + \right. \\
& \left. - \frac{2J(J+1)}{3(2J-1)(2J+3)} \right) = \\
= & \frac{1}{\sum_J (2J+1) e^{-\frac{B(J(J+1))}{k_B T}}} \sum_J (2J+1) e^{-\frac{B(J(J+1))}{k_B T}} \frac{4J(J+1)-3}{3(2J-1)(2J+3)} = \\
= & \frac{1}{\sum_J (2J+1) e^{-\frac{B(J(J+1))}{k_B T}}} \sum_J (2J+1) e^{-\frac{B(J(J+1))}{k_B T}} \frac{4J^2+4J-3}{3(2J-1)(2J+3)} = \\
= & \frac{1}{\sum_J (2J+1) e^{-\frac{B(J(J+1))}{k_B T}}} \sum_J (2J+1) e^{-\frac{B(J(J+1))}{k_B T}} \frac{(2J-1)(2J+3)}{3(2J-1)(2J+3)} = \\
= & \frac{1}{3} \frac{1}{\sum_J (2J+1) e^{-\frac{B(J(J+1))}{k_B T}}} \sum_J (2J+1) e^{-\frac{B(J(J+1))}{k_B T}} = \\
= & \frac{1}{3}
\end{aligned}
$$

Bibliography

[1] Philippe Balcou, Pascal Salières, Anne L'Huillier, and Maciej Lewenstein. Generalized phase-matching conditions for high harmonics: The role of field-gradient forces. *Phys. Rev. A*, 55:3204–3210, Apr 1997.

[2] J. Weber, S. M. Oppermann, and P. Marangos, J. Role of rotational wave packets in strong field experiments. *Phys. Rev. Lett.*, 111(263601):263601–263605, Dec 2013.

[3] C. Vozzi, C. Manzoni, F. Calegari, E. Benedetti, G. Sansone, G. Cerullo, M. Nisoli, S. De Silvestri, and S. Stagira. Characterization of a high-energy self-phase-stabilized near-infrared parametric source. *J. Opt. Soc. Am. B*, 25(7):B112–B117, Jul 2008.

[4] P. B. Corkum. Plasma perspective on strong field multiphoton ionization. *Phys. Rev. Lett.*, 71:1994–1997, Sep 1993.

[5] G. Sansone, E. Benedetti, F. Calegari, C. Vozzi, L. Avaldi, R. Flammini, L. Poletto, P. Villoresi, C. Altucci, R. Velotta, S. Stagira, S. De Silvestri, and M. Nisoli. Isolated single-cycle attosecond pulses. *Science*, 314(5798):443–446, 2006.

[6] J. Itatani, J. Levesque, D. Zeidler, Hiromichi Niikura, H. Pepin, J. C. Kieffer, P. B. Corkum, and D. M. Villeneuve. Tomographic imaging of molecular orbitals. *Nature*, 432(7019):867–871, December 2004.

[7] C. Vozzi, F. Calegari, E. Benedetti, J.-P. Caumes, G. Sansone, S. Stagira, M. Nisoli, R. Torres, E. Heesel, N. Kajumba, J. P. Marangos, C. Altucci, and R. Velotta. Controlling two-center interference in molecular high harmonic generation. *Phys. Rev. Lett.*, 95:153902, Oct 2005.

[8] M. Lewenstein, Ph. Balcou, M. Yu. Ivanov, Anne L'Huillier, and P. B. Corkum. Theory of high-harmonic generation by low-frequency laser fields. *Phys. Rev. A*, 49(3):2117–2132, Mar 1994.

[9] V. P. Krainov M. V. Ammosov, N. B. Delone. Tunnel ionization of complex atoms and atomic ions by an alternating electromagnetic field. *Soviet Physics*, 64(1191):1191–1194, 1986.

[10] V. S. Popov A. M. Perelomov and M. V. Terent'ev. Ionization of atoms in an alternating electric field. *Soviet Physics Jept*, 23(5):924–925, May 1966.

[11] K. J. Schafer, Baorui Yang, L. F. DiMauro, and K. C. Kulander. Above threshold ionization beyond the high harmonic cutoff. *Phys. Rev. Lett.*, 70:1599–1602, Mar 1993.

[12] J. B. Watson, A. Sanpera, K. Burnett, and P. L. Knight. Wave-packet recollision and pulse-shape effects in high-harmonic generation. *Phys. Rev. A*, 55:1224–1233, Feb 1997.

[13] Pascal Salières, Anne L'Huillier, and Maciej Lewenstein. Coherence control of high-order harmonics. *Phys. Rev. Lett.*, 74:3776–3779, May 1995.

[14] D Normand, L A Lompre, and C Cornaggia. Laser-induced molecular alignment probed by a double-pulse experiment. *Journal of Physics B: Atomic, Molecular and Optical Physics*, 25(20):L497, 1992.

[15] Bretislav Friedrich and Dudley Herschbach. Alignment and trapping of molecules in intense laser fields. *Phys. Rev. Lett.*, 74:4623–4626, Jun 1995.

[16] J H Posthumus, J Plumridge, M K Thomas, K Codling, L J Frasinski, A J Langley, and P F Taday. Dynamic and geometric laser-induced alignment of molecules in intense laser fields. *Journal of Physics B: Atomic, Molecular and Optical Physics*, 31(13):L553, 1998.

[17] Juan Ortigoso, Mirta Rodrguez, Manish Gupta, and Bretislav Friedrich. Time evolution of pendular states created by the interaction of molecular polarizability with a pulsed nonresonant laser field. *The Journal of Chemical Physics*, 110(8):3870–3875, 1999.

[18] P. S. Pershan, J. P. van der Ziel, and L. D. Malmstrom. Theoretical discussion of the inverse faraday effect, raman scattering, and related phenomena. *Phys. Rev.*, 143:574–583, Mar 1966.

[19] Manfred Lein. Molecular imaging using recolliding electrons. *Journal of Physics B: Atomic, Molecular and Optical Physics*, 40(16):R135, 2007.

[20] Xibin Zhou, Robynne Lock, Wen Li, Nick Wagner, Margaret M. Murnane, and Henry C. Kapteyn. Molecular recollision interferometry in high harmonic generation. *Phys. Rev. Lett.*, 100:073902, Feb 2008.

[21] R. Velotta, N. Hay, M. B. Mason, M. Castillejo, and J. P. Marangos. High-order harmonic generation in aligned molecules. *Phys. Rev. Lett.*, 87:183901, Oct 2001.

[22] M. Lein, N. Hay, R. Velotta, J. P. Marangos, and P. L. Knight. Role of the intramolecular phase in high-harmonic generation. *Phys. Rev. Lett.*, 88:183903, Apr 2002.

[23] W. Boutu, S. Haessler, H. Merdji, P. Breger, G. Waters, M. Stankiewicz, L. J. Frasinski, R. Taieb, J. Caillat, A. Maquet, P. Monchicourt, B. Carre, and P. Salieres. Coherent control of attosecond emission from aligned molecules. *Nat Phys*, 4(7):545–549, July 2008.

[24] Henrik Stapelfeldt and Tamar Seideman. Colloquium. *Rev. Mod. Phys.*, 75:543–557, Apr 2003.

[25] S. Haessler, J. Caillat, W. Boutu, C. Giovanetti-Teixeira, T. Ruchon, T. Auguste, Z. Diveki, P. Breger, A. Maquet, B. Carre, R. Taieb, and P. Salieres. Attosecond imaging of molecular electronic wavepackets. *Nat Phys*, 6(3):200–206, March 2010.

[26] R. M. Lock, S. Ramakrishna, X. Zhou, H. C. Kapteyn, M. M. Murnane, and T. Seideman. Extracting continuum electron dynamics from high harmonic emission from molecules. *Phys. Rev. Lett.*, 108(133901):133901–133905, Mar 2012.

[27] S. Ramakrishna and Tamar Seideman. Information content of high harmonics generated from aligned molecules. *Phys. Rev. Lett.*, 99(113901):113901–113904, Sep 2007.

[28] A. D. Shiner, C. Trallero-Herrero, N. Kajumba, H.-C. Bandulet, D. Comtois, F. Légaré, M. Giguère, J-C. Kieffer, P. B. Corkum, and D. M. Villeneuve. Wavelength scaling of high harmonic generation efficiency. *Phys. Rev. Lett.*, 103(073902), Aug 2009.

[29] J. Tate, T. Auguste, H. G. Muller, P. Salières, P. Agostini, and L. F. DiMauro. Scaling of wave-packet dynamics in an intense midinfrared field. *Phys. Rev. Lett.*, 98(013901), Jan 2007.

[30] C. Vozzi, F. Calegari, E. Benedetti, S. Gasilov, G. Sansone, G. Cerullo, M. Nisoli, S. De Silvestri, and S. Stagira. Millijoule-level phase-stabilized few-optical-cycle infrared parametric source. *Opt. Lett.*, 32(20):2957–2959, Oct 2007.

[31] I. J. Sola, E. Mevel, L. Elouga, E. Constant, V. Strelkov, L. Poletto, P. Villoresi, E. Benedetti, J.-P. Caumes, S. Stagira, C. Vozzi, G. Sansone, and

M. Nisoli. Controlling attosecond electron dynamics by phase-stabilized polarization gating. *Nat Phys*, 2(5):319–322, May 2006.

[32] A. M. Malvezzi, L. Garifo, and G. Tondello. Grazing-incidence high-resolution stigmatic spectrograph with two optical elements. *Appl. Opt.*, 20(14):2560–2565, Jul 1981.

[33] Luca Poletto, Giampiero Naletto, and Giuseppe Tondello. Grazing-incidence flat-field spectrometer for high-order harmonic diagnostics. *Optical Engineering*, 40(2):178–185, 2001.

[34] Luca Poletto, Giuseppe Tondello, and Paolo Villoresi. High-order laser harmonics detection in the euv and soft x-ray spectral regions. *Review of Scientific Instruments*, 72(7):2868–2874, 2001.

Ringraziamenti

Desidero ringraziare innanzitutto il mio relatore Prof. Salvatore Stagira, per avermi seguito nel persorso di scrittura della tesi e soprattutto per la sua pazienza e la sua grande disponibilitá, il gruppo di ricerca in cui sono stato coinvolto per svolgere la mia attivitá sperimentale, per il lavoro svolto insieme, per i consigli ricevuti e anche per il piacevole tempo trascorso in compagnia. Voglio inoltre dire grazie ai miei amici per la loro vicinanza e per aver allievato la solitudine di questi anni lonano da casa. Grazie anche alla Dott.ssa Sainaghi per avermi regalato dei nuovi occhi per vedere il mondo e la vita. Non ho parole, invece, per ringraziare una persona molto speciale che mi ha circondato di grande affetto in questo ultimo anno, ed in particolare mi è stata estremamente vicina in questi mesi di intenso lavoro supportandomi e sopportandomi in tutti i modi possibili, grazie davvero, molto di questo risultato lo devo e lo dedico anche a te. Vorrei infine pronunciare infinite volte la parola grazie alla mia famiglia, compresa mia sorella Tania, che mi ha permesso di studiare ció che desideravo nel luogo che preferivo, per tutte le volte che mi ha sostenuto nei momenti di difficoltá nonostante la lontananza, per aver sempre creduto in me anche quando io non lo facevo, per gli enormi sacrifici fatti in mio favore e per non avermi mai privato della libertá di scegliere il mio futuro cercando di abbattere tutte le barriere che potessero limitare la mia felicità. Devo a loro questo traguardo perchè é solo grazie all'impegno che i miei genitori hanno sempre profuso per me se sono arrivato al punto in cui mi trovo.